

## 9. SITE 1178<sup>1</sup>

Shipboard Scientific Party<sup>2</sup>

### SITE SUMMARY

The science objective of Site 1178 included sampling of slope sediments and underlying landward-dipping reflector (LDR) zone in order to clarify the structural evolution of the prism.

We recognized two fundamental lithostratigraphic units at Site 1178. Both are divided into three subunits. Interpretations of the lithostratigraphy are hampered by complexities in biostratigraphy and structural deformation. Subunit IA (upper slope–apron facies) is Quaternary to Pliocene in age and extends from the seafloor to a depth of 94.40 meters below seafloor (mbsf). Lithologies consist of hemipelagic mud, sandy mud, and volcanic ash. Subunit IB is Pliocene in age and extends from 94.40 to 127.00 mbsf. In addition to the normal hemipelagic mud, this subunit also contains abundant silt-sand turbidites and minor mud-supported gravel. Subunit IC is Pliocene to late Miocene in age and extends from 127.00 to 199.20 mbsf. Lithologies in Subunit IC consist of hemipelagic mud with variable amounts of intermixed sand, rare volcanic ash beds, and rare mixed volcanic lapilli and gravel-sized mud clasts. Strata within Unit I have been subjected to significant amounts of displacement along a submarine slide surface. Below the dislocation surface, more highly deformed strata of Unit II are late Miocene in age and almost certainly part of the Nankai accretionary prism. Subunit IIA (411.00–199.20 mbsf) contains abundant sand and silt turbidites with interbeds of carbonate-poor mudstone. Similarities are striking between Subunit IIA lithofacies and those of the axial trench–wedge environment. Subunit IIB (411.00–563.95 mbsf) contains sporadic silt to sandy silt turbidites and a greater proportion of carbonate-poor mudstone, similar in all respects to the outer trench–wedge facies at Sites 1173 and 1174. The axial trench–wedge facies is repeated below 563.95 mbsf (Subunit IIC) and extends to the bottom of Hole 1178B. This repetition of facies confirms the occurrence of one of the imbricate thrust faults

<sup>1</sup>Examples of how to reference the whole or part of this volume.

<sup>2</sup>Shipboard Scientific Party addresses.

within the accretionary prism. The low carbonate content throughout Unit II indicates deposition below the carbonate compensation depth (CCD).

Structurally, Site 1178 consists of four domains. Domain I, 0 to 200 mbsf, comprises the slope sediments, with discrete slump-folded packages and east-west-striking bedding. Domain II, from 200 to 400 mbsf, consists of accreted sediments but with only small-scale deformation features and gentle to moderate bedding dips. Domain III, in contrast, extends from 400 to 506 mbsf and is characterized by marked deformation throughout. The deformation has four chief elements: bedding dips ranging up to 55°, bedding-oblique foliation, bedding-parallel fissility, and fracture sets that brecciate the sediment into roughly trapezoidal fragments and postdate the foliation/fissility. Toward the base of this 106-m zone of shearing, scaly surfaces with downdip slickenlines probably indicate a major prism thrust fault. Domain IV, from 506 mbsf to the base of the hole, is characterized by generally weaker deformation, although moderate bedding dips are common. Steeper dips and increased deformation ~550 mbsf and between 633 mbsf and the hole bottom presumably represent additional minor thrust faults. Thus Domain IV contains several thrust slices, each internally deformed much less than the sheet overlying the major thrust at the base of Domain III but probably contributing to biostratigraphic repetitions and thickening of the section.

Biostratigraphic age control was provided by calcareous nannofossils although their abundance and states of preservation varied throughout the sequence. The interval from 199.05 to 673.17 mbsf yields assemblages especially poor in preservation and low in abundance, making zonal identification problematic. Deformation of the sediments leads to a repetition of biostratigraphic events and thus to a disturbed biostratigraphic succession. The sedimentary section spans the time interval from the late Miocene (Subzones NN11–NN10) through the Pleistocene (Subzone NN21a).

Paleomagnetic measurements of magnetic inclination and intensity in Holes 1178A and 1178B show two hiatuses at 8.5 and ~400 mbsf. Based on the results of biostratigraphy, inclination changes from the top to the bottom of Holes 1178A and 1178B are identified as two different geomagnetic polarity intervals. Normal polarity is identified from 0 to 8.5 mbsf in Hole 1178A within the Brunhes Chron (0–0.78 Ma). Inclination changes from 8.5 to ~400 mbsf are considered to be geomagnetic polarity changes from the Pliocene to late Miocene, including the Gauss (2.581–3.580 Ma), Gilbert (3.580–5.894 Ma), and C3A (5.894–6.935 Ma) Chrons. Continuous steep inclinations below 400 mbsf may be considered to be a repeat of the C4r Subchron (8.072–8.699 Ma).

The Cl concentration-depth profile exhibits a steep, continuous trend of freshening of up to 3%–4% relative to seawater Cl concentration. Superimposed on this background dilution profile are numerous smaller Cl minima. The largest ones occur at ~200 mbsf, corresponding to >6% dilution, and above the bottom-simulating reflector (BSR) at ~400 mbsf, corresponding to ~7% dilution. Based on measured core temperatures on the catwalk (a minimum of –0.5°C at 200 mbsf), the associated elevated methane concentration, and the observation that other dissolved components such as Si and Ca have similar dilution minima, we suggest that disseminated methane hydrate is widespread at this site, increasing in abundance from ~90 mbsf to the depth of the

BSR. Hydrate is probably not evenly distributed within the sediment and seems more abundant in coarser-grained horizons.

The Ca, Mg, alkalinity, and sulfate concentration profiles are intimately coupled in the top 35 mbsf, with primary dolomite formation and dolomitization of biogenic calcite the most active reactions. The inverse relation between Ca and Mg below this depth suggests that they are involved in distinct reactions—Mg in silicate reactions below the depth drilled and Ca in ash dissolution and alteration plus probably carbonate reactions linked or associated with microbially mediated reactions at the BSR.

Similar to the deep-water Sites 1173 and 1174 but unlike the shallow water Sites 1175 and 1176, an increase in Cl concentration with depth in the top 35 mbsf is a trend consistent with diffusion of lower chlorinity interglacial water into the sediment.

The total organic carbon (TOC) content for the sediment samples examined at Site 1178 ranges from 0.57 to 1.03 wt% over the first 383.6 mbsf, with an average value of 0.73 wt%, the highest TOC values measured for Nankai sediments during Leg 190. Sulfur concentrations track the TOC values in this interval and range from 0.24 to 1.45 wt%, with the highest values occurring at 200 and 350 mbsf, coincident with the highest TOC values. The moderate to low concentrations of methane throughout Holes 1178A and 1178B are attributed to the high concentrations of light hydrocarbons from ethane to hexane, indicative of older, more mature organic matter within the sediments (diagenesis) or migration (thermogenesis) of hydrocarbons from deeper depths. Overall, the concentrations of light hydrocarbon ethane to hexane reflect the thermal evolution and maturity of the sedimentary organic matter at Site 1178. The Bernard ratio ( $C_1/[C_2+C_3]$ ) for the hydrocarbons at Site 1178 also indicates that some of the lighter hydrocarbons (ethane to hexane) in these sediments were produced from more mature organic matter present in situ mixed with thermogenic hydrocarbons that have migrated in from a more mature source at depth. Significant faulting has occurred over the lower 300 m of Hole 1178B that could facilitate fluid migration of more mature hydrocarbons buried at deeper depths to shallower sediments.

Microorganisms were enumerated in 30 samples collected from the surface to 633 mbsf at Site 1178. Bacteria are present in near-surface sediments at low, but close to expected, abundances. This was probably related to high interstitial water (IW) sulfate concentrations to at least 18.3 mbsf. However, bacterial populations decline rapidly to barely detectable at 272 mbsf. This is a much greater rate of decrease than was observed at other sites during this leg. A small but statistically significant decrease from the general trend that is associated with the presence of a small amount of gas hydrate occurs at 210 mbsf. Below 272 mbsf, population sizes generally vary between not detectable and barely detectable, except for a zone between 374 and 497 mbsf, where populations increased up to a maximum of  $6 \times 10^5$  cells/cm<sup>3</sup>. These were not only locally statistically significant but were larger populations than were encountered at some of the more shallow depths at this site. No relationship was observed between bacterial populations and the IW sulfate concentration or the methane concentration; therefore, the reasons for such a rapid rate of decrease in numbers remains unclear. Seventeen whole-round cores were taken for shipboard enrichment cultures, cell viability, and shore-based microbiological analysis to measure potential bacterial activities, culture microorganisms, characterize nucleic acids, and investigate fatty acid biomarkers.

There are no obvious differences in physical properties between the slope-apron deposits of Unit I and the underlying accreted sediments of Unit II. In general, porosities at Site 1178 decrease with depth, following a typical compaction profile. Deviations from the compaction trend occur at 70–100 mbsf, 140–160 mbsf, and ~200 mbsf. In addition, porosity values within lithostratigraphic Subunits IB and IC are more scattered than in Subunit IA and Unit II, and they probably reflect lithologic variation in this sandier part of the stratigraphic section or deposition by slope-failure processes. Velocities and formation factors increase with depth and are highly variable. Uncalibrated gas-permeability measurements show a range of values similar to other Leg 190 sites, again due to differences in lithology. High values are given by volcanic ashes high in the section and by beds of silt and sand, including those down to 600 mbsf. The background hemipelagites gave uniformly low measurements.

Two in situ temperature measurements indicate a thermal gradient of 0.046°C/m.

Site 1178 drilling revealed that the LDR zone is composed of steeply dipping, pervasively foliated, and partly brecciated upper Miocene accreted sediments. This result will contribute significantly to our understanding of the tectonic evolution of the Nankai accretionary prism.

## **OPERATIONS**

### **Proposed Site ENT-09A (Site 1178)**

The vessel reached proposed Site ENT-09A (Site 1178) at 0730 hr on 8 July, and preparations for making up the bottom-hole assembly (BHA) began. Considerable ocean current was observed, so the vessel was offset upcurrent 200 m from the location to drop the beacon. The beacon was dropped at 0845 hr on 8 July, establishing Site 1178. Once the hydrophones and thrusters were lowered and the ship settled out over the site in dynamic positioning mode, it was determined that the beacon had come to rest on the seafloor 180 m downcurrent of the location.

### **Hole 1178A**

Because of the strong current, the ship had to be offset upcurrent from the location and allowed to drift back to enable the drill collars to be made up. A BHA consisting of a 9.875-in PDC bit, bit sub, seal bore drill collar, landing saver sub, modified top sub, modified head sub, nonmagnetic drill collar, seven 8.25-in drill collars, a tapered drill collar, and crossover sub was assembled.

A precision depth recorder measurement was taken that indicated a drilling depth of 1716.5 meters below sea level (mbsl) (1728.4 meters below rig floor [mbrf]). The bit was lowered to 1710 mbrf, where a bottom-water sample was collected using the water-sampling temperature probe (WSTP). The bit was then lowered to 1728 mbrf; core was taken but no sediment was recovered. The bit was lowered to 1725.6 mbsl (1737.5 mbrf), and another core was taken, with no sediment recovered. The bit was once again lowered 9.5 m to 1735.1 mbsl (1747 mbrf), and Hole 1178A was spudded at 1855 hr on 8 July. Core 1H recovered 2.9 m of sediment, establishing the seafloor depth as 1741.7 mbsl (1753.6 mbrf) (Tables **T1**, **T2**).

---

**T1.** Coring summary, p. 64.

---

---

**T2.** Coring summary by section, p. 66.

---

Cores 1H to 44X were taken from 0 to 410.8 mbsf (1753.6–2164.4 mbrf), recovering 340.19 m of core (83%). The penetration rate had decreased to <6 m/hr when the decision was made to terminate extended core barrel (XCB) coring and switch to the rotary core barrel (RCB) system. Hole 1178A was filled with 122 bbl of heavy mud, and then the pipe was tripped out of the hole. The bit cleared the rig floor at 1430 hr on 11 July, officially ending Hole 1178A. Because Hole 1178A was the last deployment of the advanced hydraulic piston corer (APC)/XCB BHA for Leg 190, it was disassembled.

### **Hole 1178B**

The ship was offset 20 m to the east while an RCB BHA was being assembled. The BHA consisted of a new 9.875-in CC-3 roller cone bit, a bit sub, 8.25-in drill collar, modified top sub, modified head sub, seven 8¼-in drill collars, a tapered drill collar, six joints of 5.5-in drill pipe, and a crossover sub to 5-in drill pipe. The bit was tripped to the seafloor, and Hole 1178B was spudded at 2015 hr on 11 July.

Hole 1178B was first drilled to 395 mbsf (1753.6–2148.6 mbrf). RCB coring then commenced, and Cores 2R through 31R were taken from 395.0 to 679.2 mbsf (2148.6–2432.8 mbrf), recovering 165.96 m of core (58%).

During operations at Site 1178, the current generally averaged between 2.5 and 3.5 kt. However, on several occasions it was believed that the current exceeded 5 kt. The bridge speed log indicated 4.8 kt during those times, and 100 turns on both screws were required to maintain station. Severe vibrations in the drill string were observed. The vibrations were transmitted up to the top drive and associated traveling equipment. The electrical supervisor reported that the hydrophones were vibrating severely within their wells. The aft side of the upper guide horn was too hot to touch with a bare hand because of the drill string rubbing against it.

Even though the ship was able to maintain position during the peak current times, we thought that the safe operational limits had been reached for two reasons. First, the automatic station keeping (ASK) system was already operating at its maximum output available from the main screws. Any increase in the 10–12 kt head winds would have exceeded the ASK system's ability to maintain station. Second, and perhaps more important, the severe vibration in the drill string and traveling equipment was of great concern. Fatiguing of drill-pipe connections, as well as possible damage to compensator rods and seals, was a distinct possibility. There were also concerns about any loose objects that might fall out of the derrick. Had the current increased above the perceived 5 kt, operations would have had to be shut down.

At 1515 hr on 12 July, three thrusters (T-2, T-4, and T-5) automatically tripped off line. Fortunately the ASK system was able to compensate for the lost thrusters and maintain ship position. With a >3-kt current running at the time, the decision was made to raise the bit from the current total depth of the hole (419.3 mbsf) to 32.7 mbsf until the ASK system problem could be resolved. The problem was traced to a faulty transformer in the forward thyrig room. This transformer supplies power to the thruster controller cards and was giving a faulty signal. The transformer was bypassed, and the ASK system performance immediately returned to normal. Operations were resumed after losing 4.5 hr.

Coring was stopped in Hole 1178B when the allotted coring time for Leg 190 expired at 0600 hr on 15 July. The hole was filled with heavy mud and the bit was tripped out. The bit cleared the seafloor at 0845 hr, and the positioning beacon was released and recovered at 1045 hr. The bit cleared the rig floor at 1250 hr on 15 July, officially ending Hole 1178B and operations at Site 1178.

### Transit from Site 1178 to Yokohama

The ship began the transit to Yokohama at 1400 hr on 15 July. The first line was ashore at 1600 hr on 16 July at Daikoku Wharf, Yokohama, Japan, officially ending Leg 190.

## LITHOSTRATIGRAPHY

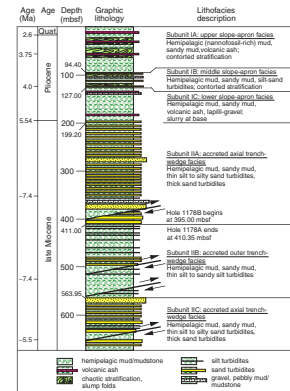
We recognized two fundamental lithostratigraphic units at Site 1178 (Fig. F1; Table T3). Unit I represents the slope-apron facies, and Unit II consists of accreted sediments. Both are divided into three subunits. Interpretations of the lithostratigraphy are hampered by complexities in biostratigraphy and deformation by thrust faulting. Another noteworthy aspect of this site is that nearly all of Unit I has been subjected to significant amounts of displacement along a submarine slide surface. Strata below the dislocation surface are almost certainly part of the Nankai Trough accretionary prism. We recognize striking similarities between their facies associations and those of the axial to outer trench-wedge environments of the Nankai Trough, as described at Sites 1173 and 1174. The widespread occurrence of such deformation features as incipient cleavage, spaced fractures, steep bedding dips, and brecciation supports the notion of frontal accretion (see “Structural Geology,” p. 9).

### Subunit IA (Upper Slope–Apron Facies)

Subunit IA is Quaternary to Pliocene in age and extends from the seafloor to a depth of 94.40 mbsf (Section 190-1178A-12X-1, 0 cm). This unit consists predominantly of nannofossil-rich hemipelagic mud (silty clay to clayey silt) with lesser amounts of sandy mud (sand-silt-clay). The hemipelagic mud and sandy mud are gray, greenish gray, or greenish brown in color. Internal structures, ranging from homogeneous to layered with sand laminae or mottled green clay-rich laminae are a result of bioturbation. The composition includes abundant clay minerals and biogenic debris together with lesser amounts of volcanic glass and lithic fragments (see “Site 1178 Smear Slides,” p. 74). Nannofossils, diatoms, and sponge spicules are common in this unit. Sandy intervals contain a typical assortment of such siliciclastic grains as quartz, plagioclase, pyroxene, and lithic fragments.

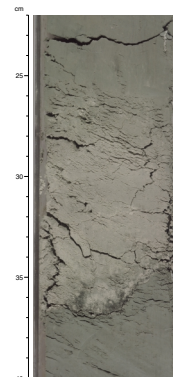
Volcanic ash beds in Subunit IA vary in thickness from <1 cm to medium bedded (19 cm). The thickest ash deposit is in Core 190-1178A-3H (14.12 mbsf). Ash layers typically have sharp, plane-parallel to irregular lower contacts and gradational upper contacts (Fig. F2). Color variations range from pale gray to dark gray, white with dark grains (salt and pepper), brown, pink, and greenish gray. Grain size varies from lapilli to fine ash; a grain-size range of 0.1–2.0 mm is most common. The volcanoclastic sediment is composed primarily of fresh glass shards or pumice, plus variable amounts of nannofossil-rich silty clay, lithic clasts,

F1. Stratigraphic column, p. 29.



T3. Stratigraphic relations, p. 75.

F2. Graded volcanic ash layer from Subunit IA, p. 30.



and crystals of quartz, plagioclase, and pyroxene (see “Site 1178 Smear Slides,” p. 74).

Intervals of disturbed stratification are common within Subunit IA (Fig. F3). Although some of the disturbance may be due to coring or drilling, we attribute most of the chaotic and folded bedding to downslope movement of poorly lithified sediment. The following intervals contain the most obvious examples of disturbed stratification: intervals 190-1178A-4H-1, 125 cm, to 4H-6, 139 cm (23.15–29.79 mbsf); 5H-2, 50 cm, to 5H-4, 130 cm (33.40–37.20 mbsf); 6H-3, 50 cm, to 7H-4, 80 cm (44.40–55.70 mbsf); and 8H-2, 35 cm, to 8H-5, 120 cm (59.35–64.70 mbsf). Additional zones of deformation may have escaped our recognition because of homogeneous lithology.

The overall facies character of Subunit IA is consistent with slope-apron sedimentation by way of hemipelagic settling of nannofossil-rich mud, mudflows, and occasional air falls of volcanic ash. A relatively high concentration of calcareous nannofossils in the hemipelagic mud indicates that deposition occurred above the CCD. Remobilization of the slope sediment by large-scale gravitational failure probably caused the internal stratal disruption of Subunit IA.

### Subunit IB (Middle Slope–Apron Facies)

Subunit IB is Pliocene in age and extends from 94.40 mbsf (Section 190-1178A-12X-1, 0 cm) to 127.00 mbsf (Section 15X-3, 80 cm). Lithification of the fine-grained strata is more advanced than in Subunit IA, but the hemipelagic deposits are also interstratified with thin beds of silty sand. These turbidites provide the most distinguishing characteristic of Subunit IB. They display sharp bases, plane-parallel laminae, and ripple cross-laminae. In addition, many of the intervening muddy intervals contain appreciable quantities of coarse silt and fine sand, some of which may have been dispersed by the coring and core-splitting process. Beds of mud-supported gravel (Fig. F4) are present in Sections 190-1178A-13X-1 and 13X-2, and 14X-2. There is also one unusual bed of volcanic lapilli and gravel-sized clasts of mudstone in Section 14X-3 (Fig. F5).

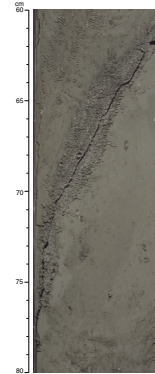
Stratal disruption is also commonplace within Subunit IB. The most clearly defined intervals of soft-sediment deformation are 190-1178A-12X-3, 30 cm, to 12X-6, 55 cm (97.61–102.36 mbsf), and 14X-6, 25 cm, to 15X-3, 80 cm (121.35–127.00 mbsf). Deposition of Subunit IB occurred during a time interval in which fine-grained turbidity currents were relatively frequent. Within a slope-apron environment, the most likely mechanism for periodic turbidite influx is overbank deposition associated with a nearby submarine canyon system.

### Subunit IC (Lower Slope–Apron Facies)

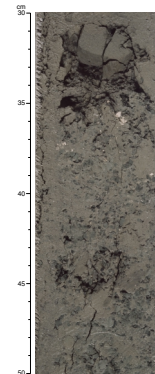
Subunit IC is Pliocene to late Miocene in age and extends from 127.00 mbsf (interval 190-1178A-15X-3, 80 cm) to 199.20 mbsf (23X-1, 0 cm). The base of Subunit IC coincides with a prominent seismic reflector; reflector orientation and lateral continuity change significantly below the subunit boundary. This dislocation surface is parallel to the present-day seafloor, so it is probably a failure plane at the base of a large submarine slump or slide.

The most common lithology of Subunit IC is greenish gray hemipelagic mud (clayey silt), with variable amounts of intermixed sand. The mud and sandy mud is fractured, and sedimentary brecciation occurs

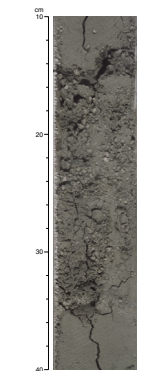
F3. Inclined volcanic ash layer in disturbed zone of Subunit IA, p. 31.



F4. Mud-supported gravel with mud and shell fragments from Subunit IB, p. 32.



F5. Gravel with pumice fragments and mud clasts from Subunit IB, p. 33.



throughout the subunit. Deformation within the lowermost interval (Sections 190-1178A-22X-4 to 22X-CC) is particularly intense, reducing most of the core to slurry. Angular clasts of green mud and mottled, pale brown patches are scattered through the subunit. There are also rare beds of volcanic ash and volcanic lapilli mixed with gravel-sized mud clasts. The original depositional setting for Subunit IC was probably an inclined slope apron without turbidite influx, similar to the environmental conditions that existed during deposition of Subunit IA.

### Subunit IIA (Accreted Axial Trench–Wedge Facies)

Subunit IIA is late Miocene in age and extends from 199.20 mbsf (Section 190-1178A-23X-1, 0 cm) to 411.00 mbsf (Section 190-1178B-4R-1, 140 cm). The most characteristic feature of this subunit is its preponderance of thin-bedded, poorly lithified turbidites, which range in texture from sand to sandy silt and silt. Most such beds are 1–10 cm in thickness with sharp bases and gradational tops. Internal sedimentary structures include plane-parallel laminae and ripple cross-laminae (Fig. F6). Normal size grading is common. In a typical 1.5-m section of core, there may be three or four sand-silt beds interlayered with hemipelagic mud, mudstone, and muddy turbidites. There are also scattered light brown carbonate-cemented mudstones.

Thicker beds of poorly lithified sand and muddy sand are present in Cores 190-1178A-30X, 40X, and 42X and in Core 190-1178B-4R. These deposits are as thick as 150 cm, poorly sorted, and normally graded; some contain dispersed clasts of mudstone. Fragments of woody organic matter are also common (Fig. F7). Common grain constituents include quartz, plagioclase, volcanic lithic fragments, and sedimentary to metasedimentary rock fragments. The base of Subunit IIA coincides with the deepest occurrence of thick-bedded sand (interval 190-1178B-4R-1, 0–140 cm).

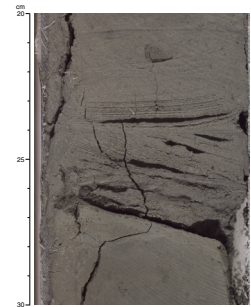
The facies character of Subunit IIA is nearly identical to the sand-rich axial trench–wedge facies that was cored at Sites 808 and 1174. Frequent turbidity currents affected the depositional environment, and rates of sedimentation were high. These environmental conditions, together with a low content of calcium carbonate, are consistent with deposition near the base of a slope. Subsequent accretion to the Nankai Trench slope occurred by frontal offscraping. The base of Subunit IIA is close to the position of a thrust fault within the prism, as described in “[Structural Geology](#),” p. 9.

### Subunit IIB (Accreted Outer Trench–Wedge Facies)

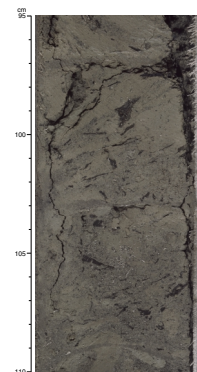
Subunit IIB is late Miocene in age and extends from 411.00 (Section 190-1178B-4R-1, 140 cm) to 563.95 mbsf (Section 190-1178B-20R-1, 35 cm). Most of this subunit is composed of gray hemipelagic mudstone (silty claystone to clayey siltstone) with local mottling and bioturbation. As subsidiary lithologies, there are sporadic interbeds of silt, sandy silt to silty sand, sandy mud (sand-silt-clay), and bands of greenish gray mudstone. Stratification is typically inclined, and many intervals of mudstone display a well-developed fissility or incipient cleavage (see “[Structural Geology](#),” p. 9). Locally, the incipient cleavage is oblique to the stratification. Inclined fractures are also common, and thrust faults are evident at ~525 and ~550 mbsf (Fig. F1).

The lithofacies character of Subunit IIB is virtually identical to what we observed in the outer trench–wedge facies at Sites 1173 and 1174, as

F6. Cross-lamination in a thin-bedded sandy turbidite, p. 34.



F7. Silty sand with wood fragments from Subunit IIA, p. 35.



well as in the correlative facies unit at Site 808 (Shipboard Scientific Party, 1991). Agents of deposition included hemipelagic settling, distal excursions of sand-silt turbidity currents onto the outer margin of the Nankai Trough, and settling of mud from the entrained layers of turbidity currents. The environmental change from Subunit IIB into IIA was gradual (i.e., an incremental increase in sandy turbidites upsection); therefore, the subunit boundary is somewhat arbitrary. Subsequent accretion to the Nankai Trench slope probably was responsible for the widespread deformation of strata within Subunit IIB.

### Subunit IIC (Accreted Axial Trench–Wedge Facies)

Most strata within Unit II are strongly deformed; spaced fractures, fissility, incipient cleavage, and steep bedding dips are common. Without observing changes in lithofacies or stratigraphic age, it is difficult to identify the location or amount of displacement on individual faults within the accretionary prism. A pronounced shift in lithofacies does occur, however, at 563.95 mbsf (Section 190-1178B-20R-1, 35 cm). Below that depth, facies relations once again are consistent with a sand-rich axial trench–wedge environment, as opposed to an outer trench–wedge environment. Beds of unlithified sand and silty sand increase in both number and thickness within Subunit IIC. The similarity of these strata to the deposits of Subunit IIA is so strong that we interpret the facies change to be the result of repetition along one of the imbricate faults of the accretionary prism. Structural criteria place such a fault at ~550 mbsf (Fig. F1).

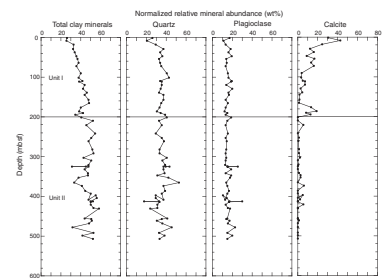
### X-Ray Diffraction Mineralogy

The results of X-ray diffraction (XRD) analysis of bulk-sediment samples from Site 1178 are shown in Figure F8 (see Tables T4 and T5 for data). Stratigraphic trends are nondescript except for a reduction in calcite content from Units I and II. The higher content of calcite within Unit I is consistent with deposition of the slope apron above the CCD. Depletion of calcite within the accreted trench-wedge deposits of Unit II is consistent with deposition of those strata below the CCD. Relative mineral abundances within Unit II are scattered and inconsistent because of the interstratification of hemipelagic mud, muddy turbidites, and sand-silt turbidites, as well as the repetition of facies by thrust faults.

## STRUCTURAL GEOLOGY

Site 1178 yielded a broad range of deformation structures consistent with penetration through slumped slope deposits into the more highly deformed rocks of the accretionary prism below (Table T6). We have divided the sequence into four structural domains (Fig. F9). Domain I (0 to 200 mbsf) comprises the slope sediments. Intervals of variably dipping beds, reaching vertical in places, are present in the silty clays, commonly bounded by subhorizontal contacts or sand layers. We interpret this arrangement to reflect a series of discrete slump packages. Paleomagnetic and Tensor tool reorientations indicate a general east-west strike for the bedding (Fig. F10A), presumably reflecting the local bathymetry of the time.

F8. Abundances of total clay minerals, quartz, plagioclase, and calcite, p. 36.

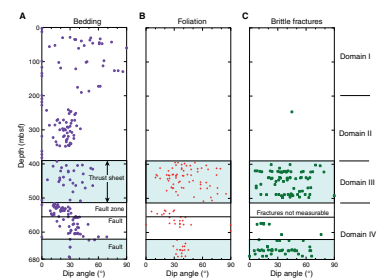


T4. Peak intensities and peak areas from XRD analysis of sediments, p. 76.

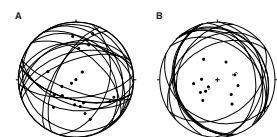
T5. Mineral abundances based on XRD analysis, p. 78.

T6. Structural data, p. 80.

F9. Synopsis of deformation structures, p. 37.



F10. Stereographic projections of bedding, p. 38.



Domain II (200 to 400 mbsf) consists of accreted sediments that appear to show only small-scale deformation features, although poor core quality precluded good observations. Structures include minor high-angle normal faults, sparse deformation bands, and a few thin, black fault seams. Few of these could be reoriented because of the small size of the drilling biscuits. Bedding dips are gentle to moderate (Fig. F9) and show no clear pattern after reorientation (Fig. F10B).

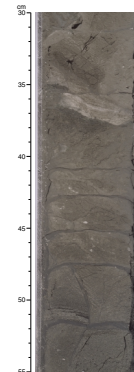
Domain III (400 to 506 mbsf) is characterized by marked deformation, although the intensity varies and is greatest at the base of the domain. The domain extends downward from 400 mbsf, where it is seen both in the lowermost cores from Hole 1178A and the uppermost cores from Hole 1178B (to 506 mbsf). The deformation is manifested in Hole 1178A in two ways, depending on lithology. In silty clays, it is recorded by an anastomosing, low-angle, penetrative foliation and an incipient breccia with irregular fine black seams (Fig. F11). In sands, it is represented by crisscrossing ribs, <1 mm across (Fig. F12), in a weblike arrangement.

Deformation in Hole 1178B has produced four chief effects in Domain III. First, bedding dips are nowhere horizontal and range up to 55° (Figs. F9, F13A). Second, a more or less penetrative foliation has developed in some silts and sands and is clearly oblique to bedding (Figs. F13B, F14). The sediment tends to break along these planes, and hence the fabric could reasonably be termed a cleavage, a structure that is little documented in the literature on poorly lithified and shallowly buried sediments. Third, many of the sediments both in this domain and in underlying undeformed intervals show a tendency to break into planes with an appearance similar to the foliation mentioned above but with an orientation parallel to bedding. Because of this bedding-parallel nature and its presence in undeformed sediments, we term this structure fissility, although its relation to the similar-looking bedding-oblique foliation in deformed intervals remains unclear. Fourth, sets of fractures are common, especially in more clayey materials, varying in spacing and orientation and causing the sediment to brecciate into slickensided fragments that are roughly trapezoidal in shape and a few millimeters to a centimeter or more in size (Figs. F13C, F15). Several of the fracture sets crosscut and clearly postdate the foliation/fissility. They may denote faulting superimposed upon the more ductile pervasive strains in the prism recorded by the foliation.

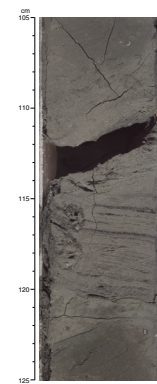
At the base of Domain III (506 mbsf), the fracture sets are spaced as little as a few millimeters and slickenlines on the fracture surfaces are uniformly approximately downdip. In places, the fractures have an anastomosing form, with the resulting lenticles having distinctly polished surfaces. Consequently, the sediment has the appearance of scaly clay. Below 506 mbsf, the spacing of fractures rapidly increases such that by 509 mbsf, deformation of the cores is negligible. Bedding dips, too, show an abrupt decrease (Fig. F9). The intensity of brittle deformation above 506 mbsf and contrast in fracture density and bedding dips across this interval suggest that this zone represents a major thrust fault in the prism.

Domain IV, therefore, is characterized by much less deformation than Domain III. It extends from 506 mbsf to the base of the hole at 673 mbsf, although significant deformation effects are seen at 550 mbsf and from 622 mbsf to the bottom of Hole 1178B. The orientation data are summarized in Figure F16. From the shallow bedding dips at ~509 mbsf, values steadily steepen to 550 mbsf, where core-scale structures also peak, and reach a maximum at 600 mbsf.

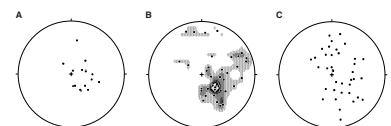
F11. Incipient breccia with irregular fine black seams, p. 39.



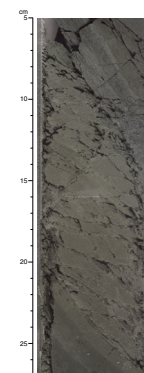
F12. Incipient weblike structure in fine sand, p. 40.



F13. Stereographic projections of structural features in Domain III, p. 41.



F14. Bedding-oblique foliation typical of Domain III, p. 42.



Below 550 mbsf, most of the cores show little deformation, although bedding dips are mostly in the 25°–45° range. Fracture sets are sporadically distributed, and some sand intervals preserve a near-vertical anastomosing grain fabric, in some cases crosscut by subhorizontal, sediment-filled veinlets. Between 622 and 673 mbsf, however, such veinlets are mutually crosscutting in a weblike arrangement (Fig. F17), fracture intensity increases, and the clay-rich sediments are crisscrossed by irregular black seams similar to those observed near the base of Hole 1178A. The sediment has the appearance of an incipient breccia, in places scaly and foliated (Fig. F18). The sets of fractures locally developed in this interval (622–673 mbsf) appear similar to those in Domain III. We therefore interpret these structures to represent zones of shearing, presumably additional thrust faults in the prism. The thrusts in Domain IV may contribute to the apparent thickening of the C4A Subchron in the magnetostratigraphy data (Fig. F19) and possible repetitions in the biostratigraphy. Thus Domain IV appears to contain several thrust slices, each internally deformed less than the sheet overlying the major thrust at the base of Domain III.

In summary, Site 1178 consists structurally of slope deposits containing packets of slumped sediment overlying an accretionary sequence that comprises several thrust sheets, one of which occupies a zone of shearing >100 m thick.

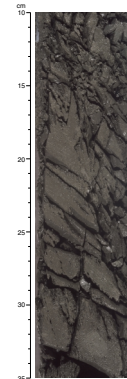
### Uncalibrated Gas-Permeability Measurements

Uncalibrated gas-permeameter measurements show a range of values similar to other Leg 190 sites, and the variation is again correlated with differences in lithology (Fig. F20). Fractured and brecciated intervals representing thrust faults were impossible to measure because of the probe design of the instrument. The background hemipelagites gave measurements ranging from  $10^{-17}$  m<sup>2</sup> to just over  $10^{-16}$  m<sup>2</sup> and showed no tendency to decrease with depth. As at other sites, there is no obvious correlation between measured uncalibrated permeability and average porosity measured shipboard. At the top of the section, some of the higher values were given by volcanic ashes, but the other high determinations were all due to silt and sand. Even at depths of ~600 mbsf, the turbiditic sands are sufficiently uncemented to give values as high as almost  $10^{-12}$  m<sup>2</sup>.

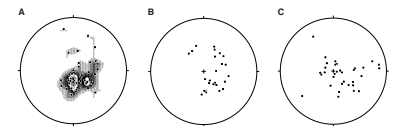
### BIOSTRATIGRAPHY

Sediments recovered from Site 1178 provide a sedimentary record from the Pleistocene through the late Miocene. Calcareous nannofossils were used for developing the biostratigraphic framework according to the zonation schemes of Martini (1971) with zonal modifications proposed by Young (1998) (Table T7). Abundance and preservation of calcareous nannofossils vary throughout the sequence. The interval (core and section) and depth (mbsf) constraints of calcareous nannofossil events recognized at Site 1178 are listed in Table T8. The epoch boundaries have been placed as in Table T9. For nannofossil ranges, see Table T10.

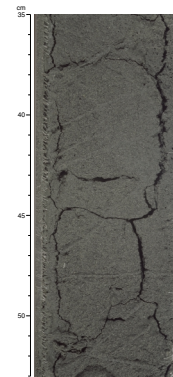
F15. Trapezoidal fragments in breccia generated by oblique fracture sets, p. 43.



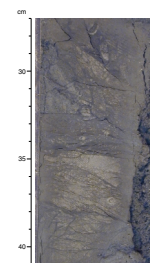
F16. Stereographic projections of structural features in Domain IV, p. 44.



F17. Incipient weblike structure in fine sand, p. 45.



F18. Incipient scaly and foliated clays with fine black seams cross-cutting the fracture fabric, p. 46.





cannot be assessed. The first appearance of *Ceratolithus cristatus* is used to identify the top of the negatively defined Zone NN12. Since *C. cristatus* is still present in Sample 190-1178A-22X-3, 57–58 cm, the interval between 118.85 and 193.37 mbsf is placed in Zones NN14–NN13.

## Miocene

Miocene sediments retrieved from Hole 1178A (204.53–410.35 mbsf) yield generally moderately to poorly preserved assemblages. Below the barren Sample 190-1178A-22X-CC at 199.05 mbsf, sediments were assigned a late Miocene age because of the presence of well-preserved specimens of *Discoaster quinquerramus*. The range of this species is used to define Zone NN11 of the late Miocene. Here it co-occurs with *Reticulefenestra pseudoumbilicus* (>7  $\mu\text{m}$ ), the presence of which in that zone is confined to Subzone NN11b, assigning these sediments to Subzone NN11b. Specimens of the Miocene species *Triquetrorhabdulus rugosus* were found in Sample 190-1178A-24X-CC. *Amaurolithus amplificus* is confined to a short range (6.05–6.8 Ma) within Subzone NN11b and was observed in Sample 190-1178A-35X-CC. The last occurrence of *Minyolitha convallis*, an event to take place within Subzone NN11a, was observed between Samples 190-1178A-39X-CC and 40X-CC. The first occurrence of *Amaurolithus primus*, marking the top of Subzone NN11a (7.2 Ma), was found between Samples 190-1178A-38X-CC and 39X-1, 19–20 cm.

## Hole 1178B

Samples analyzed from Hole 1178B (399.0–673.17 mbsf) are of late Miocene age. The duplication of biostratigraphic intervals is observed in Hole 1178B and can probably be linked to several domains of deformation structures identified (see “**Structural Geology**,” p. 9). The repetition of biostratigraphic events is difficult to exactly define because reworking is common in these sediments. The nannofossil assemblages are generally moderately preserved except for some samples in which nannofossils are altered by strong overgrowth (Samples 190-1178B-3R-CC, 9R-CC, 16R-CC, and 30R-CC). Only a few samples are actually barren of nannofossils (Samples 190-1178B-7R-4, 69–70 cm, and 11R-3, 74–75 cm).

## Miocene

Whereas the uppermost samples of Hole 1178B down to Sample 190-1178B-4R-CC are assigned to Subzone NN11a of the late Miocene because of the presence of *D. quinquerramus* and *M. convallis*, which are confined to an interval from Subzone NN11a to Zone NN9, Sample 190-1178B-5R-3, 12–13 cm, yields *Amaurolithus*, *R. pseudoumbilicus* (>7  $\mu\text{m}$ ), and *D. quinquerramus*, which indicates an assignment to Subzone NN11b. This implies a shift from older to younger sediments. *Amaurolithus* is present down to Sample 190-1178B-15R-CC, where its first occurrence (7.4 Ma) is placed. The interval from Sample 190-1178B-16R to 29R-CC contains abundant *R. pseudoumbilicus* (>7  $\mu\text{m}$ ). *D. quinquerramus* is absent in this interval, indicating an assignment to Subzone NN10a, which contains markedly older sediments. Then *Amaurolithus* spp. and *D. quinquerramus* reappear between Samples 190-1178B-29R-CC and 30R-CC. *Amaurolithus* is confined to Zones NN11B–NN14, marking a

shift toward a younger age. The investigation of additional samples may lead to the identification of additional age reversals.

## PALEOMAGNETISM

### Introduction

After measuring the natural remanent magnetization (NRM), all Hole 1178A sections of the archive-half of the core were partially demagnetized using alternating-field (AF) magnetization at 30 mT at 5-cm intervals to remove magnetic overprints acquired during XCB coring. At Hole 1178B, the AF demagnetization level was changed to 50 mT to remove the strong magnetic overprints acquired during RCB coring.

Two or three oriented discrete samples were routinely collected from each section of the working half of the core primarily for shore-based analysis of the anisotropy of magnetic susceptibility. Many discrete samples were taken for this purpose from the highly fractured Hole 1178B sediments.

### Paleomagnetic Results

Sediments were recovered from 0 to 410.8 mbsf in Hole 1178A and from 395.00 to 679.20 mbsf in Hole 1178B.

Magnetic declinations from Holes 1178A and 1178B show very scattered values, caused by rotation of small core pieces during XCB and RCB coring (Fig. F21). Identification of geomagnetic secular variation and/or geomagnetic polarity changes was therefore difficult, although the declinations were successfully used to reconstruct the structural orientation of sediments. After AF demagnetization at 30 mT, magnetic inclinations from Hole 1178A show a late Miocene to Pleistocene geomagnetic polarity record. However, noncontinuous polarity changes from the top to the bottom of both holes indicate the existence of age boundaries in the sediments. At Hole 1178B, most inclinations have continuous negative values (Fig. F21). These unanticipated inclinations may be related to repetitions in the sequence caused by thrust faults.

Sudden decreases and increases in magnetic intensity were also observed in both holes. Three step changes in the magnetic intensity record were identified, one at 8.6 mbsf (Section 190-1178A-2H-4, 120 cm), one at 209.75 mbsf (Section 190-1178A-24X-1, 95 cm), and one at 660.05 mbsf (Section 190-1178B-30R-1, 5 cm).

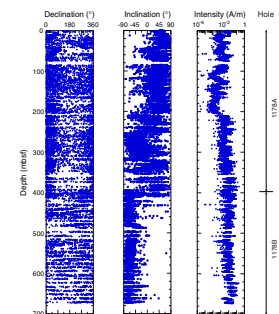
### Magnetostratigraphy

All polarity reversals determined from inclinations after AF demagnetization at 30 and 50 mT were compared with the standard geomagnetic polarity time scale of Cande and Kent (1995). The identified chrons and subchrons at Holes 1178A and 1178B are given in Table T11.

#### Hole 1178A

A clear magnetic intensity boundary at 8.5 mbsf (Section 190-1178A-1H-1, 5 cm) corresponds to the age boundary at 8.5 mbsf identified by magnetostratigraphy using inclination changes.

F21. Magnetostratigraphy, p. 49.



T11. Results of magnetostratigraphic identification, p. 97.

Based on biostratigraphic results, inclinations from the top to the bottom of Hole 1178A are grouped into two different geomagnetic polarity periods. The stable normal inclinations from 0 to 8.5 mbsf (Section 190-1178A-1H-1, 5 cm) are considered to represent normal geomagnetic polarity of the Brunhes Chron (Fig. F19). Below 8.5 mbsf, slightly steep positive inclinations are continuously observed to 43.65 mbsf (Section 190-1178A-6H-2, 125 cm).

The correspondence between the horizons of magnetic inclination and intensity change suggests that a hiatus exists at 8.5 mbsf.

According to biostratigraphic results, inclination changes between 8.5 and 323.3 mbsf (Section 190-1178A-35X-6, 100 cm) should reflect Pliocene geomagnetic polarity changes, which are interpreted to be the Gauss (2.581–3.580 Ma) and Gilbert Chrons (3.580–5.894 Ma). A narrow reversed polarity interval from 43.65 (Section 190-1178A-6H-2, 125 cm) to 53.65 mbsf (Section 7H-3, 25 cm) may be the short geomagnetic event C2An.2r (3.220–3.330 Ma) within the Gauss Chron. The beginning of Gilbert Chron (3.580 Ma) is estimated at 89.05 mbsf (Section 190-1178A-11X-3, 125 cm). Relatively stable normal inclinations from 162 mbsf (Section 190-1178A-19X-1, 60 cm) to 203.75 mbsf (Section 23X-4, 5 cm) may represent normal events within Gilbert Chron.

Inclinations change to negative values below 209.75 mbsf. Based on biostratigraphic results, these negative inclinations may represent the reversed polarity within Gilbert Chron. At 323.3 mbsf (Section 190-1178A-35X-6, 100 cm), a normal inclination was clearly observed. This normal inclination is tentatively identified as the beginning of Chron C3A (5.894 Ma). A second normal polarity interval was observed at 353.50 mbsf (Section 190-1178A-39X-1, 30 cm) and may be correlated with the normal event at the beginning Chron C3B (6.935 Ma).

At the bottom of Hole 1178A, steep negative inclinations were seen. A short normal polarity interval from 405.42 mbsf (Section 190-1178A-44X-4, 40 cm) to 408.94 mbsf (Section 44X-CC, 5 cm) was also observed. Based on biostratigraphic results, these steep reversed and normal polarity inclinations may reflect the long reversed polarity period within Chron C4 considered to be Subchron C4r (8.072–8.699 Ma). Therefore, this short normal polarity interval may be the Subchron C4r.1n (8.225–8.257 Ma). This polarity identification suggests the existence of a hiatus at ~400 mbsf.

## **Hole 1178B**

The magnetic inclinations of Hole 1178B show continuous steep negative values from the top to bottom of the hole except for some short neutral polarities (Fig. F19). Biostratigraphy results suggest that all reversed polarity inclinations may correspond to Subchron C4r (8.072–8.699 Ma). However, more detailed investigations such as rock magnetic tests are needed to verify these results.

# **INORGANIC GEOCHEMISTRY**

## **Introduction**

Two holes were drilled at Site 1178. Fifty-six pore fluid samples were squeezed from selected 10- to 50-cm-long whole-round samples for chemical and isotopic analyses from Holes 1178A and 1178B. Hole 1178A sample depths ranged from 1.4 to 408.0 mbsf, and Hole 1178B

sample depths ranged from 397.5 to 638 mbsf. Samples were collected from every Hole 1178A core except for Cores 190-1178A-10X, 30X, and 39X because of poor recovery. Samples were collected from every Hole 1178B core from Core 190-1178B-2R to 13R, except for Cores 8R and 11R because of low recovery. From Core 190-1178B-13R to 27R, samples were collected from every second or third core because of the low pore-water recovery and long squeezing times required. Pore fluid recovery from Cores 190-1178B-24R through 27R was <0.5 mL after long squeezing times; therefore, no deeper whole-round samples were squeezed from the bottom of this hole.

Elemental concentrations are reported in Table T12 and plotted as a function of depth in Figure F22. Because of time constraints, seven, instead of nine, major and minor dissolved anions and cations that sensitively reflect inorganic or microbially mediated water-rock reactions were determined for each sample with >10 mL recovered pore fluid from this site. The anions are Cl, Ca, Mg, and Si, and the cations are sulfate, alkalinity, and ammonium. K and Na concentrations will be determined at a shore-based laboratory. The smaller volume samples were not analyzed for Si, alkalinity, and ammonium. Salinity and pH were also determined.

The outstanding characteristics of the pore fluid concentration-depth profiles at Site 1178 are the variability in Cl concentrations superimposed on an overall continuous trend of Cl dilution with depth relative to seawater composition. Both features, the continuous dilution and sharp concentration variabilities, reflect the inhomogeneous distribution of gas hydrate in these sediments. The Ca and Mg profiles indicate that they are coupled at some depth intervals but decoupled at others. The sulfate-containing interval is much thicker than at any of the other sites drilled during Leg 190. It spans more than ~30 m. All other microbial reaction products also are produced at greater depths at this site. Alkalinity and ammonium maxima occur between 100 and 200 mbsf. Unlike at Sites 1175 and 1176, despite the rather low temperature gradient, both carbonate and silicate diagenetic reactions significantly imprint the pore fluid chemistry. Also, similar to the deep-water sites but unlike the other two shallow-water sites, the shallow increase in Cl is consistent with diffusion of lower-chlorinity interglacial water into the sediment. At this shallow site, sedimentation rates at the top of the section are considerably lower than at Sites 1175 and 1176 (see “Biostratigraphy,” p. 11); therefore, the glacial signal (although partially depleted by diffusion) is clearly seen.

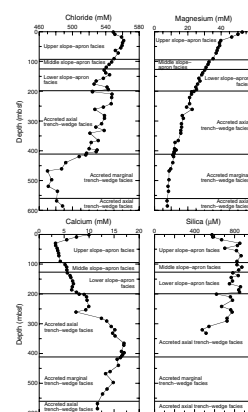
## Geochemistry Controlled by Inorganic Reactions

### Chloride

Cl concentrations were determined with a relative analytical uncertainty of 0.1% based on duplicate to quadruplicate titrations of all samples. Chloride concentrations increase in the top 32 mbsf to 562 mM. This is consistent with diffusion of lower chlorinity interglacial seawater into the sediment. At this site, volcanic ash is insignificant in this depth interval, and therefore ash hydration cannot be responsible for the observed increase. Below this maximum and throughout most of the rest of the section, between ~35 and ~500 mbsf, Cl exhibits a continuous trend of freshening with depth; the trend is steeper between 90 and 200 mbsf. Superimposed on this background Cl dilution profile are numerous smaller Cl minima produced by in situ dissociation of dis-

T12. Pore fluid composition, p. 98.

F22. Pore fluid composition as a function of depth, p. 50.



seminated gas hydrate that occurs during core recovery operation (see “Gas Hydrates” immediately below).

### **Gas Hydrates**

Although no solid gas hydrate was recovered during Leg 190, its presence was documented indirectly. Both temperature measurements of cores on the catwalk and pore fluid Cl concentrations indicate the existence of gas hydrates at two slope sites, Sites 1176 and 1178. Gas hydrate dissociates upon recovery, as its stability depends exponentially on temperature and linearly on pressure. Recovery of solid hydrate is unlikely unless it is abundant or specialized equipment is used. As a result, mainly massive hydrates have been recovered in the drilling program.

Sites 1176 and 1178 are within the stability field of seawater–methane hydrate from the seafloor to the BSR. Because methane is the dominant gas in the sediments at these sites, any gas hydrate present should be primarily methane hydrate as it is at other nonthermogenic oceanic sites. Dissociation of methane hydrate is a highly endothermic reaction; therefore, its decomposition consumes heat and cools the sediment. At Site 1176, temperatures colder than background by 4°–5°C between ~220 and 240 mbsf were measured in two cores (190-1176A-25X and 26X). Because of no or poor core recovery, there are no data for the 240–320 mbsf interval. Pore fluid Cl concentrations suggest minor addition of water, ~1% beyond other dilution processes.

At Site 1178, gas hydrate is considerably more abundant than at Site 1176. Based on pore fluid Cl concentrations, methane hydrate (inferred from gas composition) is present between ~120 and 400 mbsf, with highest concentrations between 150 and 200 mbsf. At ~200 mbsf, in Core 190-1178A-23X, the lowest catwalk core temperature of –0.5°C was measured. Temperatures colder than background by 4°–6°C were measured in several cores, mostly between 150 and 200 mbsf.

The Cl concentration–depth profile has a steep continuous trend of freshening between 90 and 200 mbsf with two intense Cl minima. One minimum is present at 170–185 mbsf; the second, with the lowest Cl value of 524 mM compared with bottom-water value of 557 mM, was measured in Core 190-1178A-23X ( $T = -0.5^{\circ}\text{C}$ ), which corresponds to >6% dilution by methane hydrate dissociation. The background dilution throughout the 150–200 mbsf interval is 3%. Between 200 and 400 mbsf, Cl concentrations continue to gradually decrease with depth from 545 to a minimum of 517 mM at the BSR depth, which corresponds to >7% dilution. Superimposed on the background Cl dilution profile are numerous smaller Cl minima. This indicates that throughout the sediment section (90–400 mbsf), disseminated gas hydrate is present and is responsible for the background 3%–4% Cl dilution and that specific sediment horizons, probably the coarsest-grained ones, have higher hydrate concentrations, equivalent to 6%–7% Cl dilution. Concentration–depth profiles of other components, specifically Si and Ca, show similar fluctuations in concentration with depth, supporting the conclusion that they have a common origin of dilution by methane hydrate dissociation.

Cl concentrations sharply decrease below the BSR depth and reach a minimum of 470 mM, almost a 16% dilution, centered at ~500 mbsf. The origin of this low-Cl zone is as yet unclear. It may represent a more methane hydrate-rich paleo-BSR that has not had enough time to dissipate the dilution signal caused by dissociation of the hydrate. Consistent with this scenario, higher methane concentrations are found at

this depth. Sedimentation and/or tectonics could have caused such an upward migration of the BSR.

### **Silica**

Dissolved Si concentrations increase steeply with depth in the top 35 m and below, and although variable, they remain almost constant at  $800 \pm 50 \mu\text{M}$  to ~200 mbsf. In this depth interval, diatoms are abundant. Despite their abundance, Si concentrations are slightly lower than the opal-A solubility value. This may be because competing reactions consume Si released by diatom dissolution or because the opal-A dissolution rate is slower than the Si diffusion rate. This becomes important where sedimentation rates are slow to medium. At greater depth, where diatoms and sponge spicules are present but less abundant and not very well preserved, Si concentrations gradually decrease with depth. A sharp decrease in Si concentrations is observed at ~300 mbsf, where diatoms steeply disappear with depth (see "**Biostratigraphy**," p. 11). Because of the low volumes of pore fluid recovered below this depth and the disappearance of biogenic Si remains, the deeper part of this sediment section was not analyzed for Si.

### **Calcium and Magnesium**

Ca and Mg concentrations steeply decrease with depth in the top ~35 mbsf, the sulfate-containing zone. Ca decreases by ~7.5 mM from seawater concentration to 3.3 mM, whereas Mg concentrations decrease by ~15 mM from seawater concentration to 39 mM. Because the Ca/Mg molar ratio in dolomite is 1, it is clear that Mg is intensely involved in more than one diagenetic reaction at this depth interval. One reaction is authigenic dolomite precipitation; the other is either dolomitization of a calcite precursor and/or involvement in a silicate reaction. Alkalinity increases sharply in this depth interval, promoting carbonate diagenesis. Between ~35 mbsf and the depth of the BSR, Ca and Mg have an inverse relationship, suggesting either dolomitization of calcite or involvement in silicate reactions. The former is probably less important because of the low abundance of biogenic calcite in this section (2–5 wt%) (see "**Organic Geochemistry**," p. 19). The most common silicate reactions that increase Ca concentrations above seawater concentrations are volcanic ash dissolution and alteration. Simultaneously, a Mg-rich clay may form. At the present prevailing low temperatures, because of the moderate geothermal gradient (~4°C/100 m), the formation of an authigenic clay mineral must be extremely slow. Thus, dissolution of volcanic ash and Mg clay formation are likely decoupled reactions. The Mg diffusional profile suggests a sink at great depth, whereas the Ca profile indicates a sink at the depth of the BSR. The possibility of a linkage between the BSR depth and carbonate diagenesis is intriguing; if correct, the involved reactions are most probably linked with bacterial activity.

## **Geochemistry Controlled by Microbially Mediated Reactions**

### **Alkalinity**

Alkalinity steeply increases in the sulfate-containing zone to ~20 mM and then remains approximately constant to a depth of ~200 mbsf, sug-

gesting involvement in carbonate reactions. Below, it decreases monotonically with depth and reaches seawater concentrations at ~500 mbsf. This suggests a sink at greater depth, probably a common sink with Mg.

### Ammonium

Ammonium produced by bacterially mediated decomposition of organic matter increases in concentration to 12 mM at ~200 mbsf. Because of the few data points below this depth, ammonium's behavior is unclear; most likely it has a sink as at all the other sites. Because K and Na data are as yet unavailable and Mg is involved in more than one reaction, the ion exchange influence is less clear.

### Sulfate

Sulfate concentration reaches zero at ~35 mbsf and remains practically zero throughout the section. At this anaerobic condition, magnetite would become unstable and weaken the sediment magnetic properties at depth.

## ORGANIC GEOCHEMISTRY

Site 1178 is an upper slope location drilled to evaluate the chemical, physical, and structural characteristics of an older portion of the accretionary prism and possibly to sample gas hydrates. Monitoring of volatile hydrocarbons was conducted for safety reasons, and organic, petrological, and geochemical studies were carried out to assess the types of organic matter and the molecular compositions of the hydrocarbons found in the sediments.

A total of 75 sediment samples were collected at Site 1178 from Holes 1178A and 1178B (at ~10-m intervals) from 1.5 to 669.0 mbsf. All sediments were analyzed for their methane concentrations and light hydrocarbon compositions during headspace analyses (Table T13). In addition, molecular gas compositions, total organic carbon (TOC), inorganic carbon (carbonate), and sulfur analyses were performed (Table T14) (see "Organic Geochemistry," p. 14, in the "Explanatory Notes" chapter for analytical procedures).

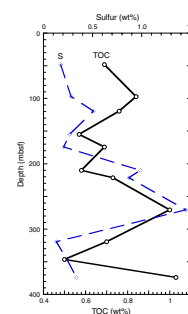
The TOC contents of the sediment samples examined at Site 1178 ranged from 0.57 to 1.03 wt% over the first 383.6 mbsf, with an average value of 0.73 wt% (Fig. F23). The high TOC values reflect a more mature sedimentary package and a mixture of mostly marine and some terrestrial matter (wood pieces) in this interval and range from 0.24 to 1.45 wt% with the highest values found at 200 and 350 mbsf, coincident with the highest TOC values.

The inorganic carbon values were generally low at Site 1178, with a few scattered values that ranged between 0.04 and 2.74 wt%. Thus, the bulk carbonate values were also low (1.46–5.00 wt%), except for a few samples that varied from 8.08 to 22.81 wt%, with an overall average concentration of carbonate in the sediments of ~5 wt%. In general, carbonate contents were confined to very thin layers throughout the hole with the higher carbonate concentrations found over the first 90 mbsf in the upper slope–apron facies (Subunit 1A). Because Site 1178 was the last site drilled during Leg 190, TOC, sulfur, and bulk carbonate analyses of the lower 300 mbsf were not performed.

T13. Headspace gas and vacutainer analysis, p. 99.

T14. Carbon, nitrogen, sulfur, and hydrogen analyses, p. 101.

F23. Total organic carbon (TOC) and sulfur concentrations, p. 52.



## Hydrocarbon Gases

Headspace gas concentrations of methane were moderate to low (thousands of parts per million) throughout Hole 1178A with low concentrations in the first 20 mbsf (the sulfate-reducing zone) followed by an abrupt increase in methane concentration (1152 to ~16,000 ppm) over the next 100 mbsf. Below, concentrations decrease sharply to ~1000 ppm and remain in that range to total depth. Some higher concentrations (~10,000 ppm range) were measured throughout Hole 1178A; however, the average concentration was a few thousand parts per million and remained in this range into Hole 1178B to the base of the hole at 669 mbsf.

The moderate to low concentrations of methane throughout Holes 1178A and 1178B are attributed to the elevated concentrations of light hydrocarbons from ethane to hexane, indicative of older, more mature organic matter within the sediments (diagenesis) or migration (thermogenesis) of hydrocarbons from greater depths. Ethane and propane are present in most of the sediment samples measured, increasing in concentration with depth ( $C_2 = 0\text{--}118$  ppm;  $C_3 = 0\text{--}121.5$  ppm), also consistent with an increase in maturity. Propane concentrations are higher than ethane concentrations from 250 to 408 mbsf in Hole 1178A, which may be attributed to diffusive migration of ethane from the sediments or to preferential removal of ethane from sediments by microbial processes. In Hole 1178B, the ethane to propane ratios decrease with depth and ethane exceeds propane in sediment samples from 566 to total depth at 669 mbsf, consistent with production of these hydrocarbons in more mature sediments.

The same low ethane/high propane concentrations were also observed in the shallower sediments at Sites 808 during Leg 131 (Taira et al., 1991) and at Site 1174 (see “[Organic Geochemistry](#),” p. 24 in the “Site 1174” chapter). Carbon isotopic studies of ethane in sediments from Site 808 did not display significant isotopic changes in sediments from shallower and deeper (below the décollement) depths, indicating that low concentrations of ethane can not be explained by diffusion (Berner and Faber, 1993). It was concluded that ethane and propane in these sediments were likely generated from isotopically different precursors within the kerogen (i.e., terrigenous vs. marine) in the sediments. A more complete assessment of the organic matter in both Sites 1178 and 1174 sediments is needed to address these unusual concentration ratios for ethane and propane that appear to be consistent throughout the sites drilled in the Nankai accretionary system.

## Light Hydrocarbons

Site 1178 is the only location drilled during Leg 190 that had significant levels of light hydrocarbons heavier than propane. Normal butane and pentane concentrations are low in Hole 1178A sediments (0.5–7 ppm) but increase with depth in Hole 1178B sediments with concentrations up to 18.3 ppm for butane and 13.7 ppm for pentane. Isobutane and isopentane concentrations display a similar trend with values up to 13.7 and 16.7 ppm, respectively, at 566 mbsf, whereas normal hexane and isohexane concentrations are generally low (0–2 ppm). Overall, concentrations of  $C_2\text{--}C_6$  hydrocarbons reflect the thermal evolution of the sedimentary organic matter at Site 1178. Since the formation reactions for lighter hydrocarbons are strongly temperature dependent, concentration and isotopic variations of these gases are sensitive indica-

tors of the thermal maturation of organic matter. Although diagenetic processes at low temperature could explain the presence of  $C_2$ – $C_6$  hydrocarbons, the unusual  $C_2/C_3$  ratios, especially in the upper 400 mbsf, coupled with increasing concentrations of butane and pentane with depth, suggest that some thermally produced hydrocarbons have migrated in and mixed with in situ biogenic hydrocarbons (mostly methane).

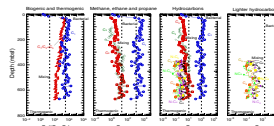
The Bernard ratios ( $C_1/[C_2+C_3]$ ) (Fig. F24) for hydrocarbons at Site 1178 also indicate that some contribution of the lighter hydrocarbons ( $C_2$ – $C_6$ ) in these sediments was produced from more mature organic matter present in situ mixed with thermogenic hydrocarbons that migrated from a more mature source at depth. Methane concentrations are constant throughout and are likely derived from biogenic or microbially mediated processes.  $C_4$ – $C_6$  plot exclusively in the thermogenic zone, again suggesting that these hydrocarbons formed in more mature sediments at higher temperature. The relatively low temperatures at Site 1178 ( $25^\circ$ – $40^\circ\text{C}$ ), coupled with the young age (early Miocene) of the sediments drilled, also support these conclusions. Moreover, unlike at any of the other sites drilled during Leg 190, significant faulting has been observed throughout the lower 300 m of Hole 1178B, which would facilitate fluid migration of more mature hydrocarbons from greater depths to shallower sediments.

## Conclusions

Organic geochemical analyses at Site 1178 lead to the following conclusions:

1. TOC contents for the sediment samples examined at Site 1178 ranged from 0.57 to 1.03 wt% over the first 383.6 mbsf with an average value of 0.73 wt%, the highest TOC values measured for Nankai sediments during Leg 190.
2. Sulfur concentrations track the TOC values in this interval and range from 0.24 to 1.45 wt% with the highest values found at 200 and 350 mbsf, coincident with the highest TOC values.
3. The moderate to low concentrations of methane throughout Holes 1178A and 1178B are attributed to the high concentrations of light hydrocarbons from  $C_2$  to  $C_6$ , indicative of older, more mature organic matter within the sediments (diagenesis) or migration (thermogenesis) of hydrocarbons from greater depths.
4. Propane concentrations are higher than ethane concentrations from 250 to 408 mbsf in Hole 1178A, consistent with results for these gases at Sites 1174 and 808. A more thorough assessment of the organic matter at these sites is needed to address the unusual ratios of ethane to propane that appear to be consistent throughout the sites drilled within the Nankai accretionary system.
5. Overall, the concentrations of light hydrocarbons ( $C_2$ – $C_6$ ) reflect the thermal evolution and maturity of the sedimentary organic matter at Site 1178.
6. The Bernard ratio ( $C_1/[C_2+C_3]$ ) for the hydrocarbons at Site 1178 also indicates some contribution of the lighter hydrocarbons ( $C_2$ – $C_6$ ) in these sediments from more mature organic matter

F24. Bernard ratios, p. 53.



present in situ mixed with themogenic hydrocarbons that have migrated in from a more mature source at depth.

- The significant faulting observed in the lower 300 m of Hole 1178B has facilitated fluid migration of more mature hydrocarbons buried from greater depths.

## MICROBIOLOGY

Thirty samples were obtained from Holes 1178A and 1178B for direct microscopic enumeration of bacteria on board ship. Seventeen whole-round cores were taken for shipboard enrichment cultures, cell viability, and shore-based microbiological analysis to measure potential bacterial activities, culture microorganisms, characterize nucleic acids, and investigate fatty acid biomarkers.

### Total Bacterial Enumeration

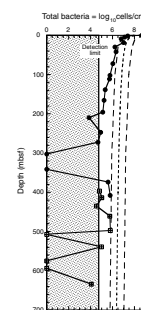
Bacteria are present in 23 of the samples (Table T15; Fig. F25), and populations are all below the general model for bacterial populations in deep-sea sediments (Parkes et al., 1994). The surface sample (Sample 190-1178A-1H-1, 0–1 cm) contains  $4.75 \times 10^8$  cells/cm<sup>3</sup>, which follows a general trend observed at other Ocean Drilling Program (ODP) sites where near-surface bacterial populations decrease as overlying water depths increase (Table T16). Populations rapidly decrease in the upper few meters, and from ~72 mbsf (Sample 190-1178A-9X-5, 149–150 cm) bacterial populations deviate significantly even from the lower prediction limit. This decrease steadily continues to 272 mbsf (Sample 190-1178A-30X-4, 149–150 cm) apart from a single datum at 210 mbsf (Sample 190-1178A-24X-1, 129–130 cm) where populations showed an additional significant decrease. This was a sample from the vicinity of a small amount of methane hydrate and consisted of cold, spongy, foaming sediment. Local reductions in bacterial populations around hydrates have been previously observed at Leg 146 sites (Cragg et al., 1995).

Bacteria were not detected at 302 or 341 mbsf (Samples 190-1178A-33X-5, 122–123 cm, and 37X-5, 124–125 cm) but return to relatively high concentrations ( $\sim 4 \times 10^5$  cells/cm<sup>3</sup>) between 374 and 408 mbsf (Samples 190-1178A-41X-2, 0–1 cm, and 44X-5, 124–125 cm). Although the overlap between Hole 1178A and 1178B shows differing bacterial abundance, the variability of these data indicate no significant difference. Between 396 and 498 mbsf (Samples 190-1178B-2R-2, 0–1 cm, to 190-1178A-13R-1, 112–113 cm) bacterial populations are present at, or just below, the lower prediction limit (Fig. F25). Overall, between these depths, they are present in greater numbers than between 166 and 272 mbsf (Samples 190-1178A-19X-3, 129–130 cm, to 190-1178A-30X-4, 149–150 cm). Below 500 mbsf, bacteria are either below detection or present in barely detectable numbers.

No correlation was observed with methane concentrations, which were low but relatively constant, averaging ~4100 ppmv throughout both Holes 1178A and 1178B. Between 72 and 120 mbsf, methane concentrations almost doubled to ~7500 ppmv (see “Organic Geochemistry,” p. 19). Nevertheless, this increase was not reflected in any change in bacterial abundance. The reasons for the unusually rapid decline in bacterial populations remain unclear.

T15. Total bacterial populations in sediments, p. 102.

F25. Depth distribution of total bacterial populations in sediment samples, p. 54.



T16. Comparison of surface sediment bacterial populations, p. 103.

## Contamination Tests

The chemical tracer test was conducted during APC, XCB, and RCB coring at this site (Cores 190-1178A-8H and 11X and 190-1178B-19R). The particulate tracer was used during XCB coring (Core 190-1178A-11X). In order to estimate the amount of drilling fluid intrusion into the recovered cores, chemical and particulate tracers were deployed as previously described (Smith et al., 2000).

### Chemical Tracer

Perfluoro(methylcyclohexane) was used as the perfluorocarbon tracer (PFT). Calibration of the gas chromatograph (HP 5890) with standard solutions yielded a slope of  $9.2 \times 10^{11}$  area units/gram of PFT. The detection limit for these samples was equivalent to 0.01  $\mu\text{L}$  of drilling fluid. The tracer was detected on the outer edge all of sections of core examined (Table T17). Because of the hardness of the sediment in Core 190-1178B-19R, the samples were not be taken with syringes. Instead, the outer edge of the core was pared away with a hammer and chisel. Estimates of drilling fluid intrusion into the interior of the cores range from below detection to 0.2–36  $\mu\text{L/g}$  for samples midway between the core liner and below detection to 0.86–0.07  $\mu\text{L/g}$  in samples collected in the center of the core (Table T17).

### Particulate Tracer

Fluorescent microspheres were detected on the outside of all three sections examined in Core 190-1178A-11X (Table T18). Microspheres were not observed in the center samples from any of the cores.

---

T17. Drilling fluid intrusion estimated based on PFT experiments, p. 104.

---

---

T18. Fluorescent microsphere tracer experiments, p. 105.

---

## PHYSICAL PROPERTIES

### Introduction

At Site 1178, laboratory measurements were made to provide a downhole profile of physical properties through slope-apron sediments and the upper portion of the accretionary complex. With the exception of short (<50 cm) and small-diameter sections, all cores were initially passed through the multisensor track (MST) before being split. Gamma-ray attenuation (GRA) and magnetic susceptibility measurements were taken at 4-cm intervals with 2-s acquisition times for all cores. Because of time constraints at this last site, *P*-wave velocity and natural gamma-ray (NGR) measurements were not made. Voids and cracking caused by gas expansion, noted in cores between the mudline and ~400 mbsf, degraded MST measurements. Biscuiting in XCB and RCB cores also degraded measurements.

In each full core, four samples were selected for index properties measurements from undisturbed core. Measurements of dry volume and wet and dry mass were uploaded to the Janus database and were used to calculate water content, bulk density, grain density, porosity, void ratio, and dry bulk density. *P*-wave velocities were measured on split cores or discrete samples at a frequency of two to three per core. Measurements were taken in three directions when core conditions permitted.

Shear strength measurements were made near the *P*-wave core measurement locations from between the mudline and 60 mbsf, at which point the cores became too stiff for insertion of the vane shear device. Electrical conductivity measurements were taken at least once per core. Raw data and calculated physical properties data are available from the Janus database for all MST, moisture and density, thermal conductivity, velocity, and shear strength measurements (see the “[Related Leg Data](#)” contents list). Because electrical conductivity data are not currently available from the database, they are included in Table T19.

## Density and Porosity

Sediment bulk density was determined by both the GRA method on unsplit cores and the mass/volume method (“index properties”) on discrete samples (see “[Physical Properties](#),” p. 19, in the “[Explanatory Notes](#)” chapter). The GRA density data and the bulk densities determined by the mass/volume method are in good agreement for APC and XCB cores (Fig. F26A, F26B). Both moisture and density measured on discrete samples and GRA density measurements show similar downhole trends. However, GRA densities exhibit considerable scatter and average GRA densities from APC cores are generally higher than core measurements, whereas those from XCB and RCB cores are generally lower than those measured on discrete samples.

Grain densities determined from dry mass and volume measurements are essentially constant throughout lithostratigraphic Subunit IA (upper slope–apron facies), with a mean value of 2.65 g/cm<sup>3</sup> (Fig. F26C). At the base of Subunit IA (94 mbsf), grain densities increase sharply to a mean value of 2.72 g/cm<sup>3</sup> and remain nearly constant to the base of the hole. Scatter in grain density values also increases below 94 mbsf (Fig. F26C).

Overall, porosity at Site 1178 is characterized by a typical compaction trend, decreasing gradually with depth from ~63%–70% at the mudline to 26%–35% at 672 mbsf. Porosity values within lithostratigraphic Subunits IB and IC (middle and lower slope–apron facies) are more scattered than within Subunit IA and Unit II. The increased scatter may be attributed to lithologic variations in this relatively sand-rich part of the section.

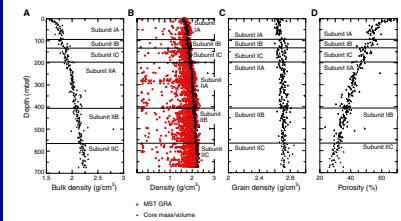
Deviations from the general compaction trend occur at 70–100 and 140–160 mbsf, where porosity increases. In general, the boundaries between lithostratigraphic units are not characterized by large changes in porosity (Fig. F26A, F26D), although the boundary between lithostratigraphic Units I and II at 199 mbsf does coincide with a short interval of slightly decreased porosity.

## Shear Strength

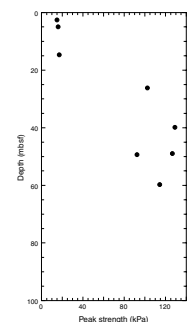
Undrained shear strength measurements were made using a miniature automated vane shear (AVS) and were conducted exclusively in fine-grained silty clays. Shear strengths increase gradually downhole from 15 kPa at the seafloor to values >130 kPa at 60 mbsf (Fig. F27). Scatter in the data reflects opening of fractures at the tips of the AVS vanes during some measurements. For this reason, actual sediment strength is probably best reflected by the highest measured values.

T19. Electrical conductivities and formation factor data obtained for cube samples, p. 106.

F26. Bulk density, grain density, and porosity, p. 55.



F27. Undrained peak shear strength, p. 56.



## Thermal Conductivity and Projected Temperatures

Thermal conductivity was measured using one of two methods, depending on core condition. For shallow, nonindurated samples, a needle probe was inserted into the unsplit core for a full-space conductivity measurement. Below 342 mbsf (Core 190-1178A-37X), insertion of the needle caused fracturing, so a half-space method was used on split cores. Half-space measurements were sparse because of lack of core pieces of sufficient size.

Within lithostratigraphic Subunit IA (upper slope-apron facies), thermal conductivity averages 1.1 W/(m·°C), which is slightly higher than seen at similar depths at other sites. A drop in thermal conductivity is observed at the bottom of this subunit. Between 100 and 340 mbsf, thermal conductivity averages 1.2 W/(m·°C) and does not show any distinct changes at lithologic or stratigraphic boundaries. Between 340 mbsf and the bottom of Hole 1178B, the limited measurements indicate values of 1.5 W/(m·°C) or greater.

A conductive heat flow of ~51 mW/m<sup>2</sup> was defined by shipboard thermal conductivity and downhole temperature measurements to ~115 mbsf (see “[In Situ Temperature and Pressure Measurements Section](#),” p. 26). Using this estimated heat flow and measured shipboard thermal conductivity, projected downhole temperatures reach ~20°C at 400 mbsf, the depth of the BSR, and ~25°C at the bottom of Hole 1178B (Fig. F28B).

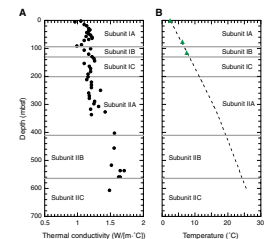
## Acoustic Velocity

In APC cores, *P*-wave velocities were measured using the *P*-wave sensors 1 and 2 (PWS1 and PWS2) insertion probe system along the core axis (*z*-axis) and across the core axis (*y*-axis), respectively. The PWS3 contact probe system was used to measure *P*-wave velocities across the liner (*x*-axis). In XCB cores, sample cubes were cut and measurements in all three directions were performed using the PWS3 contact probe system. Poor core quality in RCB cores prevented measurements in Cores 190-1178A-10X through 18X. Subsequent measurements were compromised by fissility, foliation, and fractures. Samples taken below 200 mbsf also exhibited high attenuation, which made determination of travel times difficult. Velocities generally increase with depth (Fig. F29) but display large scatter and some abnormally low values between 320 and 410 mbsf. The BSR lies near the base of this interval, at ~400 mbsf on the depth-converted seismic section.

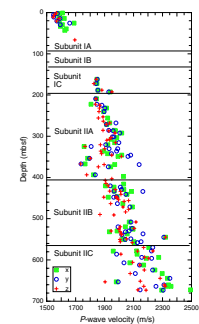
## Electrical Conductivity

Measurements were made on APC cores with a four-needle 30-kHz electrode array. On XCB cores, conductivity was measured on the same sample cubes used for *P*-wave measurements with a 30-kHz two-electrode system. Apparent formation factor measured on unsplit cores is given in Table T20. The electrical conductivity and formation factor measured on the sample cubes are given in Table T19. Values appear more scattered than at the other sites, most notably in the *z*-direction (Fig. F30A). Vertical anisotropy develops below 220 mbsf, but values are scattered in both the horizontal and vertical planes (Fig. F30B). Most sample cubes were cut relative to the core axis, but bedding dip was generally steeper than at the other sites, and zones of steep bedding dip were not confined to narrow intervals. Furthermore, a dipping folia-

F28. Thermal conductivity and temperature trends, p. 57.

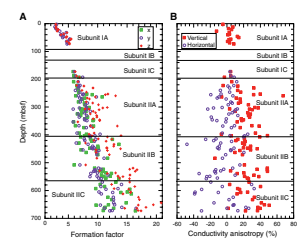


F29. *P*-wave velocity, p. 58.



T20. Formation factor data from the needle-probe method, p. 108.

F30. Formation factor and anisotropy of electrical conductivity, p. 59.



tion, often parallel to bedding, was observed in many cores (see “**Structural Geology**,” p. 9). These observations caused us to reconsider our sampling procedure, and subsequent samples (below 651.4 mbsf) were cut parallel to the foliation. Samples cubes cut parallel to foliation or bedding appear in italics in Table T19. These data have a higher and more consistent vertical anisotropy (where the vertical axis is considered to be perpendicular to foliation or bedding) of 35%–50% and a lower horizontal anisotropy. This suggests that changes in foliation and bedding dip may be partially responsible for the data scatter.

### Magnetic Susceptibility

Volumetric magnetic susceptibilities were measured on unsplit cores by the MST (Fig. F31). Uncorrected values of magnetic susceptibility from the Janus database were used. Magnetic susceptibility data show wide scatter in the uppermost 20 m. Between 20 and 80 mbsf, peaks of magnetic susceptibility data with values as high as  $120 \times 10^{-5}$  SI are observed. Between 80 and 190 mbsf, the magnetic susceptibility data show low scatter and almost constant values ( $20 \times 10^{-5}$  to  $40 \times 10^{-5}$  SI). Between 190 and 360 mbsf, magnetic susceptibilities slightly increase and many peaks (as high as  $170 \times 10^{-5}$  SI) exist. Below 360 mbsf, the scatter of magnetic susceptibility data increases. Values range from  $20 \times 10^{-5}$  to  $100 \times 10^{-5}$  SI between 520 and 560 mbsf. Between 560 mbsf and the bottom of Hole 1178B, magnetic susceptibility values show large scatter.

### Summary and Discussion

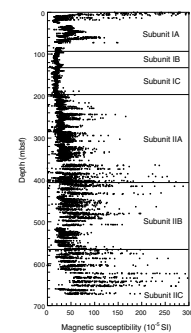
Porosities at Site 1178 decrease with depth, from values of 63%–70% at the mudline to 26%–35% at 672 mbsf. Deviations from this compaction trend occur at 70–100 mbsf, 140–160 mbsf, and ~200 mbsf. Porosity values within lithostratigraphic Subunits IB and IC are more scattered than in Subunit IA and Unit II and probably reflect either lithologic variations in this sandier part of the stratigraphic section or deposition by slope failure processes. Grain density increases abruptly at the boundary between the upper and middle slope-apron facies (94 mbsf). Velocities and formation factors generally increase with depth and show considerable scatter. In general, there are no obvious differences in physical properties between the slope-apron deposits of Unit I and the underlying accreted sediments of Unit II.

## IN SITU TEMPERATURE AND PRESSURE MEASUREMENTS

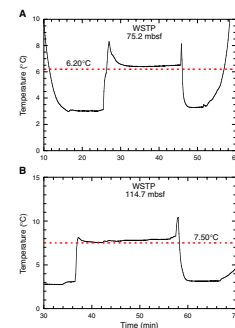
Two determinations of downhole temperatures were made at Site 1178 using the WSTP temperature tool. Runs were attempted with the Adara APC temperature tool and Davis-Villinger temperature probe but were not successful because of equipment failure. The temperature data are shown in Figure F32. In situ temperatures were estimated by extrapolation of the station data to correct for the frictional heating on penetration. Both records are noisy, and only the initial part of each curve could be used for the extrapolation.

The mudline temperature and the two measurements define a linear gradient of  $0.046^\circ\text{C}/\text{m}$  (Fig. F33). Thermal conductivities from core

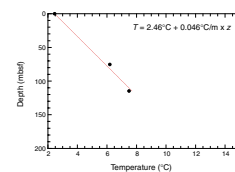
F31. Magnetic susceptibility, p. 60.



F32. Temperatures measured during the deployment of the WSTP temperature tool, p. 61.



F33. Temperature vs. depth, p. 62.



samples of the upper 106 m averaged  $1.1 \text{ W}/(\text{m}\cdot^{\circ}\text{C})$  (see “Physical Properties,” p. 23), indicating a vertical conductive heat flow of  $51 \text{ mW}/\text{m}^2$ .

## SEISMIC STRATIGRAPHY

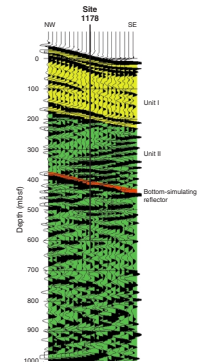
Reflections on three-dimensional (3-D) seismic line 278 can be correlated with lithostratigraphic boundaries at Site 1178 (Fig. F34). Specific correlations should be considered preliminary at this time because the velocity structure at this site is not well known. Any inaccuracies in velocity will produce errors in depth conversion. Additional velocity work will be carried out postcruise to improve depth conversions and stratigraphic correlations.

Lithostratigraphic Unit I is recognized on the seismic line as a sequence bounded at the top by the seafloor and at the bottom by an angular unconformity (Fig. F34) at  $\sim 200 \text{ mbsf}$ . The upper part of the unit has a thin seismic stratigraphic sequence that onlaps to the northwest. The lower part of the unit is characterized by discontinuous low-amplitude reflections that dip to the southeast. The strong unconformity at the base of the unit dips to the southeast.

Lithostratigraphic Unit II underlies the strong unconformity at  $200 \text{ mbsf}$ . The top of the unit is truncated by the unconformity. Reflections within the unit are moderate-amplitude and generally dip to the northwest, although dips are shallow downsection.

A strong bottom-simulating reflection crosses Unit II at  $\sim 400 \text{ mbsf}$  at Site 1178. It dips southeast and cuts across the northwest-dipping reflections of Unit II.

F34. Three-dimensional seismic reflection line 278, p. 63.



## REFERENCES

- Berner, U., and Faber, E., 1993. Light hydrocarbons in sediments of the Nankai Accretionary Prism (Leg 131, Site 808). *In* Hill, I.A., Taira, A., Firth, J.V., et al., *Proc. ODP, Sci. Results*, 131: College Station, TX (Ocean Drilling Program), 185–195.
- Cande, S.C., and Kent, D.V., 1995. Revised calibration of the geomagnetic polarity timescale for the Late Cretaceous and Cenozoic. *J. Geophys. Res.*, 100:6093–6095.
- Cragg, B.A., Parkes, R.J., Fry, J.C., Weightman, A.J., Rochelle, P.A., Maxwell, J.R., Kastner, M., Hovland, M., Whiticar, M.J., and Sample, J.C., 1995. The impact of fluid and gas venting on bacterial populations and processes in sediments from the Cascadia Margin accretionary system (Sites 888–892) and the geochemical consequences. *In* Carson, B., Westbrook, G.K., Musgrave, R.J., and Suess, E. (Eds.), *Proc. ODP, Sci. Results*, 146 (Pt 1): College Station, TX (Ocean Drilling Program), 399–411.
- Martini, E., 1971. Standard Tertiary and Quaternary calcareous nannoplankton zonation. *In* Farinacci, A. (Ed.), *Proc. 2<sup>nd</sup> Int. Conf. Planktonic Microfossils Roma*: Rome (Ed. Tecnosci.), 2:739–785.
- Parkes, R.J., Cragg, B.A., Bale, S.J., Getliff, J.M., Goodman, K., Rochelle, P.A., Fry, J.C., Weightman, A.J., and Harvey, S.M., 1994. A deep bacterial biosphere in Pacific Ocean sediments. *Nature*, 371:410–413.
- Shipboard Scientific Party, 1991. Site 808. *In* Taira, A., Hill, I., Firth, J.V., et al., *Proc. ODP, Init. Repts.*, 131: College Station, TX (Ocean Drilling Program), 71–269.
- Smith, D.C., Spivack, A.J., Fisk, M.R., Haveman, S.A., Staudigel, H., and ODP Leg 185 Scientific Party, 2000. Methods for quantifying potential microbial contamination during deep ocean coring. *ODP Tech. Note*, 28 [Online]. Available from World Wide Web: <<http://www-odp.tamu.edu/publications/tnotes/tn28/INDEX.HTM>>.
- Taira, A., Hill, I., Firth, J.V., et al., 1991. *Proc. ODP, Init. Repts.*, 131: College Station, TX (Ocean Drilling Program).
- Young, J.R., 1998. Neogene. *In* Bown, P.R. (Ed.), *Calcareous Nannofossil Biostratigraphy* (Vol. 8): Dordrecht (Kluwer Academic), 225–265.

Figure F1. Stratigraphic column for Site 1178, showing lithostratigraphic units, ages, and characteristic lithologies.

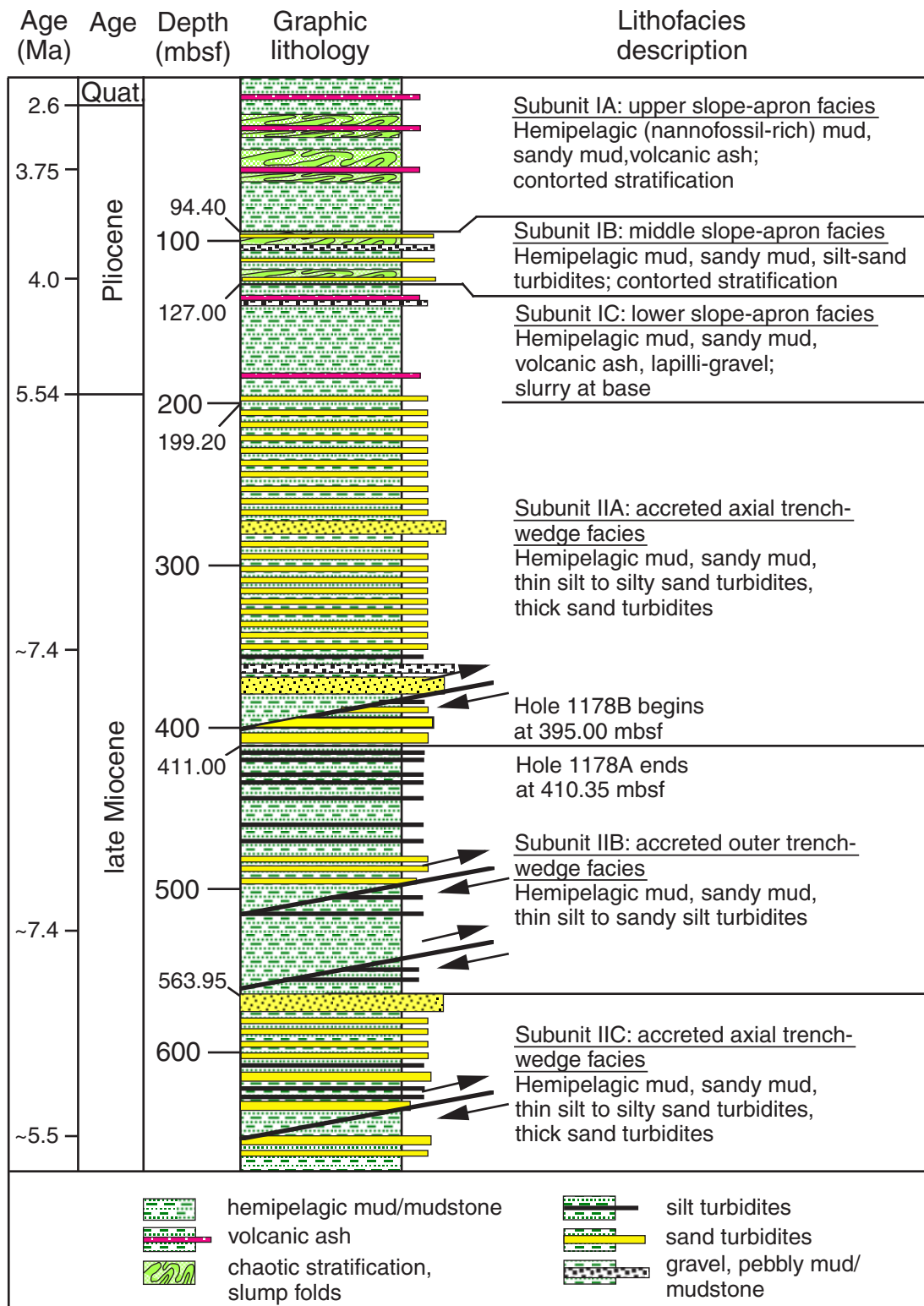


**Figure F2.** Graded volcanic ash layer from Subunit IA (interval 190-1178A-7H-1, 22–40 cm).

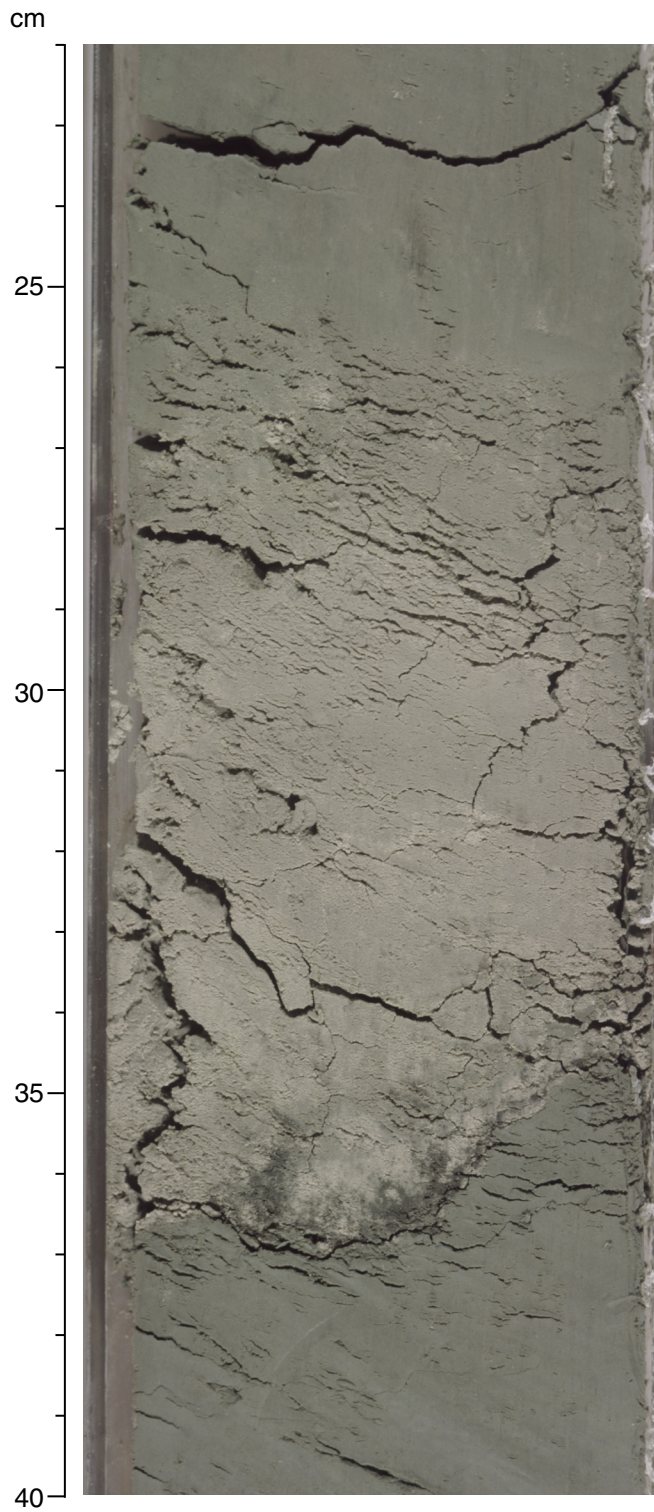


**Figure F3.** Inclined volcanic ash layer in a disturbed zone of Subunit IA (interval 190-1178A-6H-5, 60–80 cm).

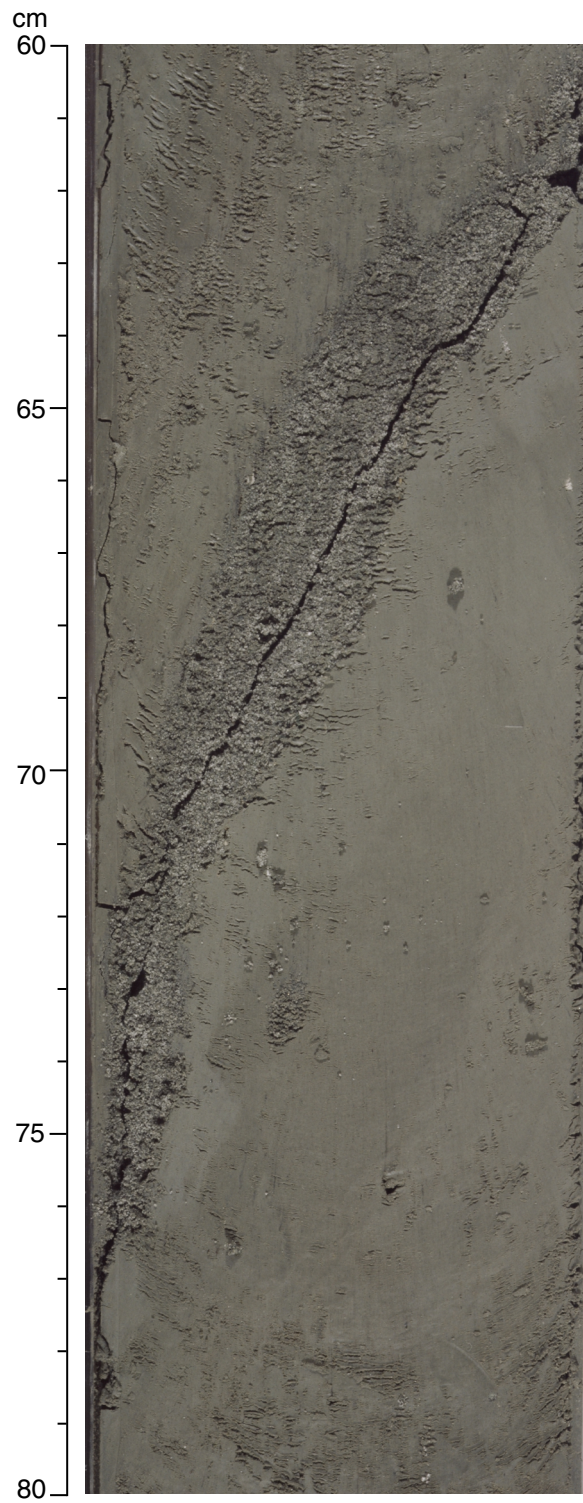
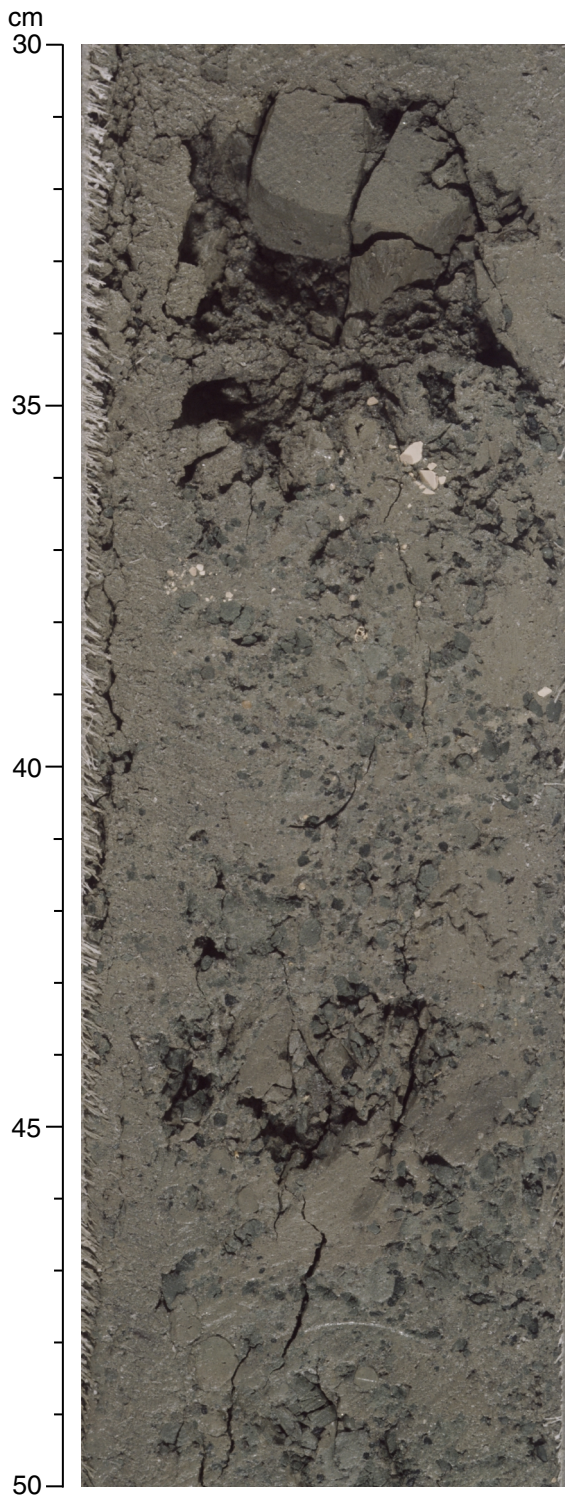


Figure F4. Mud-supported gravel with mud and shell fragments from Subunit IB (interval 190-1178A-13X-2, 30–50 cm).



**Figure F5.** Gravel with pumice fragments and mud clasts from Subunit IB (interval 190-1178A-14X-3, 10–40 cm).



Figure F6. Cross-lamination in a thin-bedded sandy turbidite from Subunit IIA (interval 190-1178A-35X-5, 20–30 cm).

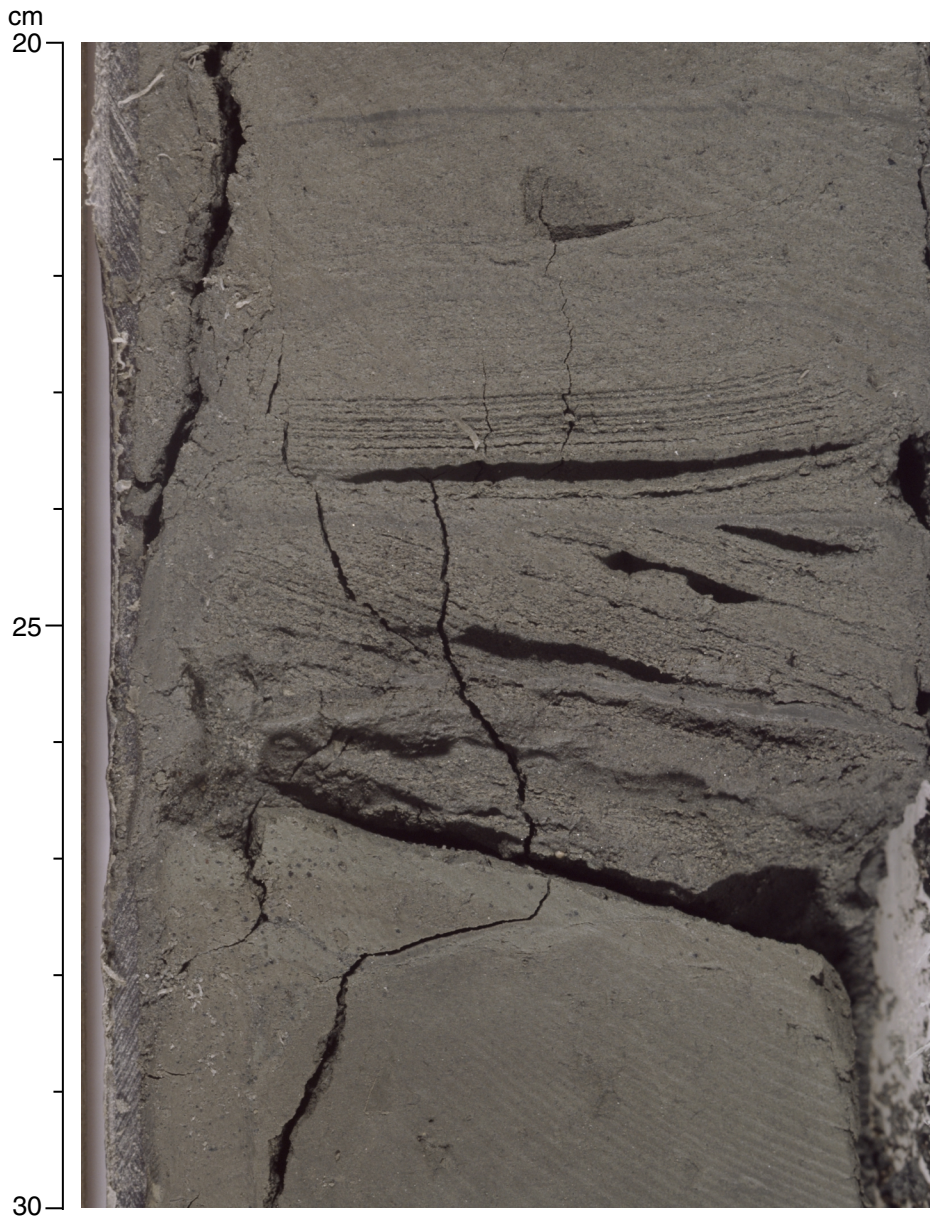
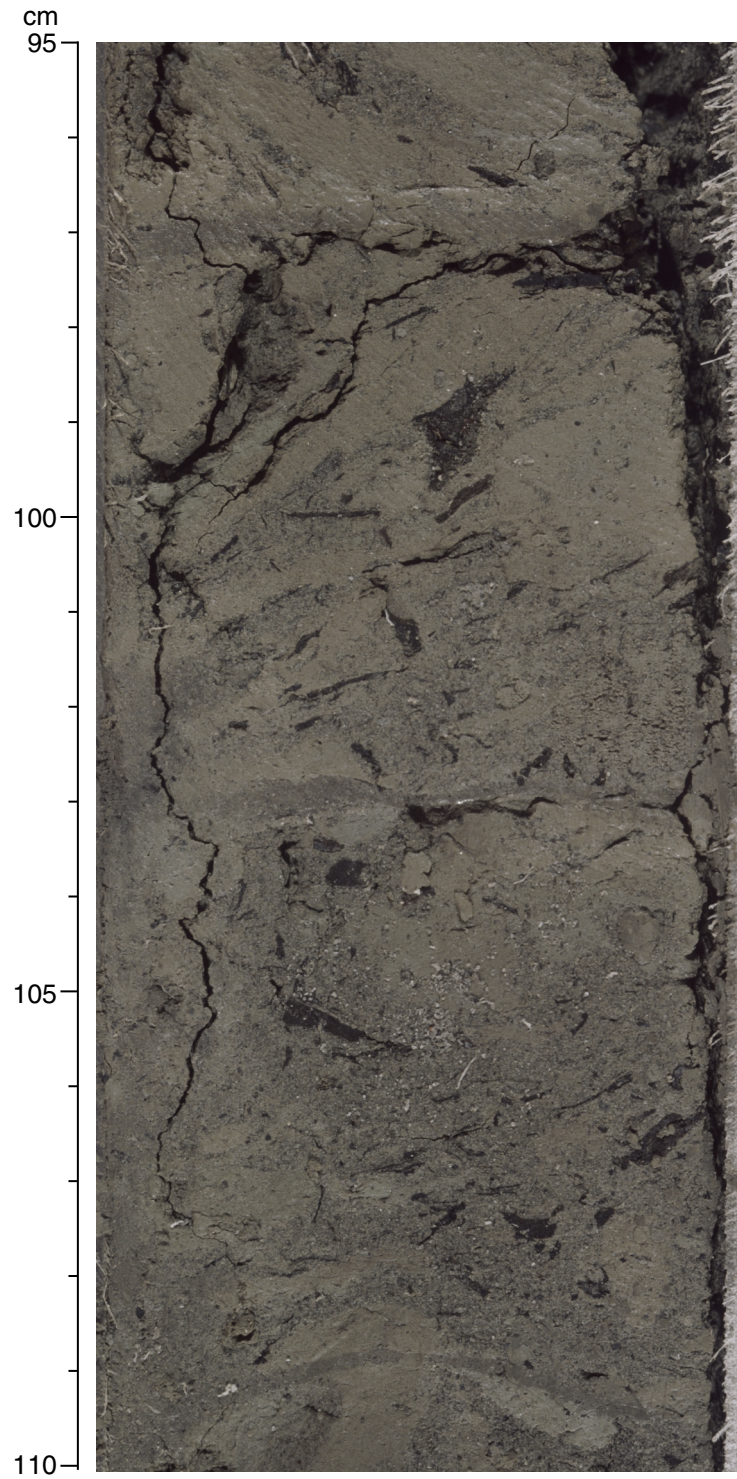
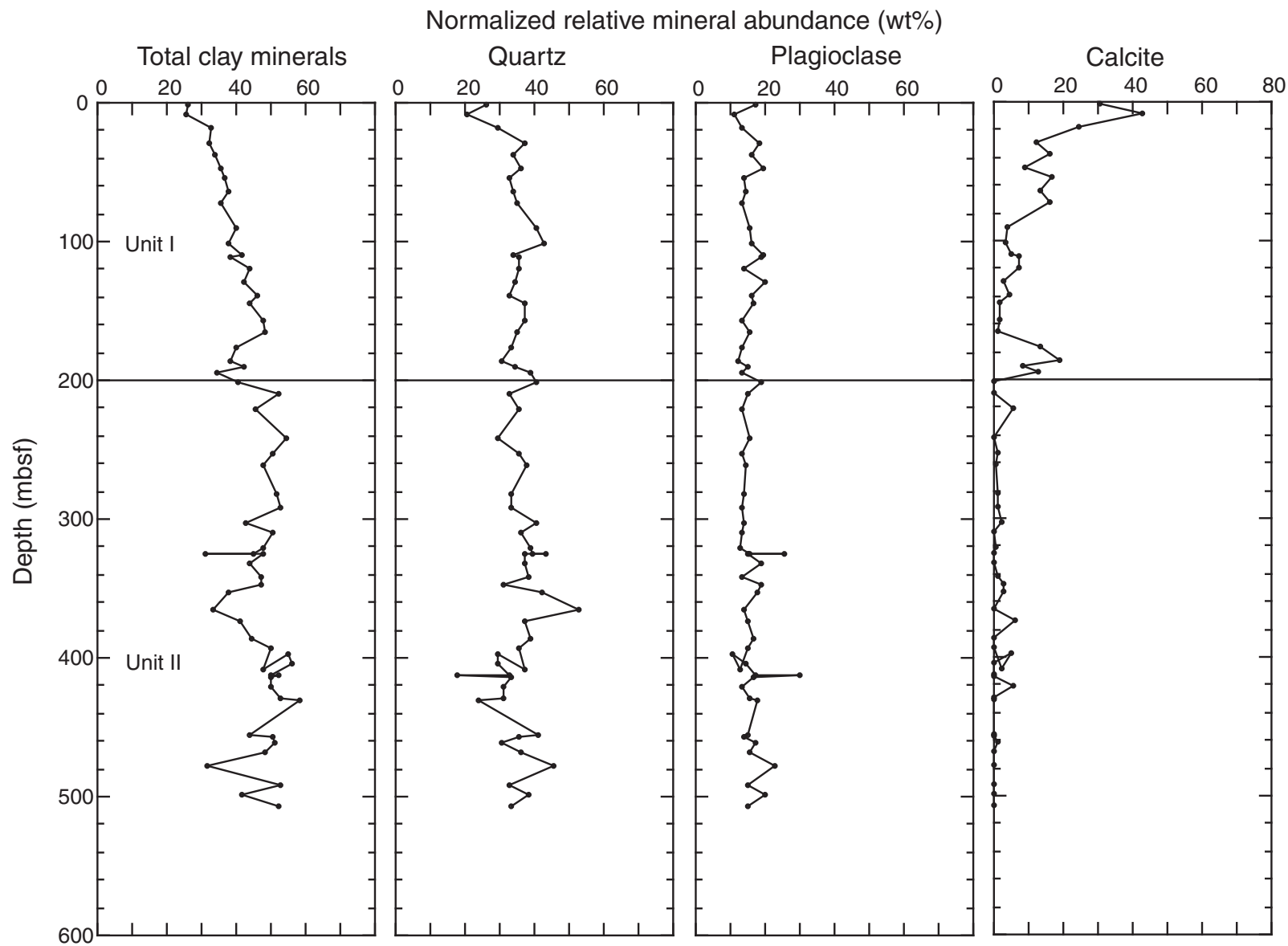


Figure F7. Silty sand with wood fragments from Subunit IIA (interval 190-1178A-41X-2, 95–110 cm).



**Figure F8.** Normalized relative abundances of total clay minerals, quartz, plagioclase, and calcite at Site 1178 based on X-ray diffraction analysis of random bulk-sediment powders.



**Figure F9.** Synopsis of deformation structures at Site 1178 presented as variation of dip angle with depth and showing the delineation of the four structural domains. **A.** Variation of bedding dip with depth. **B.** Variation of foliation dip with depth. **C.** Variation of fracture dip with depth. Note that the fault at 550 mbsf is partly defined by core fractures not depicted here because their orientation was not possible to measure.

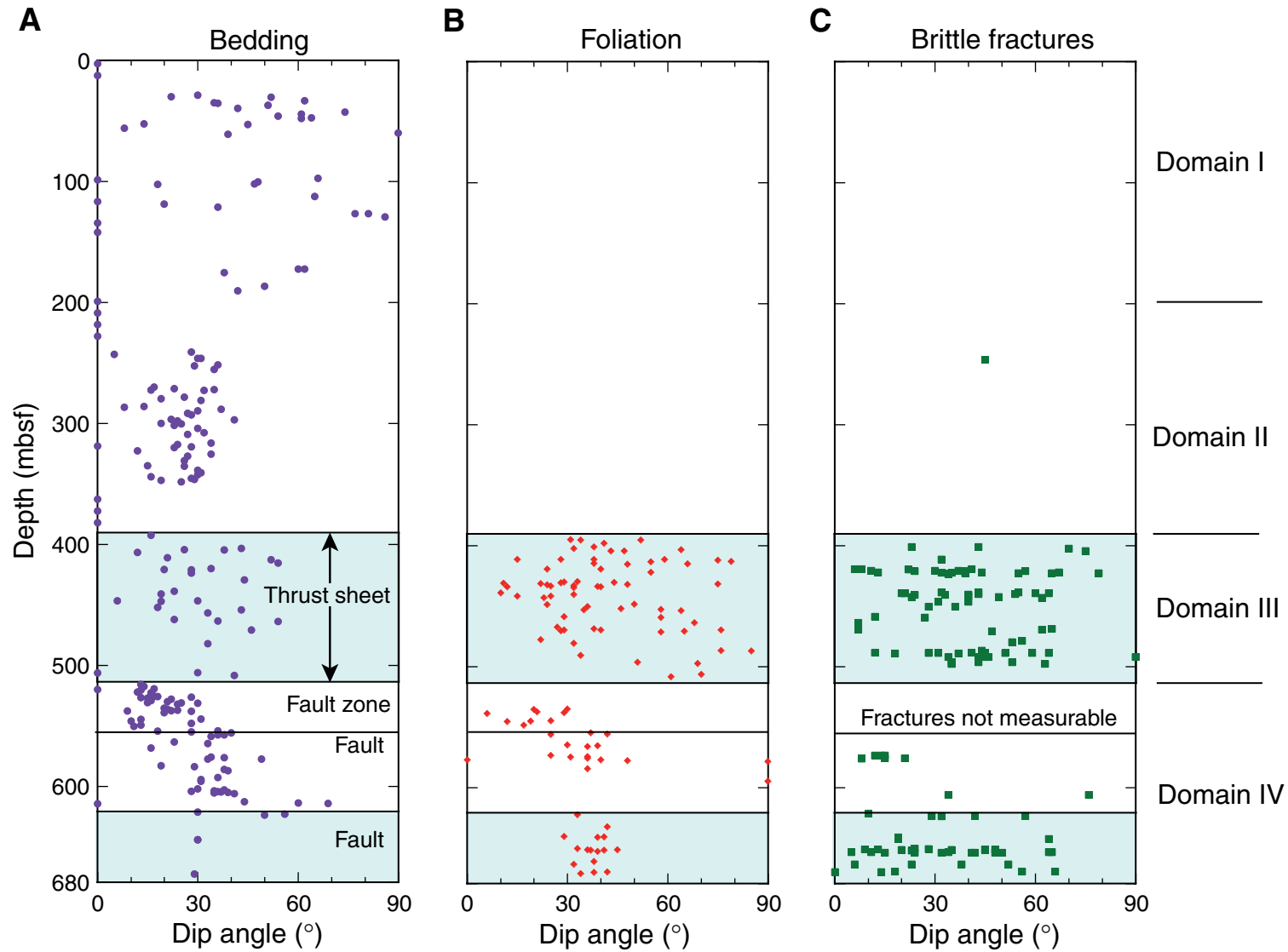


Figure F10. Equal-area lower-hemisphere stereographic projections of bedding in Hole 1178A. A. Domain I (above 200 mbsf), showing possible east-west orientation resulting from slump folding. B. Domain II (below 200 mbsf), showing a lack of preferred orientation.

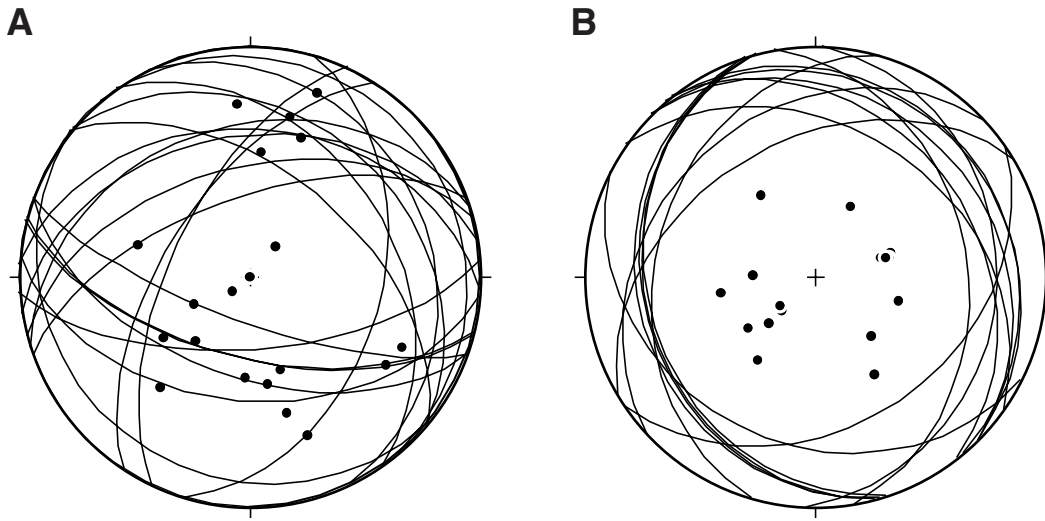


Figure F11. Incipient breccia with irregular fine black seams (interval 190-1178A-42X-4, 30–55 cm).

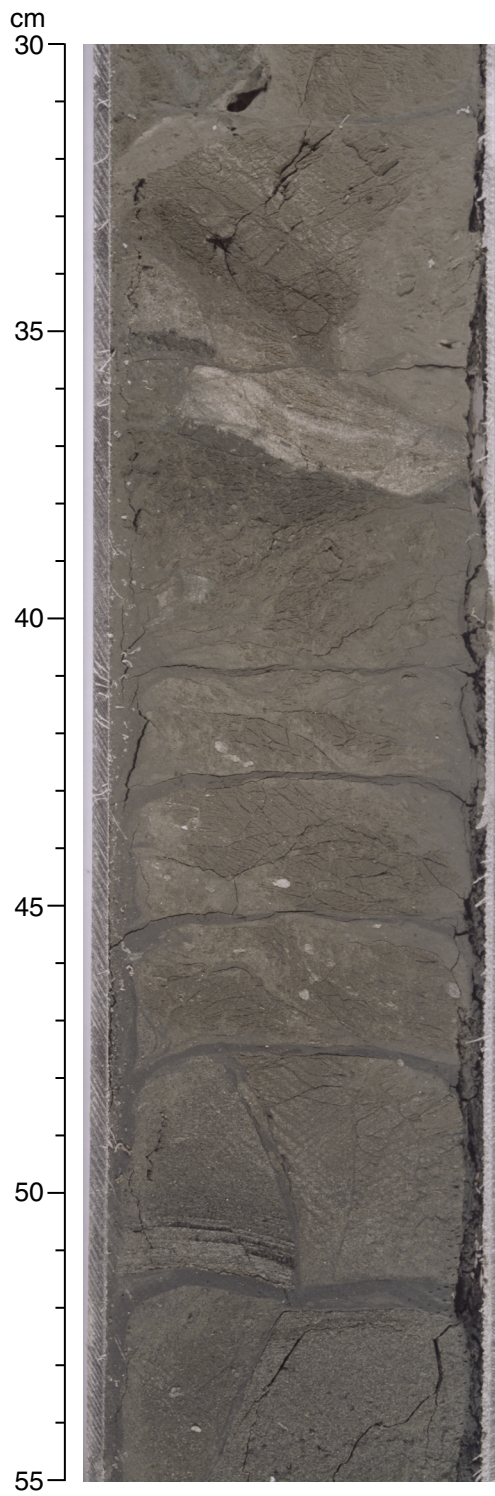
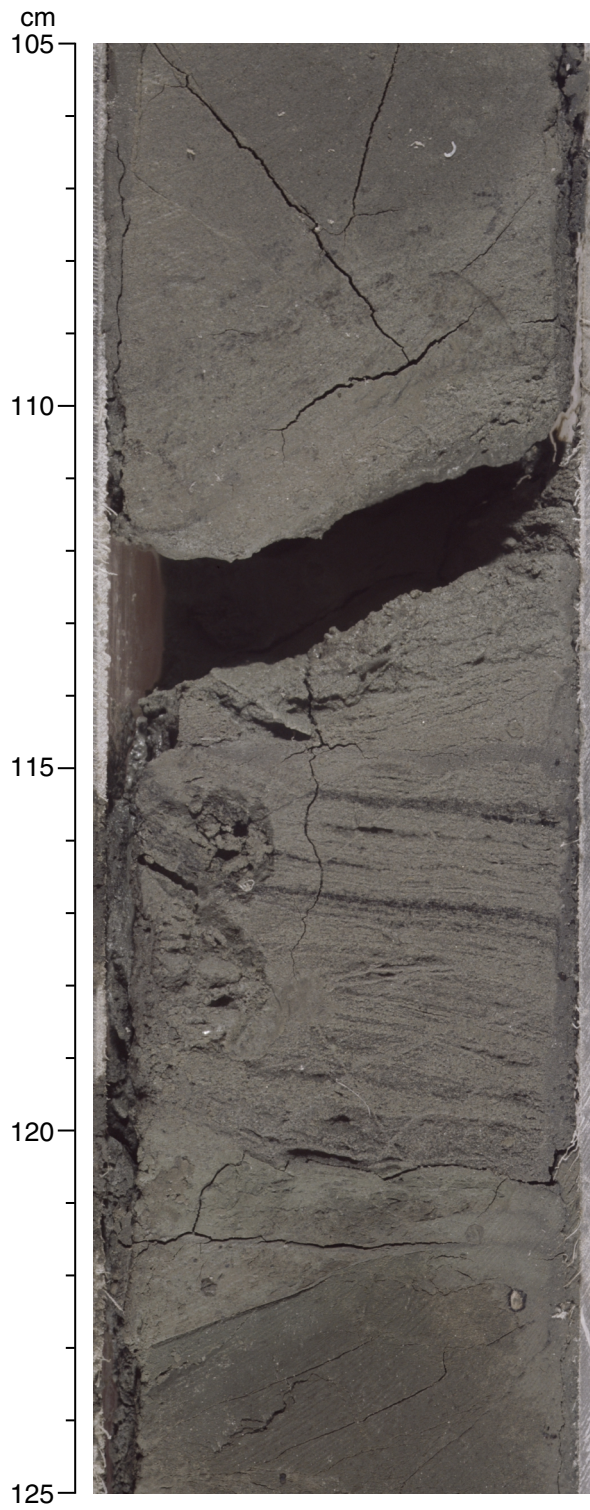
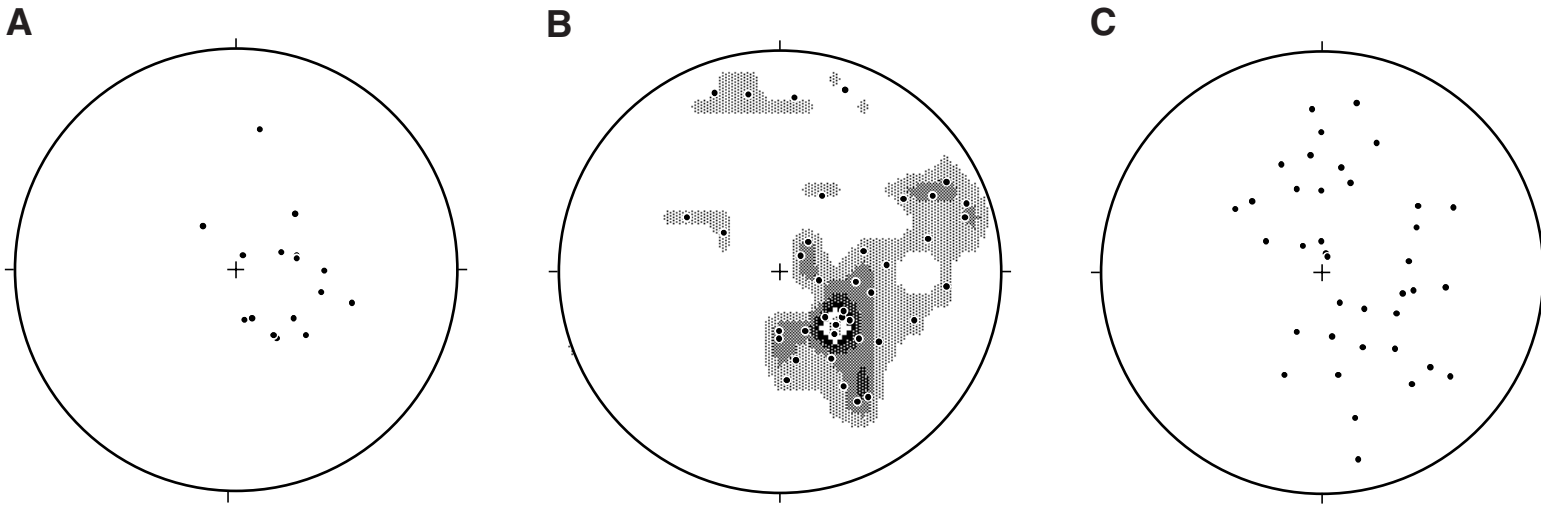


Figure F12. Incipient weblike structure in fine sand (interval 190-1178A-42X-3, 105–125 cm).



**Figure F13.** Equal-area lower-hemisphere stereographic projections of structural features in Domain III after paleomagnetic reorientation. **A.** Bedding. **B.** Foliation showing contour intervals. Number of points = 39, contour interval = 2.0%/1% area. **C.** Fractures.



**Figure F14.** Bedding-oblique foliation typical of Domain III (interval 190-1178B-9R-5, 5–27 cm). Steeply dipping bedding can be observed over intervals 5–10 cm and 22–27 cm, bounding an interval with lower-angle foliation.

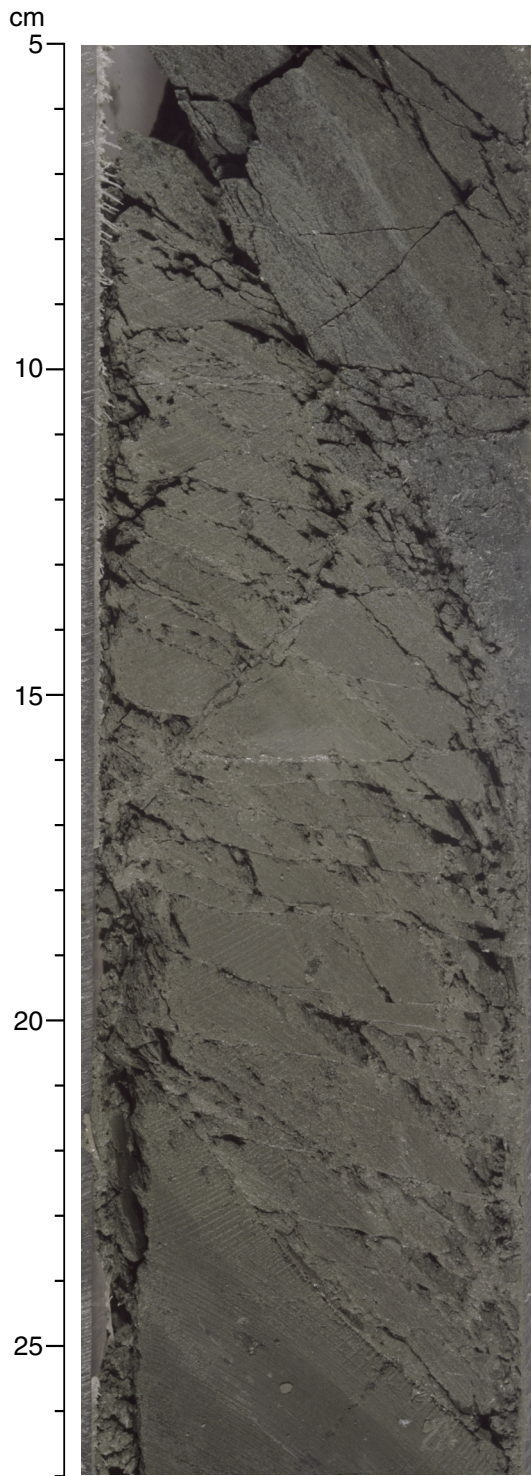
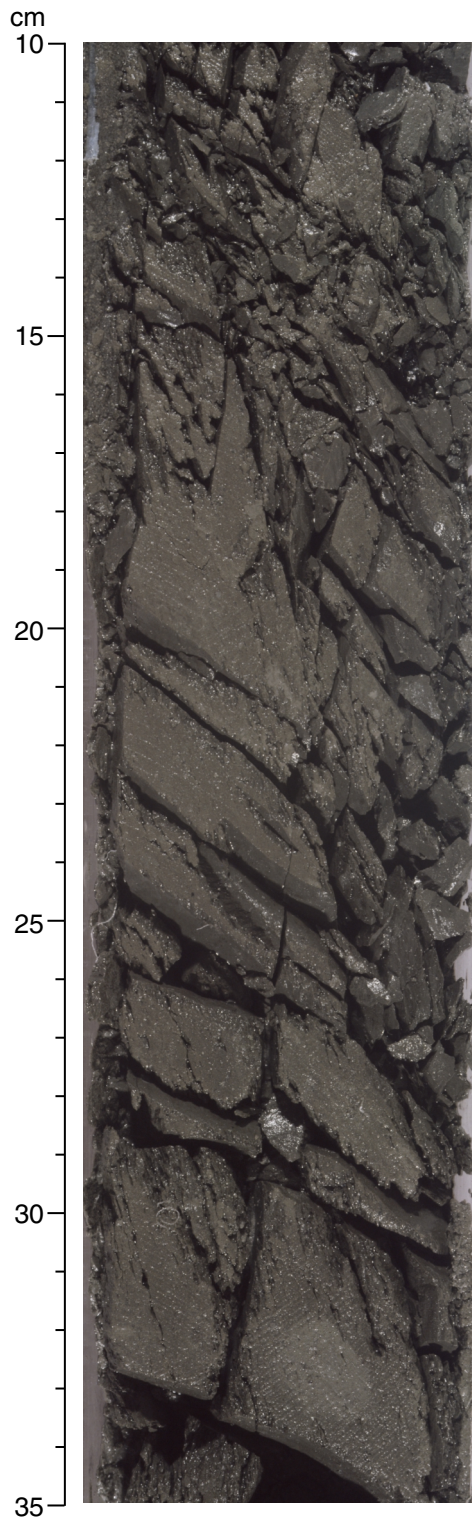


Figure F15. Trapezoidal fragments in breccia generated by oblique fracture sets (interval 190-1178B-12R-1, 10-35 cm).



**Figure F16.** Equal-area lower-hemisphere stereographic projections of structural features in Domain IV after paleomagnetic reorientation. **A.** Bedding showing contour intervals. Number of points = 47. Contour interval = 2.0%/1% area. **B.** Foliation. **C.** Fractures.

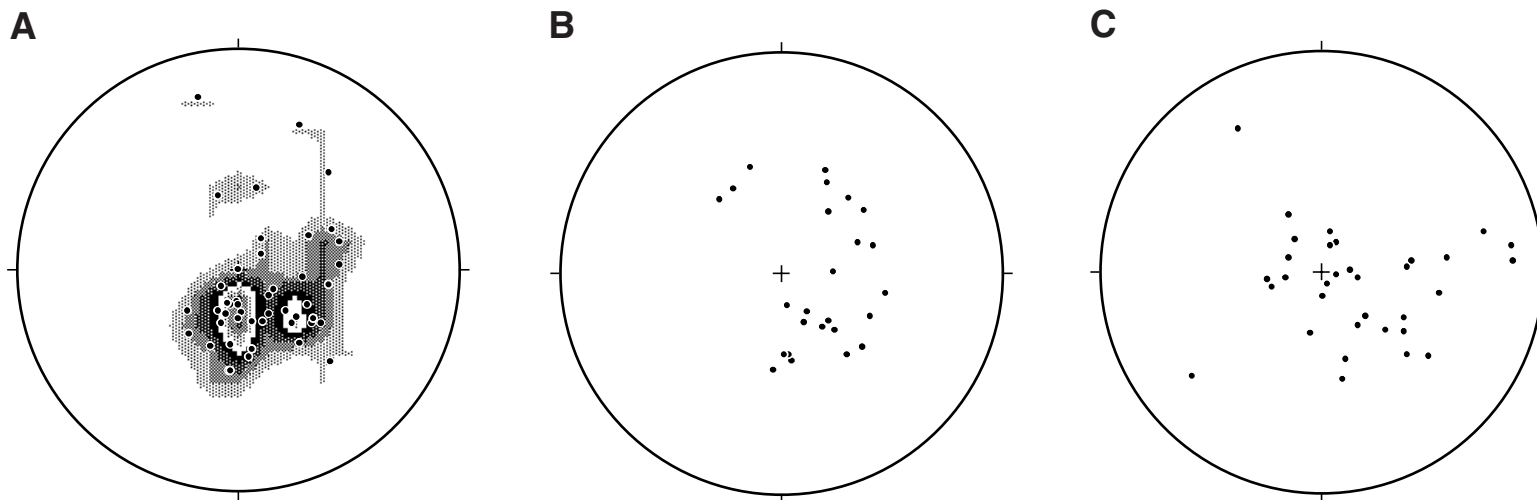
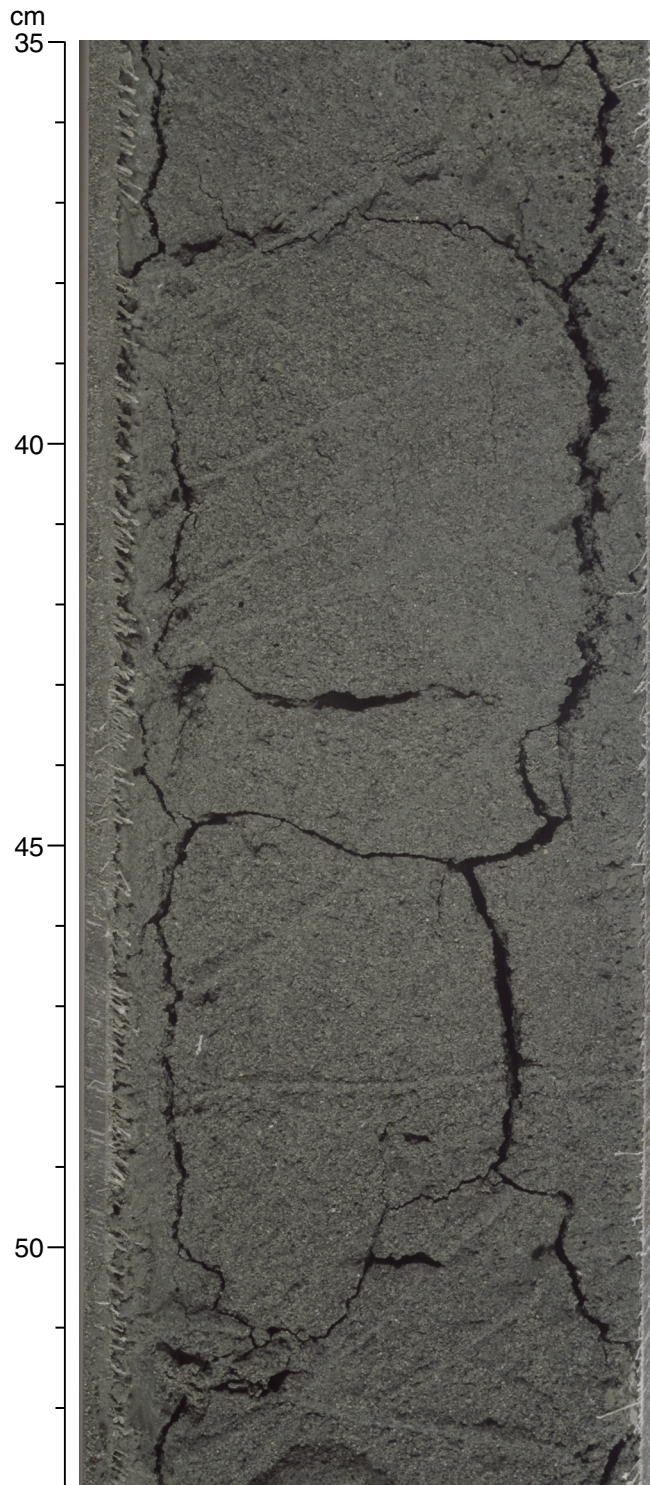


Figure F17. Incipient weblike structure in fine sand (interval 190-1178B-27R-3, 35–53 cm).



**Figure F18.** Incipient scaly and foliated clays with fine black seams crosscutting the fracture fabric (interval 190-1178B-29R-3, 27–41 cm).

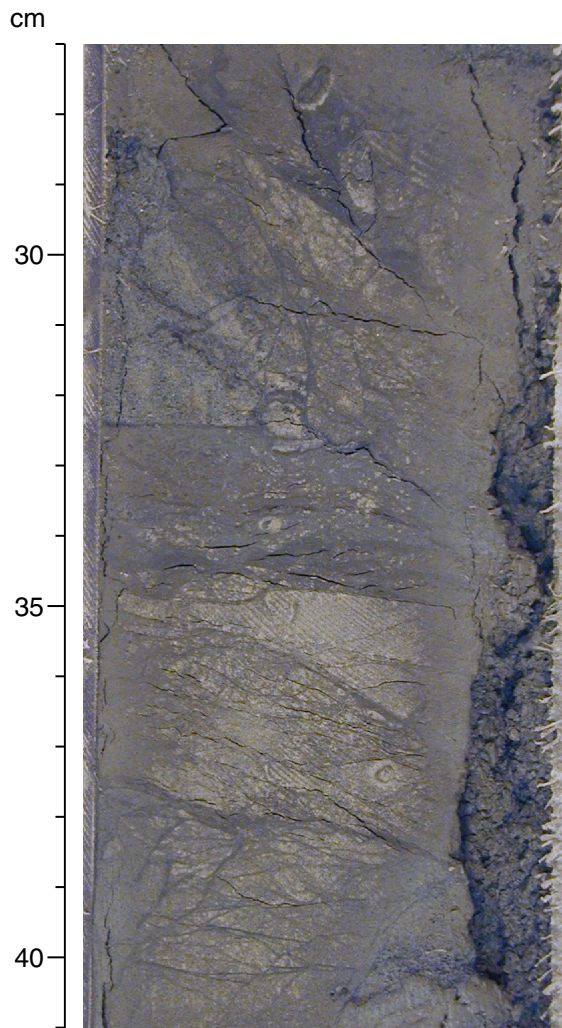


Figure F19. Paleomagnetic declination, inclination, and intensity after AF demagnetization at Holes 1178A and 1178B. Scattered declinations reflect the rotation of small core pieces during XCB and RCB coring.

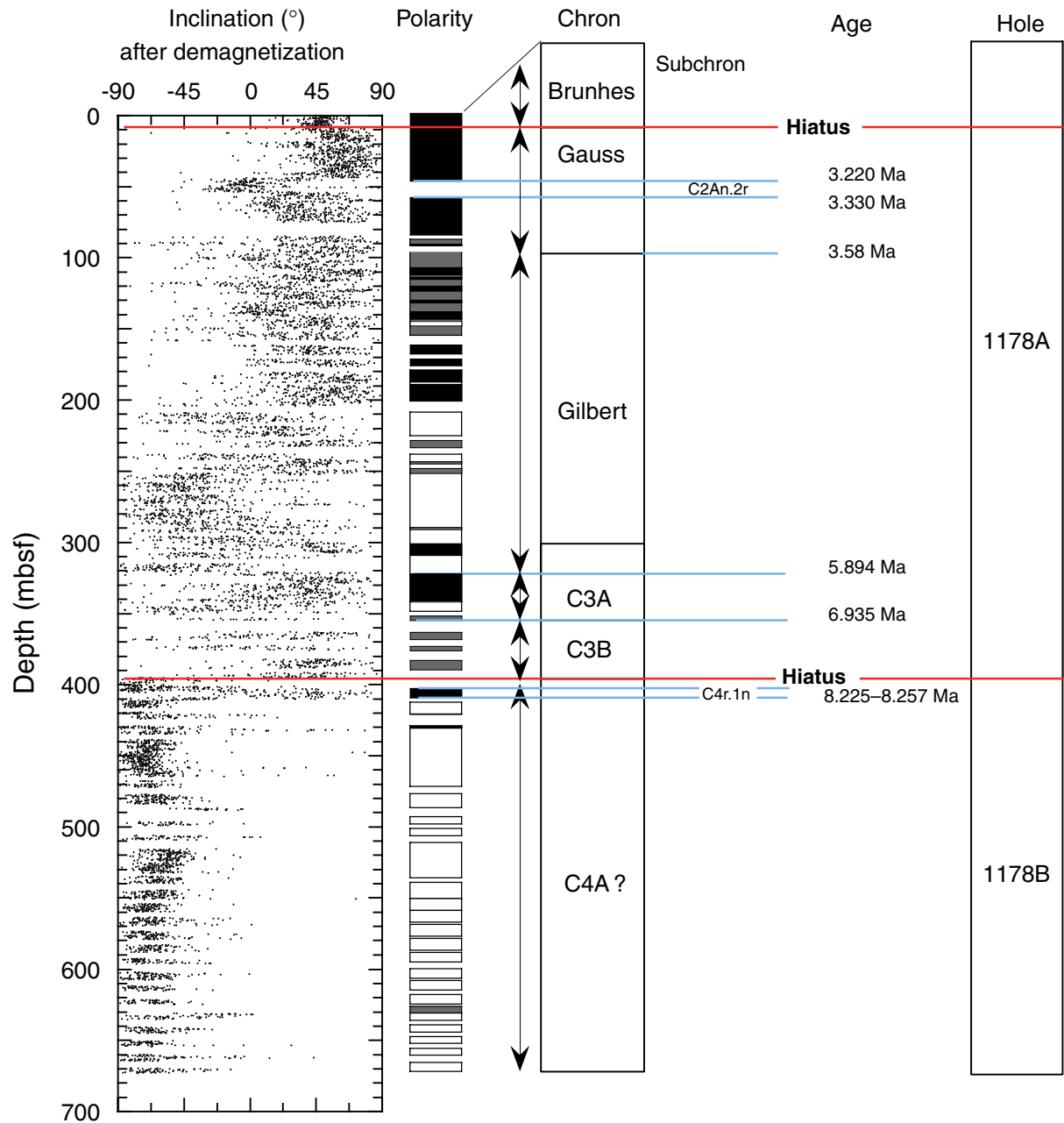


Figure F20. Uncalibrated gas-permeameter measurements from Site 1178.

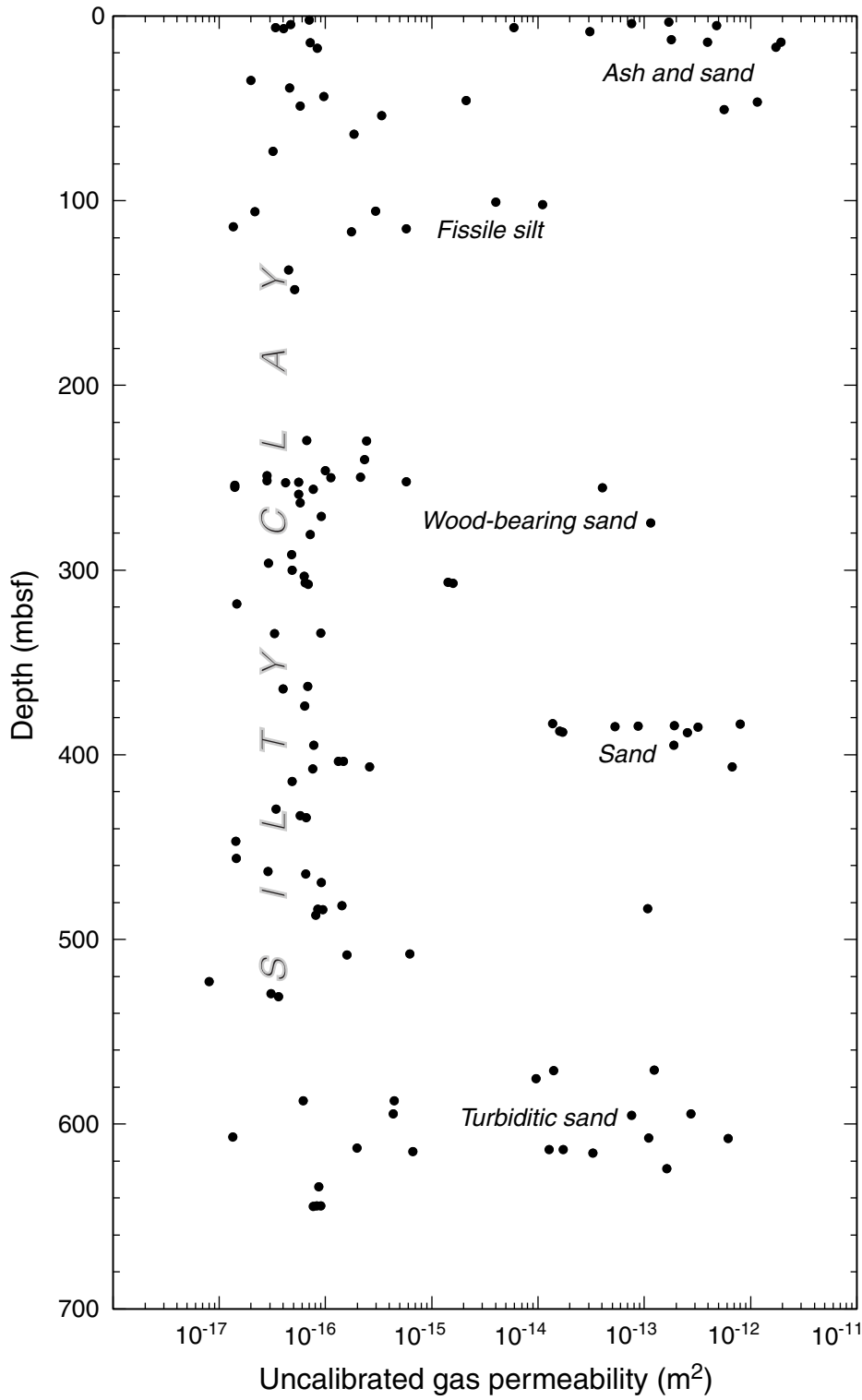


Figure F21. Site 1178 magnetostratigraphy. Black = normal polarity, white = reversed polarity, gray = unknown polarity.

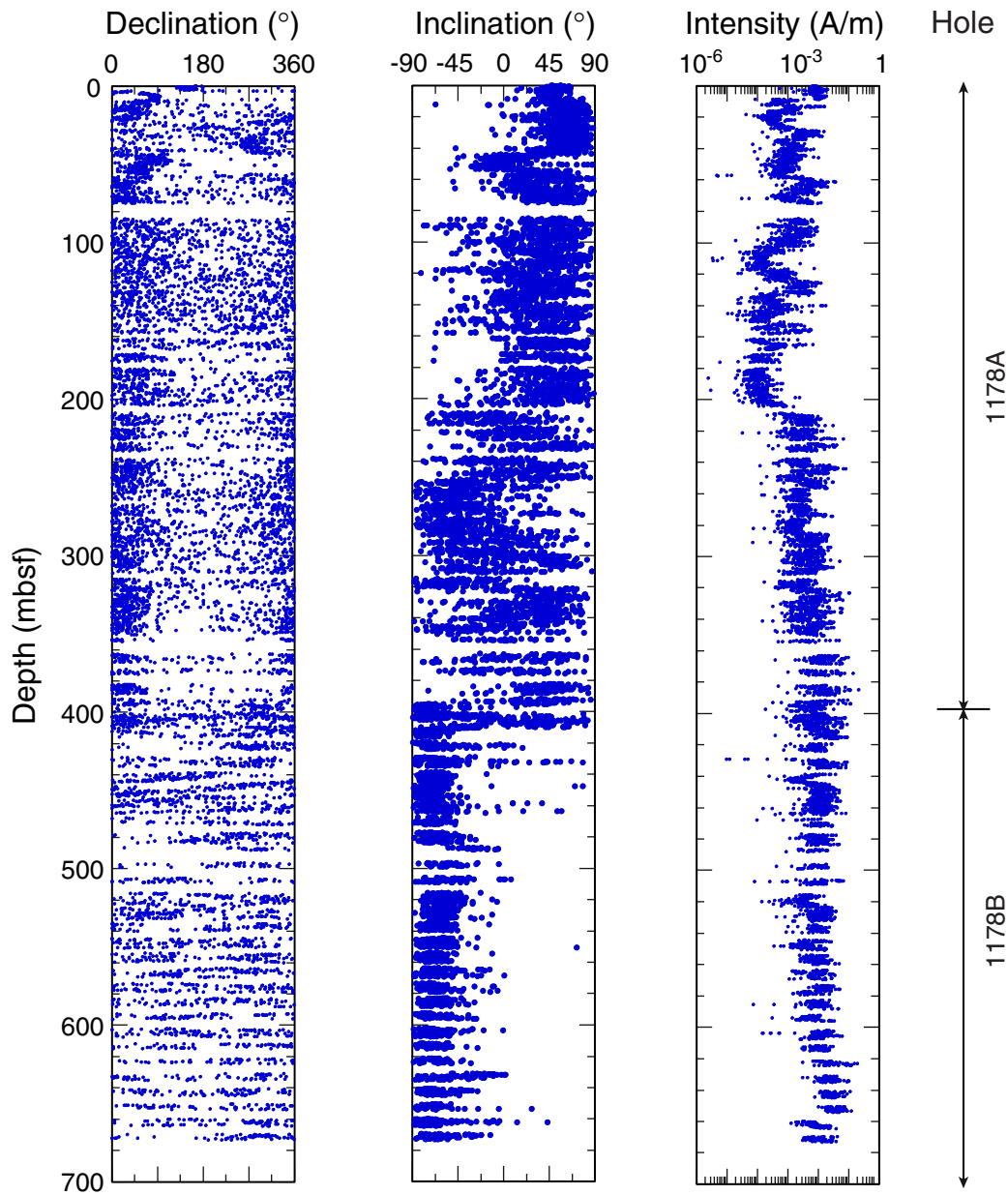


Figure F22. Pore fluid composition as a function of depth at Site 1178. Solid horizontal lines indicate litho-stratigraphic boundaries. (Continued on next page.)

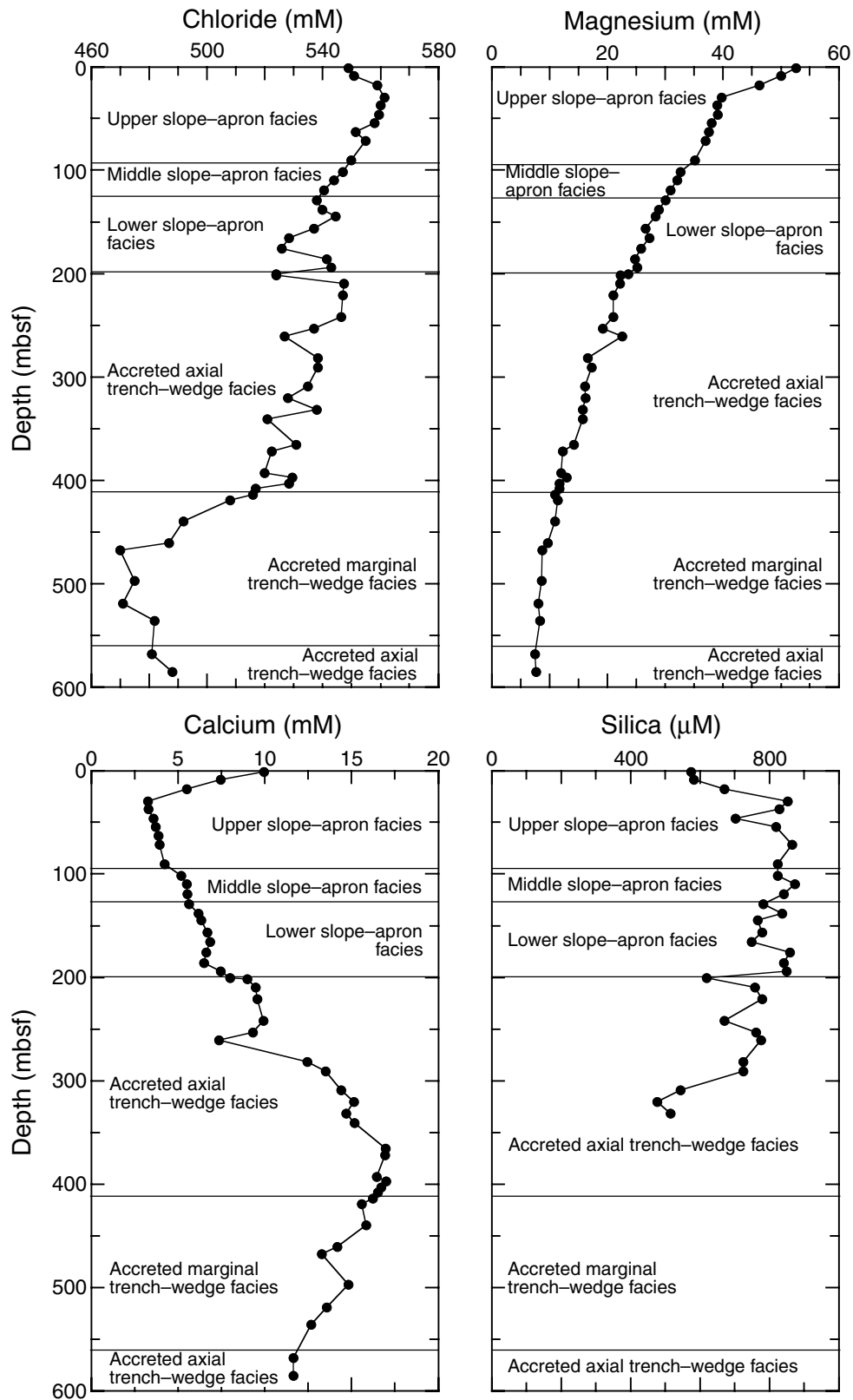


Figure F22 (continued).

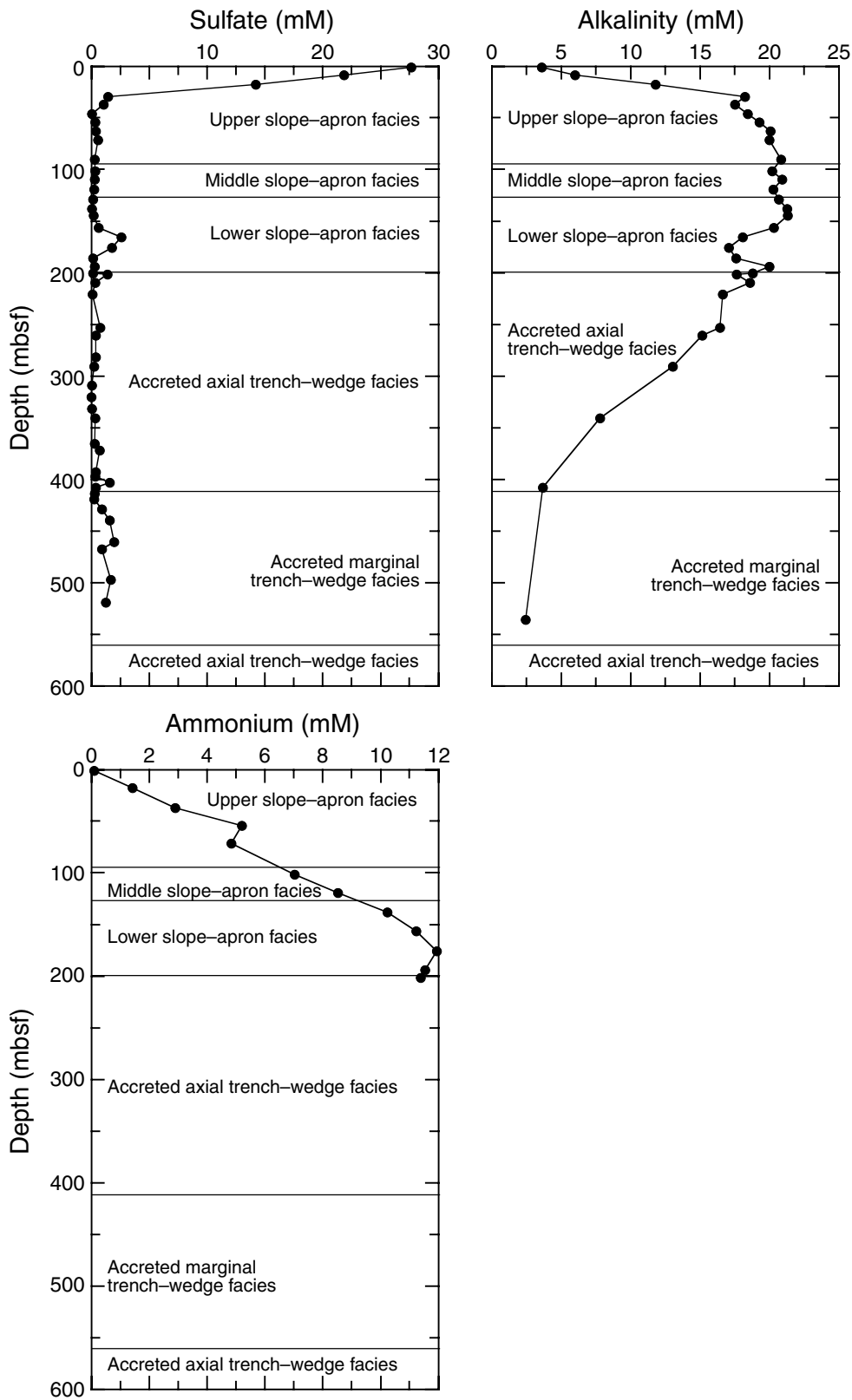
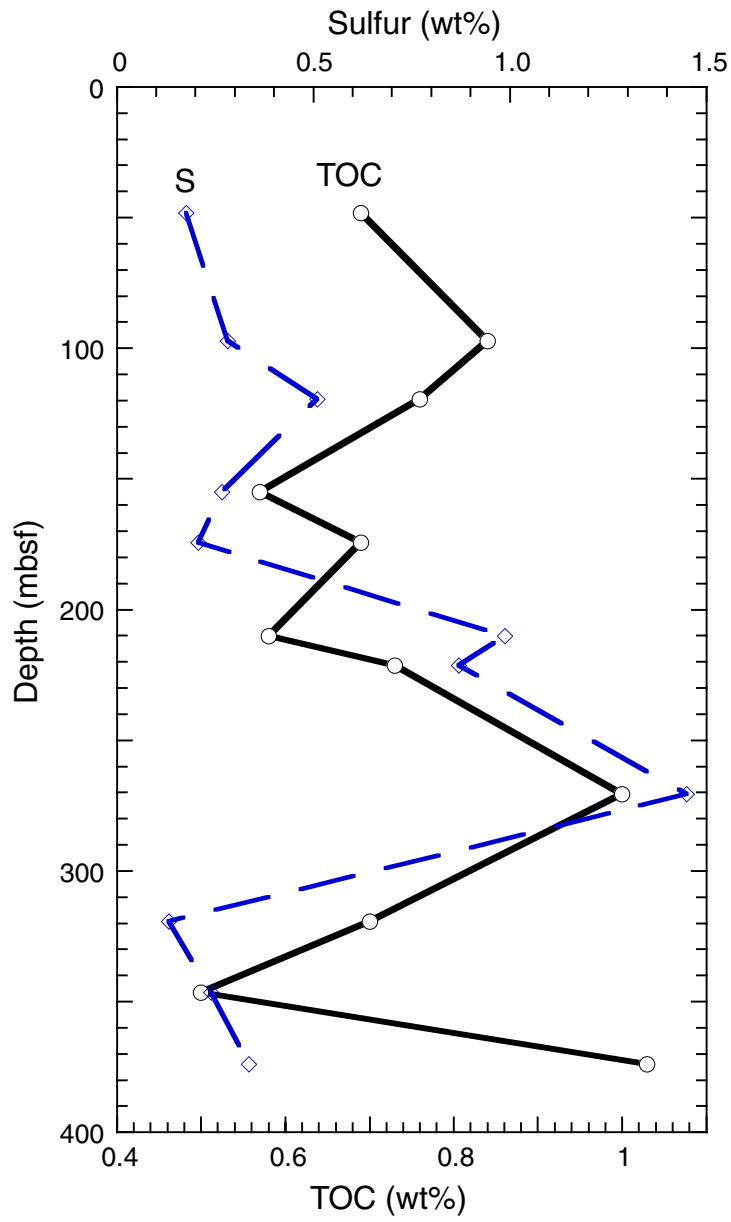


Figure F23. Total organic carbon (TOC) and sulfur concentrations in sediments at Site 1178.



**Figure F24.** Bernard ratios ( $C_1/[C_2+C_3]$ ) at Site 1178 indicate that biogenic methane is present throughout Site 1178 and that light hydrocarbons ( $C_2-C_6$ ) are being produced from more thermally mature organic matter with increasing depth.

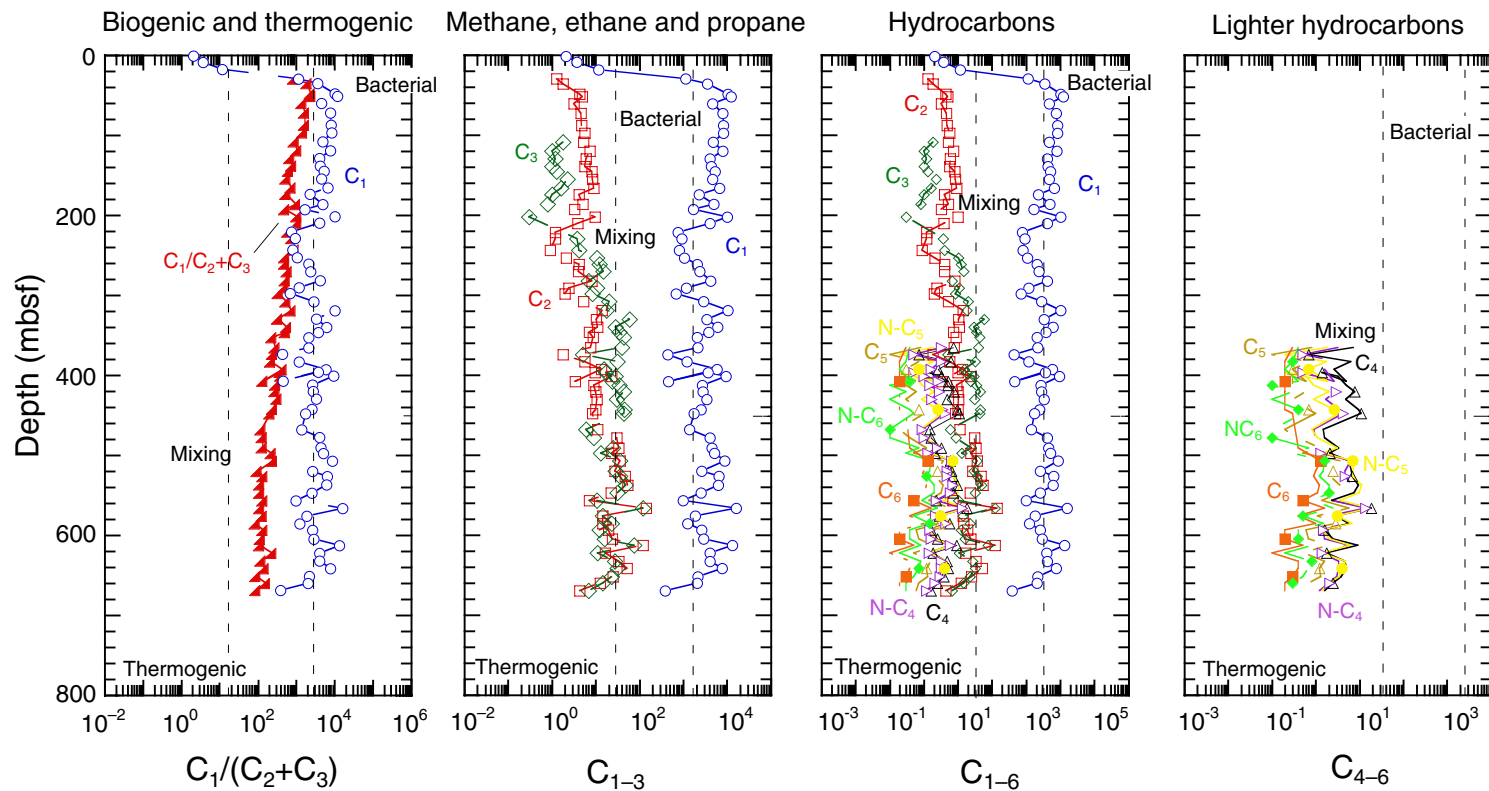
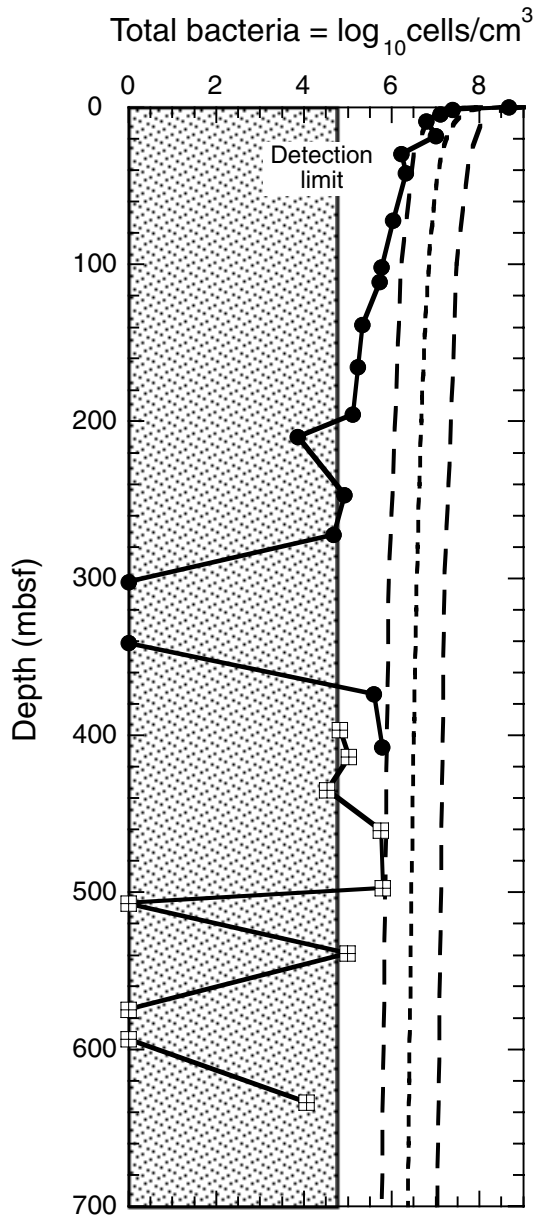


Figure F25. Depth distribution of total bacterial populations in sediment samples from Holes 1178A (solid circles) and 1178B (open squares). The dashed line represents a general regression line of bacterial numbers vs. depth in deep-sea sediments (Parkes et al., 1994), with 95% upper and lower prediction limits shown by the lines of longer dashes. The shaded area on the left of the figure indicates where bacterial populations are too low to be detected with the acridine orange direct counts; the detection limit was  $6 \times 10^4$  cells/cm<sup>3</sup> (any values within this area are constructed from sums of three enumerations and have no measure of error).



**Figure F26.** A. Site 1178 bulk density measurements. Lithostratigraphic Subunits IA (upper slope–apron facies), IB (middle slope–apron facies), IC (lower slope–apron facies), IIA (accreted axial trench–wedge facies), IIB (accreted outer trench–wedge facies), and IIC (accreted axial trench–wedge facies) are indicated. B. MST GRA and mass/volume bulk density. C. Grain density. D. Porosity.

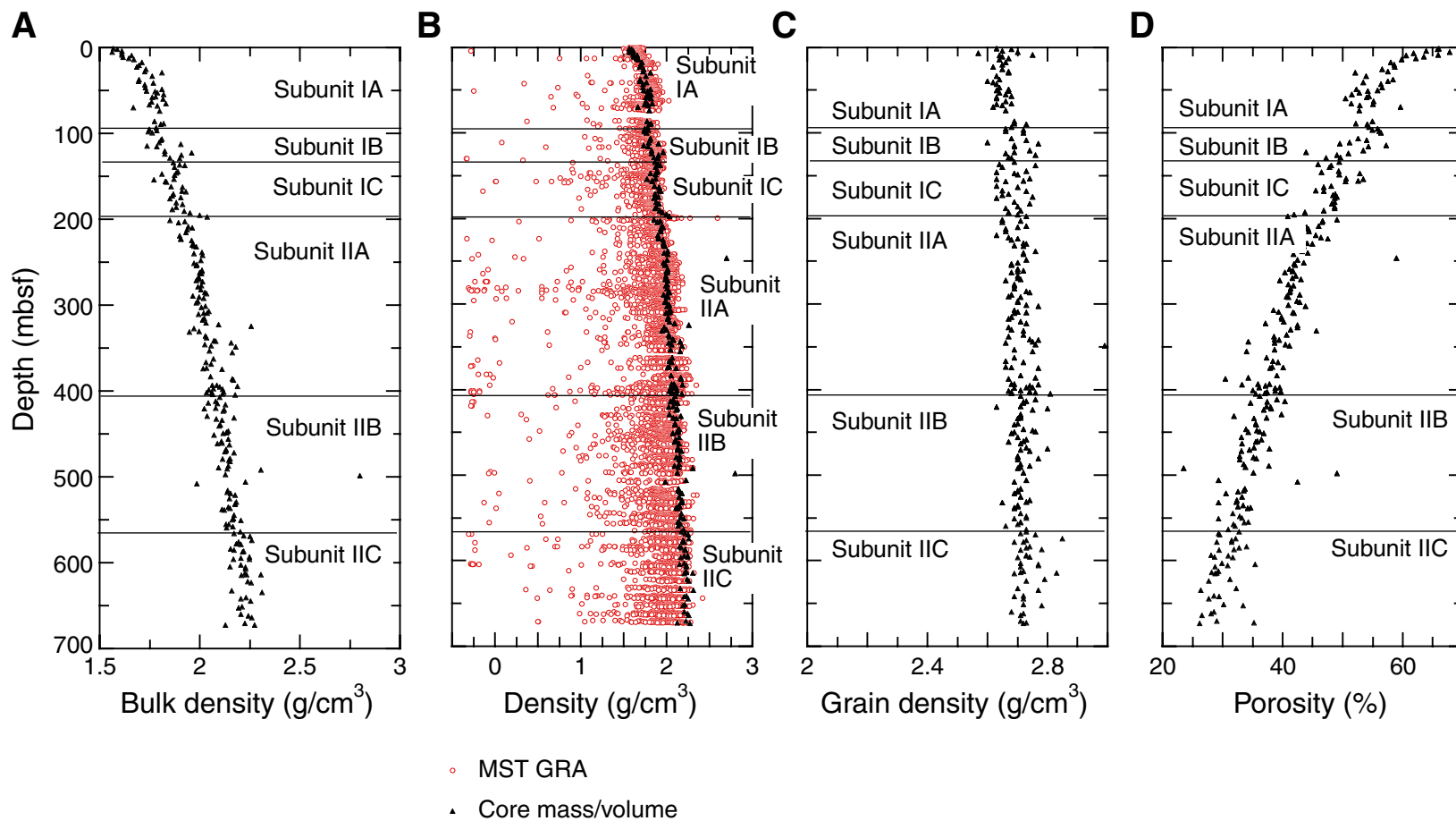


Figure F27. Site 1178 undrained peak shear strength values.

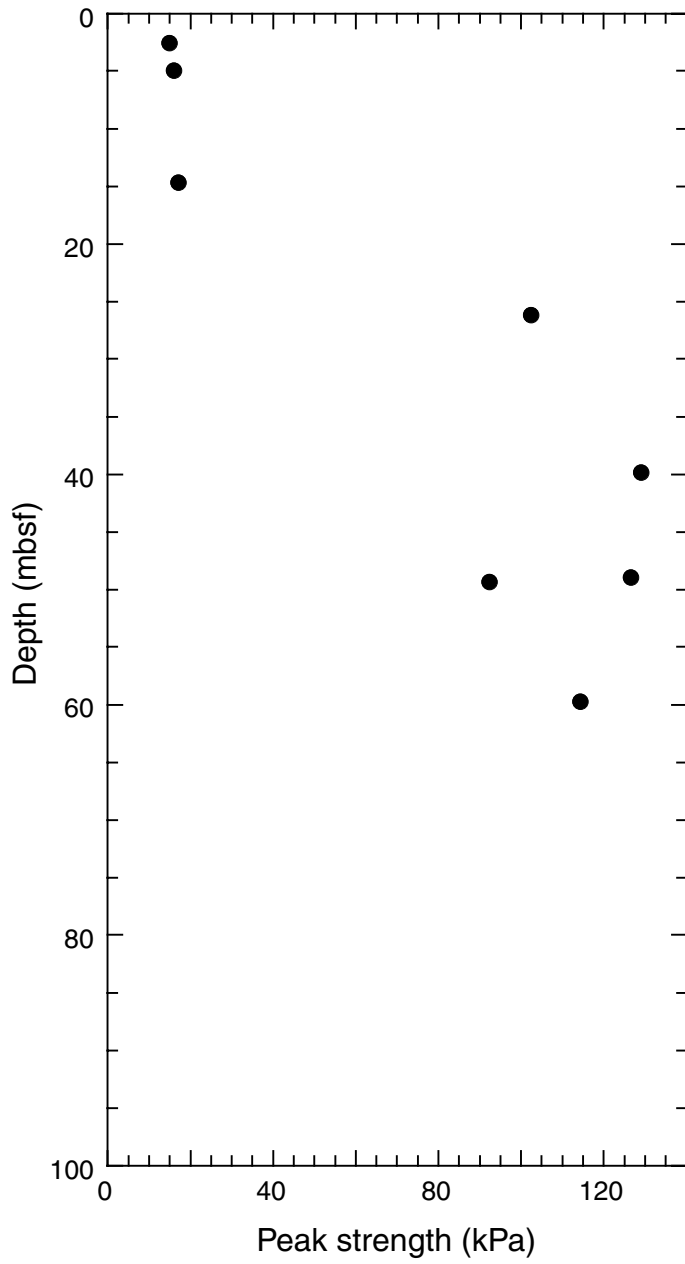


Figure F28. A. Site 1178 thermal conductivity. B. Observed (triangles) and projected (dashed line) temperatures.

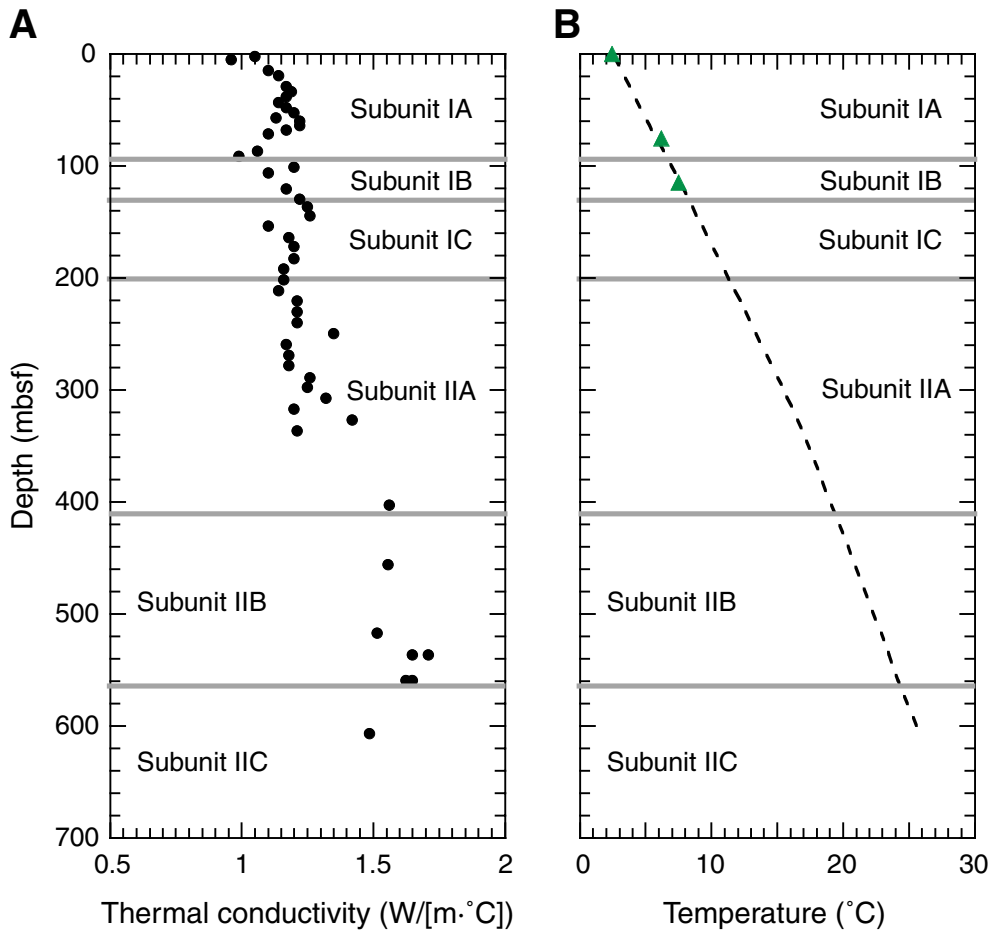


Figure F29. Site 1178 *P*-wave velocity.

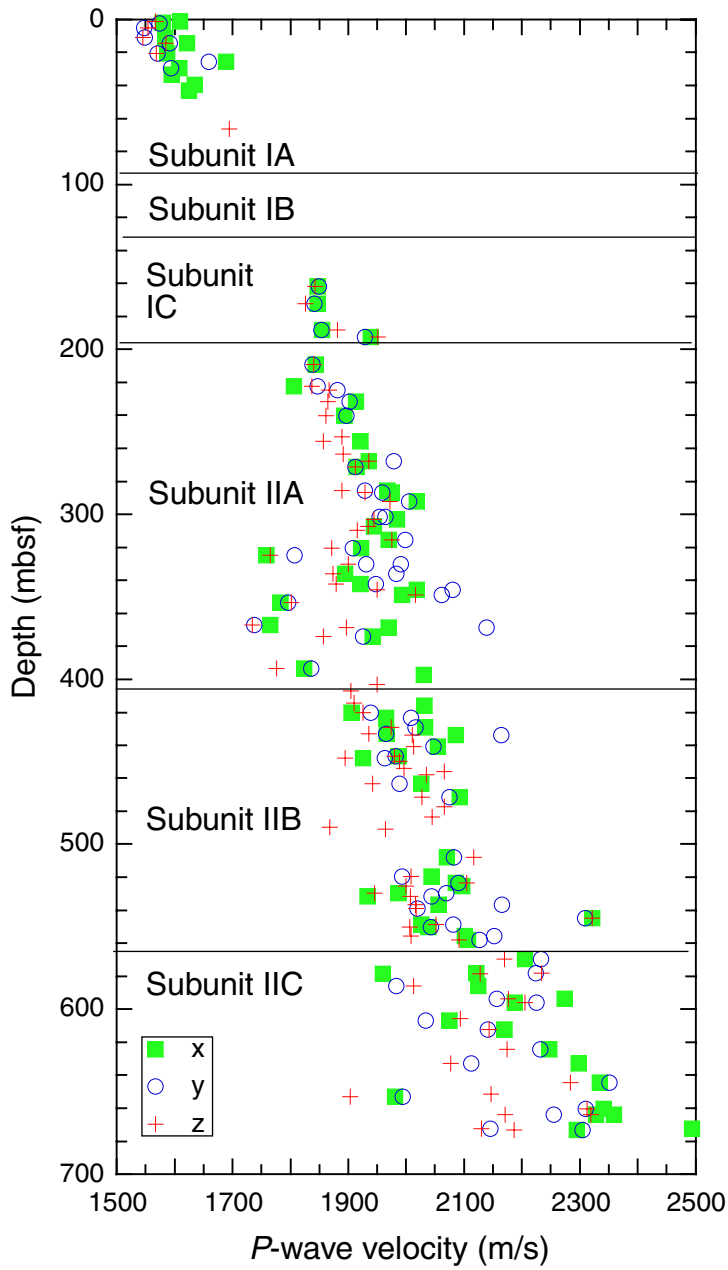


Figure F30. A. Site 1178 formation factor. B. Anisotropy of electrical conductivity in the horizontal (x- and y-axes) and vertical (z-axis) planes (parallel and perpendicular to foliation).

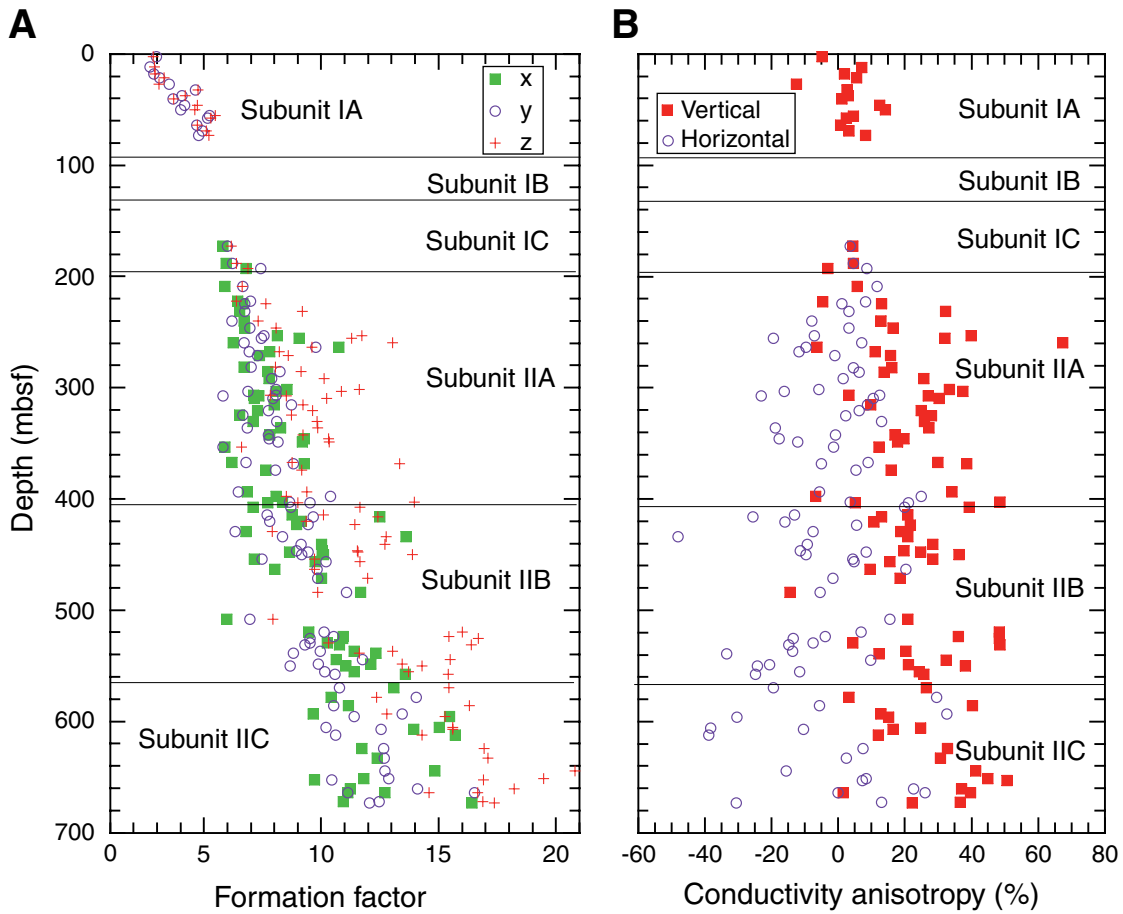


Figure F31. Site 1178 magnetic susceptibility.

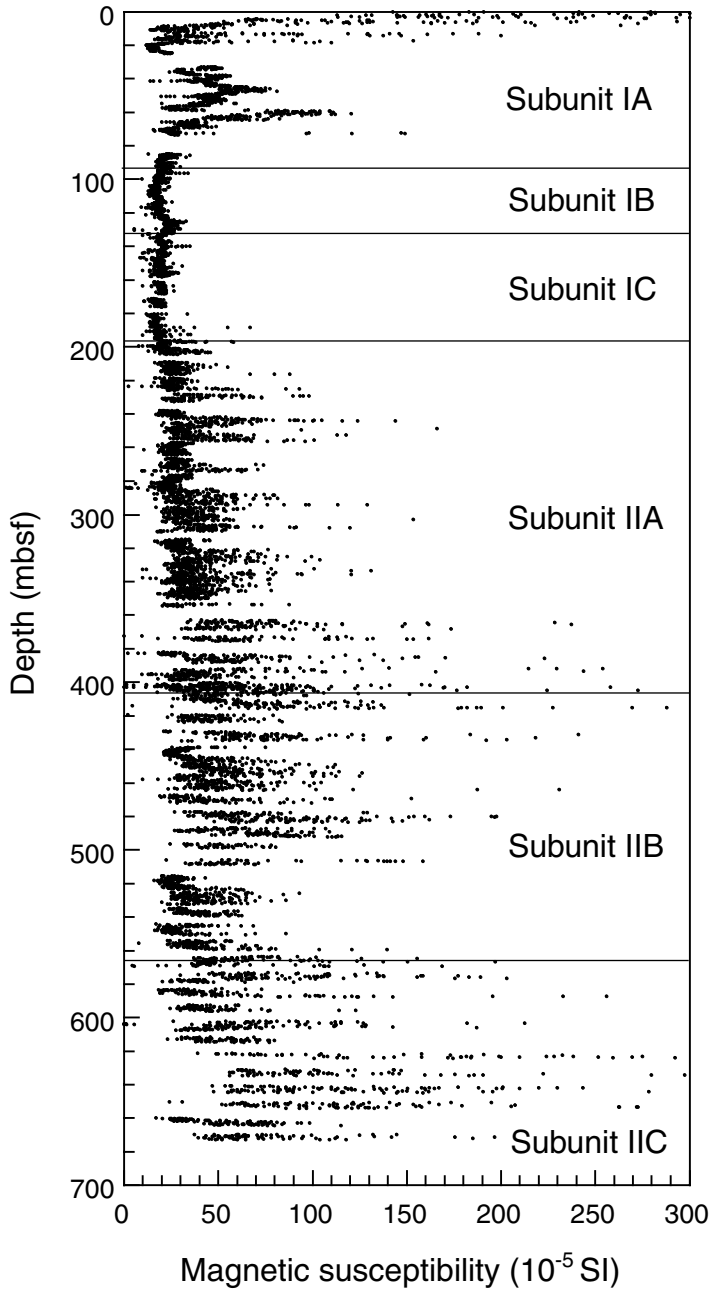


Figure F32. Temperatures measured during the deployment of the water-sampling temperature probe (WSTP) temperature tool in Hole 1178A (A) before Core 1178A-10X and (B) before Core 14X. Dashed lines = extrapolated temperatures, solid line = mudline temperature from a WSTP bottom-water sampling run.

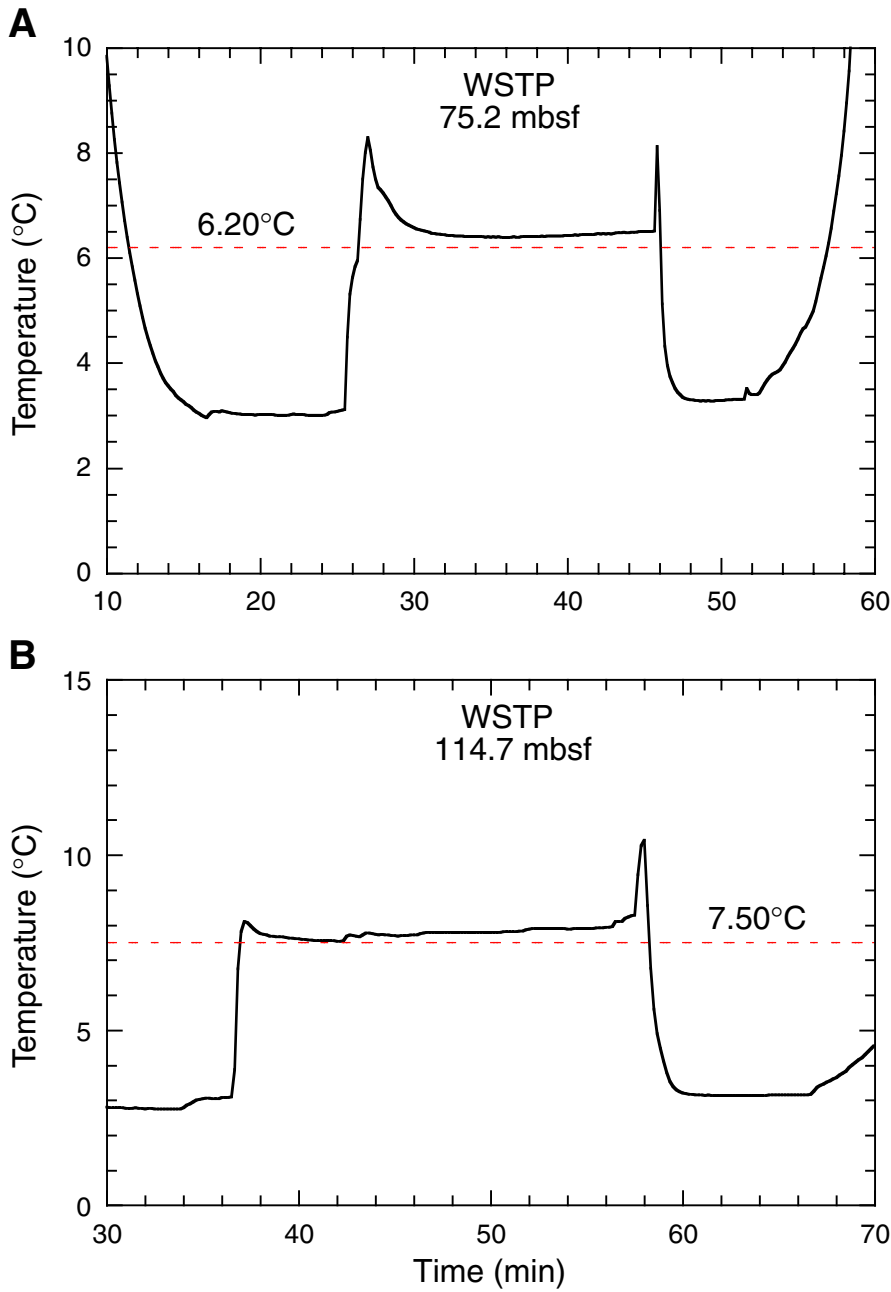


Figure F33. Hole 1178A observed (circles) and extrapolated best-fit (line) temperatures. The equation shows linear best fit for the two measurements and the mudline temperature.  $T$  = temperature,  $z$  = mbsf.

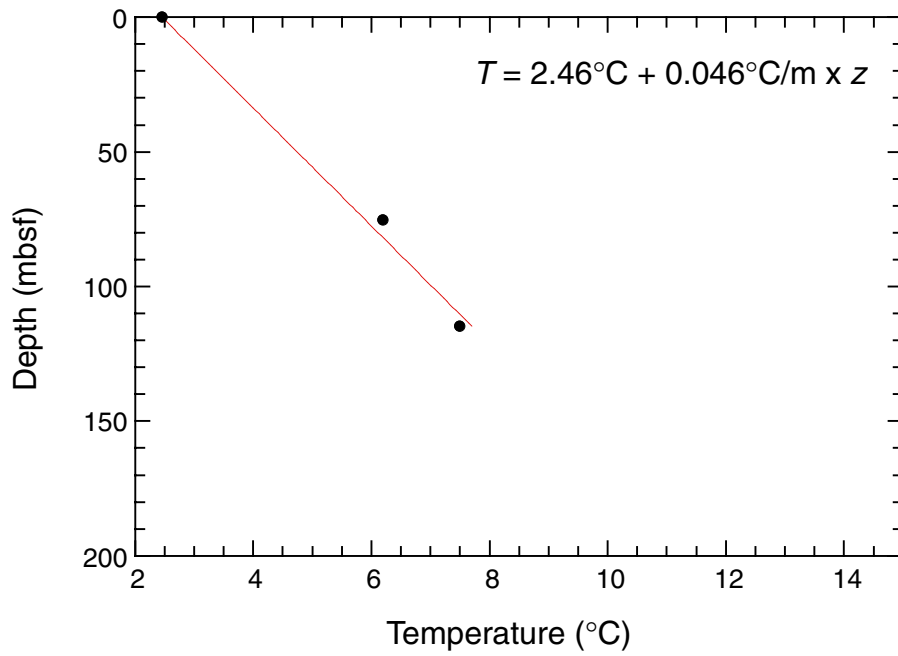
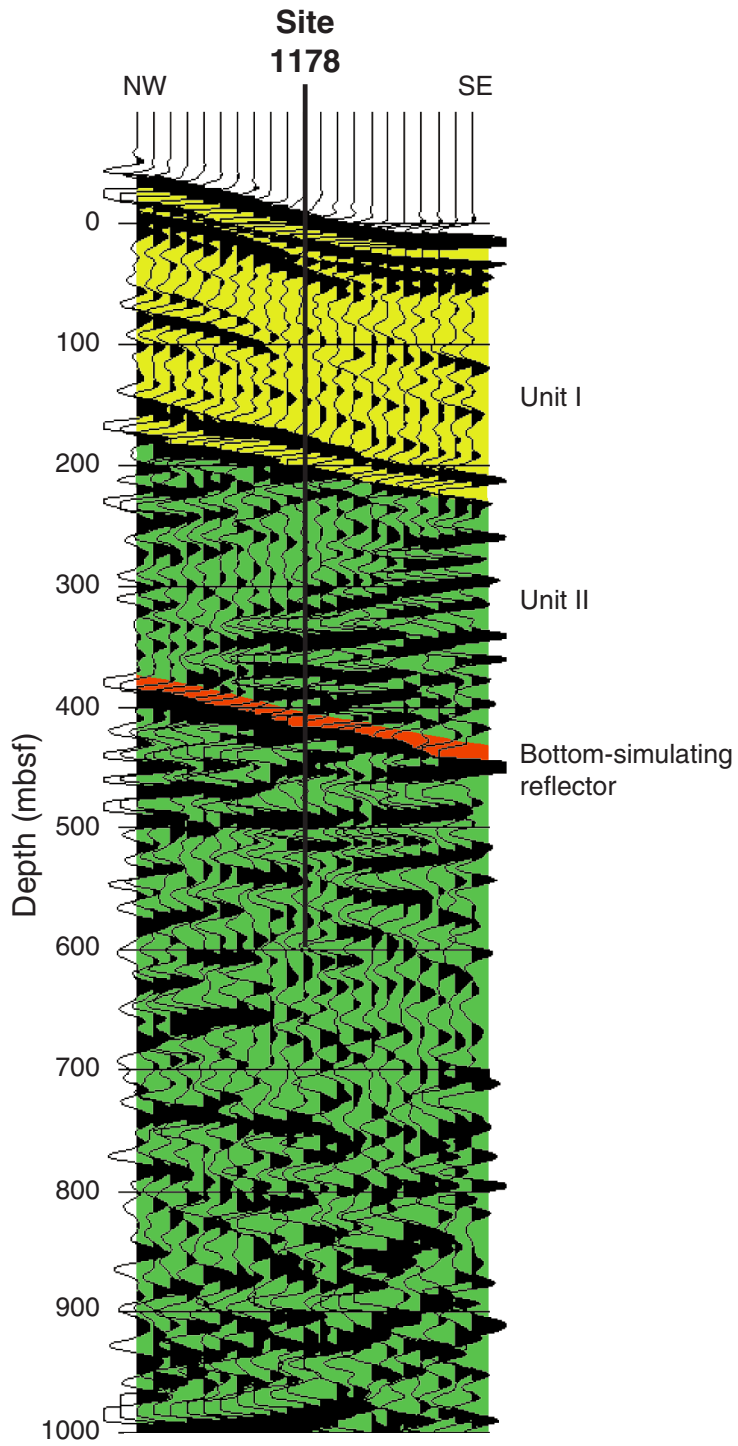


Figure F34. Three-dimensional seismic reflection line 278 across Site 1178. This line has been 3-D stacked and migrated.



**Table T1.** Coring summary, Site 1178. (See table note. Continued on next page.)

Core	Date (July 2000)	Time (local)	Depth (mbsf)		Length (m)		Recovery (%)	Comments
			Top	Bottom	Cored	Recovered		
190-1178A-								
1H	8	1930	0.0	2.9	2.9	2.90	100.0	
2H	8	2030	2.9	12.4	9.5	9.42	99.2	Tensor in at 20:25
3H	8	2125	12.4	21.9	9.5	9.91	104.3	
4H	8	2230	21.9	31.4	9.5	9.67	101.8	Split liner: liner split for entire length
5H	8	2345	31.4	40.9	9.5	10.07	106.0	
6H	9	0050	40.9	50.4	9.5	9.69	102.0	
7H	9	0135	50.4	57.5	7.1	7.13	100.4	Camera out at 01:35; DVTP at 1811.10 m
8H	9	0435	57.5	65.6	8.1	8.10	100.0	Tracer, camera in at 03:30, out at 04:45
9X	9	0610	65.6	75.2	9.6	9.57	99.7	Tracer
10X	9	0825	75.2	84.8	9.6	0.00	0.0	WSTP at 1828.8 m; tracer, Whirl-Pak
11X	9	0915	84.8	94.4	9.6	9.60	100.0	Whirl-Pak, tracer
12X	9	1005	94.4	104.0	9.6	8.94	93.1	
13X	9	1125	104.0	113.6	9.6	9.41	98.0	WSTP at 1867.2 m
14X	9	1320	113.6	123.2	9.6	9.98	104.0	
15X	9	1430	123.2	132.7	9.5	9.60	101.1	
16X	9	1535	132.7	142.2	9.5	9.46	99.6	
17X	9	1635	142.2	151.8	9.6	8.52	88.8	
18X	9	1745	151.8	161.4	9.6	6.75	70.3	
19X	9	1840	161.4	171.0	9.6	7.10	74.0	
20X	9	1930	171.0	180.4	9.4	5.66	60.2	Expanding core
21X	9	2025	180.4	189.8	9.4	8.34	88.7	
22X	9	2120	189.8	199.2	9.4	9.26	98.5	
23X	9	2225	199.2	208.8	9.6	5.34	55.6	
24X	9	2340	208.8	218.4	9.6	7.76	80.8	
25X	10	0040	218.4	228.1	9.7	7.71	79.5	
26X	10	0140	228.1	237.8	9.7	4.89	50.4	
27X	10	0245	237.8	247.4	9.6	9.58	99.8	
28X	10	0350	247.4	257.0	9.6	9.13	95.1	
29X	10	0455	257.0	266.6	9.6	7.79	81.1	
30X	10	0610	266.6	276.2	9.6	8.22	85.6	
31X	10	0800	276.2	285.9	9.7	9.88	101.9	Sinker bars out
32X	10	0945	285.9	295.5	9.6	8.80	91.7	
33X	10	1110	295.5	305.1	9.6	9.76	101.7	
34X	10	1300	305.1	314.8	9.7	6.21	64.0	
35X	10	1440	314.8	324.4	9.6	9.01	93.9	
36X	10	1600	324.4	334.0	9.6	9.58	99.8	
37X	10	1710	334.0	343.6	9.6	9.26	96.5	
38X	10	1900	343.6	353.2	9.6	6.98	72.7	
39X	10	2100	353.2	362.9	9.7	2.18	22.5	
40X	10	2235	362.9	372.5	9.6	6.15	64.1	
41X	11	0020	372.5	382.1	9.6	3.31	34.5	
42X	11	0225	382.1	391.6	9.5	6.51	68.5	
43X	11	0520	391.6	401.2	9.6	3.91	40.7	
44X	11	0750	401.2	410.8	9.6	9.15	95.3	Total depth 1178A at 07:55
			Totals:		410.8	340.2	83	
190-1178B-								
1W	12	1345	0.0	395.0	0.0	0.0	N/A	
2R	12	1500	395.0	400.0	5.0	4.01	80.2	
3R	12	1655	400.0	409.6	9.6	5.43	56.6	
4R	12	1900	409.6	419.3	9.7	6.6	68.0	
5R	13	0215	419.3	429.0	9.7	4.91	50.6	
6R	13	0405	429.0	438.6	9.6	6.23	64.9	
7R	13	0540	438.6	448.2	9.6	9.39	97.8	
8R	13	0715	448.2	457.8	9.6	9.4	97.9	
9R	13	0840	457.8	467.4	9.6	6.96	72.5	
10R	13	1015	467.4	477.1	9.7	4.92	50.7	
11R	13	1205	477.1	486.7	9.6	6.92	72.1	
12R	13	1350	486.7	496.4	9.7	6.72	69.3	
13R	13	1620	496.4	506.0	9.6	2.67	27.8	
14R	13	1805	506.0	515.6	9.6	3.18	33.1	
15R	13	1955	515.6	525.2	9.6	8.58	89.4	
16R	13	2130	525.2	534.8	9.6	7.3	76.0	
17R	13	2335	534.8	544.4	9.6	5.07	52.8	
18R	14	0145	544.4	554.0	9.6	6.68	69.6	
19R	14	0325	554.0	563.6	9.6	5.92	61.7	Tracer
20R	14	0530	563.6	573.3	9.7	6.18	63.7	
21R	14	0755	573.3	582.9	9.6	5.98	62.3	

**Table T1 (continued).**

Core	Date (July 2000)	Time (local)	Depth (mbsf)		Length (m)		Recovery (%)	Comments
			Top	Bottom	Cored	Recovered		
22R	14	0955	582.9	592.5	9.6	5.24	54.6	
23R	14	1205	592.5	602.1	9.6	3.97	41.4	
24R	14	1415	602.1	611.7	9.6	5.74	59.8	
25R	14	1640	611.7	621.4	9.7	3.42	35.3	
26R	14	1900	621.4	631.0	9.6	3.22	33.5	
27R	14	2115	631.0	640.7	9.7	4.24	43.7	
28R	14	2340	640.7	650.4	9.7	4.6	47.4	
29R	15	0155	650.4	660.0	9.6	4.03	42.0	
30R	15	0355	660.0	669.6	9.6	4.87	50.7	
31R	15	0545	669.6	679.2	9.6	3.58	37.3	
			Total:		284.2	166	58	

Note: WSTP = water-sampling temperature probe.

**Table T2.** Coring summary by section, Site 1178. (See table notes. Continued on next eight pages.)

Core	Date (July 2000)	Time (local)	Core depth (mbsf)		Length (m)		Recovery (%)	Section	Length (m)		Section depth (mbsf)		Catwalk samples	Comment
			Top	Bottom	Cored	Recovered			Liner	Curated	Top	Bottom		
190-1178A- 1H	8	1930	0.0	2.9	2.9	2.90	100.0							
								1	1.5	1.5	0.0	1.5	IW, BACT	
								2	1.24	1.24	1.5	2.74	HS, BGAS, BACT	
								CC(w/CC)	0.16	0.16	2.74	2.9	PAL	
								Totals:	2.9	2.9				
2H	8	2030	2.9	12.4	9.5	9.42	99.2							
								1	1.5	1.5	2.9	4.4	WRY, WRS, BACT	
								2	1.5	1.5	4.4	5.9		
								3	1.5	1.5	5.9	7.4		
								4	1.5	1.5	7.4	8.9	IW, BACT	
								5	1.5	1.5	8.9	10.4	HS, BGAS	
								6	1.5	1.5	10.4	11.9		
								7	0.27	0.27	11.9	12.17		
								CC(w/7)	0.15	0.15	12.17	12.32	PAL	
								Totals:	9.42	9.42				
3H	8	2125	12.4	21.9	9.5	9.91	104.3							
								1	1.5	1.5	12.4	13.9		
								2	1.5	1.5	13.9	15.4		
								3	1.5	1.5	15.4	16.9		
								4	1.5	1.5	16.9	18.4	BACT, IW	
								5	1.5	1.5	18.4	19.9	HS, BGAS	
								6	1.5	1.5	19.9	21.4		
								7	0.63	0.63	21.4	22.03		
								CC(w/7)	0.28	0.28	22.03	22.31	PAL	
								Totals:	9.91	9.91				
4H	8	2230	21.9	31.4	9.5	9.67	101.8							
								1	1.5	1.5	21.9	23.4		
								2	1.5	1.5	23.4	24.9		
								3	1.5	1.5	24.9	26.4		
								4	1.5	1.5	26.4	27.9		
								5	0.5	0.5	27.9	28.4		
								6	1.5	1.5	28.4	29.9	BACT, IW	
								7	1.03	1.03	29.9	30.93	HS, BGAS	
								CC(w/CC)	0.64	0.64	30.93	31.57	PAL	
								Totals:	9.67	9.67				
5H	8	2345	31.4	40.9	9.5	10.07	106.0							
								1	1.5	1.5	31.4	32.9		
								2	1.5	1.5	32.9	34.4		
								3	1.5	1.5	34.4	35.9	WRMT	
								4	1.5	1.5	35.9	37.4	HS, BGAS, IW	
								5	1.5	1.5	37.4	38.9		
								6	1.5	1.5	38.9	40.4		
								7	0.85	0.85	40.4	41.25		
								CC(w/7)	0.22	0.22	41.25	41.47	PAL	
								Totals:	10.07	10.07				
6H	9	50	40.9	50.4	9.5	9.69	102.0							
								1	1.5	1.5	40.9	42.4	WRY, WRS, BACT	
								2	1.5	1.5	42.4	43.9		
								3	1.5	1.5	43.9	45.4		
								4	1.5	1.5	45.4	46.9	IW	
								5	1.5	1.5	46.9	48.4		
								6	1.5	1.5	48.4	49.9	HS, BGAS	
								7	0.69	0.69	49.9	50.59	PAL	
								Totals:	9.69	9.69				
7H	9	135	50.4	57.5	7.1	7.13	100.4							
								1	1.5	1.5	50.4	51.9		
								2	1.5	1.5	51.9	53.4	HS	
								3	1.5	1.5	53.4	54.9	IW	
								4	1.5	1.5	54.9	56.4		
								5	0.84	0.84	56.4	57.24		
								CC(w/5)	0.29	0.29	57.24	57.53	PAL	
								Totals:	7.13	7.13				
8H	9	435	57.5	65.6	8.1	8.10	100.0							
								1	1.5	1.5	57.5	59.0	SMTCR	
								2	1.5	1.5	59.0	60.5		
								3	1.5	1.5	60.5	62.0	SMTCR, HS, BGAS	

Table T2 (continued).

Core	Date (July 2000)	Time (local)	Core depth (mbsf)		Length (m)		Recovery (%)	Section	Length (m)		Section depth (mbsf)		Catwalk samples	Comment
			Top	Bottom	Cored	Recovered			Liner	Curated	Top	Bottom		
9X	9	610	65.6	75.2	9.6	9.57	99.7	4	1.5	1.5	62.0	63.5	IW	
								5	1.5	1.5	63.5	65.0	SMTCR	
								6	0.59	0.59	65.0	65.6		
								CC(NS)	0.01	0.01	65.59	65.6	PAL	
								Totals:	8.1	8.1				
								1	1.5	1.5	65.6	67.1		
								2	1.5	1.5	67.1	68.6		
10X	9	825	75.2	84.8	9.6	0.00	0.0	3	1.5	1.5	68.6	70.1		
								4	0.64	0.64	70.1	70.74		
								5	1.5	1.5	70.74	72.24	BACT, IW	
								6	1.31	1.31	72.24	73.55	HS, BGAS	
								7	1.25	1.25	73.55	74.8		
								CC(w/CC)	0.37	0.37	74.8	75.17		
								Totals:	9.57	9.57				
11X	9	915	84.8	94.4	9.6	9.60	100.0	1	0	0				
								Totals:	0	0				
12X	9	1005	94.4	104.0	9.6	8.94	93.1	1	1.5	1.5	84.8	86.3	SMTCR	
								2	1.5	1.5	86.3	87.8		
								3	1.5	1.5	87.8	89.3	HS, BGAS, SMTCR	
								4	1.5	1.5	89.3	90.8	IW	
								5	1.5	1.5	90.8	92.3	SMTCR	
								6	1.5	1.5	92.3	93.8		
								7	0.24	0.24	93.8	94.04		
CC(w/7)	0.36	0.36	94.04	94.4	PAL									
Totals:	9.6	9.6												
13X	9	1125	104.0	113.6	9.6	9.41	98.0	1	1.41	1.41	94.4	95.81		
								2	1.5	1.5	95.81	97.31		
								3	1.5	1.5	97.31	98.81	HS, BGAS	
								4	1.5	1.5	98.81	100.31		
								5	1.5	1.5	100.31	101.81	BACT, IW	
								6	1.3	1.3	101.81	103.11		
								CC(w/CC)	0.23	0.23	103.11	103.34	PAL	
Totals:	8.94	8.94												
14X	9	1320	113.6	123.2	9.6	9.98	104.0	1	1.5	1.5	104.0	105.5		
								2	1.5	1.5	105.5	107.0		
								3	1.5	1.5	107.0	108.5		
								4	1.5	1.5	108.5	110.0	HS, BGAS, IW	
								5	1.5	1.5	110.0	111.5	WRY, WRS, BACT	
								6	1.5	1.5	111.5	113.0		
								CC(w/CC)	0.41	0.41	113.0	113.41	PAL	
Totals:	9.41	9.41												
15X	9	1430	123.2	132.7	9.5	9.60	101.1	1	1.5	1.5	113.6	115.1		
								2	1.5	1.5	115.1	116.6		
								3	1.5	1.5	116.6	118.1		
								4	1.5	1.5	118.1	119.6	IW	
								5	1.5	1.5	119.6	121.1	HS, BGAS	
								6	1.5	1.5	121.1	122.6		
								7	0.55	0.55	122.6	123.15		
CC(w/7)	0.43	0.43	123.15	123.58	PAL									
Totals:	9.98	9.98												
16X	9	1535	132.7	142.2	9.5	9.46	99.6	1	1.5	1.5	123.2	124.7		
								2	1.5	1.5	124.7	126.2		
								3	1.5	1.5	126.2	127.7		
								4	1.5	1.5	127.7	129.2	IW	
								5	1.5	1.5	129.2	130.7	HS, BGAS	
								6	1.5	1.5	130.7	132.2		
								7	0.44	0.44	132.2	132.64		
CC(w/7)	0.16	0.16	132.64	132.8	PAL									
Totals:	9.6	9.6												
16X	9	1535	132.7	142.2	9.5	9.46	99.6	1	1.5	1.5	132.7	134.2		

**Table T2 (continued).**

Core	Date (July 2000)	Time (local)	Core depth (mbsf)		Length (m)		Recovery (%)	Section	Length (m)		Section depth (mbsf)		Catwalk samples	Comment		
			Top	Bottom	Cored	Recovered			Liner	Curated	Top	Bottom				
17X	9	1635	142.2	151.8	9.6	8.52	88.8	2	1.5	1.5	134.2	135.7	BACT, IW HS, BGAS, VAC			
								3	1.5	1.5	135.7	137.2				
								4	1.5	1.5	137.2	138.7				
								5	1.5	1.5	138.7	140.2				
								6	1.06	1.06	140.2	141.26				
								7	0.52	0.52	141.26	141.78				
								CC(w/7)	0.38	0.38	141.78	142.16				
								Totals:	9.46	9.46						
18X	9	1745	151.8	161.4	9.6	6.75	70.3	1	1.5	1.5	142.2	143.7	IW HS, BGAS VAC			
								2	1.5	1.5	143.7	145.2				
								3	1.5	1.5	145.2	146.7				
								4	1.5	1.5	146.7	148.2				
								5	1.5	1.5	148.2	149.7				
								6	0.85	0.85	149.7	150.55				
								CC(w/6)	0.17	0.17	150.55	150.72				
								Totals:	8.52	8.52						
19X	9	1840	161.4	171.0	9.6	7.10	74.0	1	1.0	1.0	151.8	152.8	HS, IW PAL			
								2	0.86	0.86	152.8	153.66				
								3	1.5	1.5	153.66	155.16				
								4	1.5	1.5	155.16	156.66				
								5	1.5	1.5	156.66	158.16				
								CC(w/CC)	0.39	0.39	158.16	158.55				
								Totals:	6.75	6.75						
								20X	9	1930	171.0	180.4			9.4	5.66
2	1.5	1.5	162.9	164.4												
3	1.5	1.5	164.4	165.9												
4	1.5	1.5	165.9	167.4												
5	0.89	0.89	167.4	168.29												
CC(w/5)	0.21	0.21	168.29	168.5												
Totals:	7.1	7.1														
21X	9	2025	180.4	189.8	9.4	8.34	88.7						1	0.34		
								2	1.5	1.5	171.34	172.84				
								3	1.5	1.5	172.84	174.34				
								4	1.24	1.24	174.34	175.58				
								5	0.8	0.8	175.58	176.38				
								CC(w/5)	0.28	0.28	176.38	176.66				
								Totals:	5.66	5.66						
								22X	9	2120	189.8	199.2	9.4	9.26	98.5	1
2	1.5	1.5	181.9	183.4												
3	1.5	1.5	183.4	184.9												
4	1.5	1.5	184.9	186.4												
5	1.5	1.5	186.4	187.9												
6	0.64	0.64	187.9	188.54												
CC(w/6)	0.2	0.2	188.54	188.74												
Totals:	8.34	8.34														
23X	9	2225	199.2	208.8	9.6	5.34	55.6	1	1.5	1.5	189.8	191.3	HS, BGAS, IW WRY, WRS, BACT PAL			
								2	1.5	1.5	191.3	192.8				
								3	1.5	1.5	192.8	194.3				
								4	1.5	1.5	194.3	195.8				
								5	1.5	1.5	195.8	197.3				
								6	1.42	1.42	197.3	198.72				
								CC(w/CC)	0.34	0.34	198.72	199.06				
								Totals:	9.26	9.26						
24X	9	2340	208.8	218.4	9.6	7.76	80.8	1	1.5	1.5	199.2	200.7	IW IW HS, BGAS PAL			
								2	1.5	1.5	200.7	202.2				
								3	1.5	1.5	202.2	203.7				
								4	0.65	0.65	203.7	204.35				
								CC(w/4)	0.19	0.19	204.35	204.54				
								Totals:	5.34	5.34						
								1	1.5	1.5	208.8	210.3			IW, BACT	

Table T2 (continued).

Core	Date (July 2000)	Time (local)	Core depth (mbsf)		Length (m)		Recovery (%)	Section	Length (m)		Section depth (mbsf)		Catwalk samples	Comment
			Top	Bottom	Cored	Recovered			Liner	Curated	Top	Bottom		
								2	1.39	1.39	210.3	211.69	HS, BGAS	
								3	1.5	1.5	211.69	213.19		
								4	1.5	1.5	213.19	214.69		
								5	1.5	1.5	214.69	216.19		
								6	0.36	0.36	216.19	216.55		
								CC(w/6)	0.01	0.01	216.55	216.56	PAL	
								Totals:	7.76	7.76				
25X	10	40	218.4	228.1	9.7	7.71	79.5							
								1	1.47	1.47	218.4	219.87		
								2	1.5	1.5	219.87	221.37	IW	
								3	1.5	1.5	221.37	222.87	HS, BGAS	
								4	1.43	1.43	222.87	224.3		
								5	1.52	1.52	224.3	225.82		
								CC(w/CC)	0.29	0.29	225.82	226.11	PAL	
								Totals:	7.71	7.71				
26X	10	140	228.1	237.8	9.7	4.89	50.4							
								1	1.5	1.5	228.1	229.6	IW	
								2	1.5	1.5	229.6	231.1	HS, BGAS	
								3	1.46	1.46	231.1	232.56		
								CC(w/CC)	0.43	0.43	232.56	232.99	PAL	
								Totals:	4.89	4.89				
27X	10	245	237.8	247.4	9.6	9.58	99.8							
								1	1.5	1.5	237.8	239.3		
								2	1.5	1.5	239.3	240.8		
								3	1.5	1.5	240.8	242.3	IW	
								4	1.5	1.5	242.3	243.8		
								5	1.5	1.5	243.8	245.3	HS, BGAS	
								6	1.3	1.3	245.3	246.6		
								7	0.45	0.45	246.6	247.05	BACT	
								CC(w/CC)	0.33	0.33	247.05	247.38	PAL	
								Totals:	9.58	9.58				
28X	10	350	247.4	257.0	9.6	9.13	95.1							
								1	1.5	1.5	247.4	248.9		
								2	1.5	1.5	248.9	250.4		
								3	1.5	1.5	250.4	251.9		
								4	1.5	1.5	251.9	253.4	IW	
								5	1.5	1.5	253.4	254.9	HS, BGAS	
								6	1.42	1.42	254.9	256.32		
								CC(w/CC)	0.21	0.21	256.32	256.53	PAL	
								Totals:	9.13	9.13				
29X	10	455	257.0	266.6	9.6	7.79	81.1							
								1	1.5	1.5	257.0	258.5		
								2	1.21	1.21	258.5	259.71		
								3	1.45	1.45	259.71	261.16	IW	
								4	1.48	1.48	261.16	262.64	HS, BGAS	
								5	1.5	1.5	262.64	264.14		
								6	0.4	0.4	264.14	264.54		
								CC(w/CC)	0.25	0.25	264.54	264.79	PAL	
								Totals:	7.79	7.79				
30X	10	610	266.6	276.2	9.6	8.22	85.6							
								1	1.5	1.5	266.6	268.1		
								2	1.1	1.1	268.1	269.2		
								3	1.5	1.5	269.2	270.7		
								4	1.5	1.5	270.7	272.2	BACT, HS	
								5	1.5	1.5	272.2	273.7		
								6	0.83	0.83	273.7	274.53		
								CC(w/6)	0.29	0.29	274.53	274.82	PAL	
								Totals:	8.22	8.22				
31X	10	800	276.2	285.9	9.7	9.88	101.9							
								1	1.5	1.5	276.2	277.7		
								2	1.5	1.5	277.7	279.2		
								3	1.5	1.5	279.2	280.7		
								4	1.4	1.4	280.7	282.1	IW	
								5	1.42	1.42	282.1	283.52	HS, BGAS	
								6	1.0	1.0	283.52	284.52		
								7	1.33	1.33	284.52	285.85		
								CC(w/CC)	0.23	0.23	285.85	286.08	PAL	
								Totals:	9.88	9.88				

**Table T2 (continued).**

Core	Date (July 2000)	Time (local)	Core depth (mbsf)		Length (m)		Recovery (%)	Section	Length (m)		Section depth (mbsf)		Catwalk samples	Comment
			Top	Bottom	Cored	Recovered			Liner	Curated	Top	Bottom		
32X	10	945	285.9	295.5	9.6	8.80	91.7							
								1	1.5	1.5	285.9	287.4		
								2	0.95	0.95	287.4	288.35		Dropped
								3	1.5	1.5	288.35	289.85		
								4	1.5	1.5	289.85	291.35	IW	
								5	1.5	1.5	291.35	292.85	HS	
								6	1.5	1.5	292.85	294.35		
								CC(w/CC)	0.35	0.35	294.35	294.7		
								Totals:	8.8	8.8				
33X	10	1110	295.5	305.1	9.6	9.76	101.7							
								1	1.5	1.5	295.5	297.0		
								2	1.5	1.5	297.0	298.5		
								3	1.5	1.5	298.5	300.0	HS, BGAS	
								4	1.5	1.5	300.0	301.5		
								5	1.5	1.5	301.5	303.0	BACT, WRS, WRY	
								6	1.5	1.5	303.0	304.5		
								7	0.46	0.46	304.5	304.96		
								CC(w/7)	0.3	0.3	304.96	305.26	PAL	
								Totals:	9.76	9.76				
34X	10	1300	305.1	314.8	9.7	6.21	64.0							
								1	1.5	1.5	305.1	306.6		
								2	1.5	1.5	306.6	308.1		
								3	1.5	1.5	308.1	309.6	HS, BGAS, IW	
								4	0.7	0.7	309.6	310.3		
								CC(w/CC)	1.01	1.01	310.3	311.31	PAL	
								Totals:	6.21	6.21				
35X	10	1440	314.8	324.4	9.6	9.01	93.9							
								1	1.5	1.5	314.8	316.3		
								2	1.5	1.5	316.3	317.8	BGAS	
								3	1.5	1.5	317.8	319.3		
								4	1.5	1.5	319.3	320.8	HS, IW	
								5	1.5	1.5	320.8	322.3		
								6	1.25	1.25	322.3	323.55		
								CC(w/CC)	0.26	0.26	323.55	323.81	PAL	
								Totals:	9.01	9.01				
36X	10	1600	324.4	334.0	9.6	9.58	99.8							
								1	1.5	1.5	324.4	325.9		
								2	1.5	1.5	325.9	327.4		
								3	1.5	1.5	327.4	328.9		
								4	1.5	1.5	328.9	330.4		
								5	1.5	1.5	330.4	331.9	HS, BGAS, IW	
								6	1.47	1.47	331.9	333.37		
								CC(w/CC)	0.61	0.61	333.37	333.98	PAL	
								Totals:	9.58	9.58				
37X	10	1710	334.0	343.6	9.6	9.26	96.5							
								1	1.5	1.5	334.0	335.5		
								2	1.5	1.5	335.5	337.0		
								3	1.5	1.5	337.0	338.5		
								4	1.5	1.5	338.5	340.0		
								5	1.5	1.5	340.0	341.5	HS, IW, BACT	
								6	1.27	1.27	341.5	342.77		
								CC(w/CC)	0.49	0.49	342.77	343.26		
								Totals:	9.26	9.26				
38X	10	1900	343.6	353.2	9.6	6.98	72.7							
								1	1.5	1.5	343.6	345.1		
								2	1.5	1.5	345.1	346.6		
								3	1.5	1.5	346.6	348.1	HS, BGAS, IW	
								4	1.5	1.5	348.1	349.6		
								5	0.61	0.61	349.6	350.21		
								CC(w/5)	0.37	0.37	350.21	350.58		
								Totals:	6.98	6.98				
39X	10	2100	353.2	362.9	9.7	2.18	22.5							
								1	1.5	1.5	353.2	354.7	HS, BGAS	
								2	0.44	0.44	354.7	355.14		
								CC(w/2)	0.24	0.24	355.14	355.38	PAL	
								Totals:	2.18	2.18				
40X	10	2235	362.9	372.5	9.6	6.15	64.1							
								1	1.5	1.5	362.9	364.4		

Table T2 (continued).

Core	Date (July 2000)	Time (local)	Core depth (mbsf)		Length (m)		Recovery (%)	Section	Length (m)		Section depth (mbsf)		Catwalk samples	Comment
			Top	Bottom	Cored	Recovered			Liner	Curated	Top	Bottom		
41X	11	20	372.5	382.1	9.6	3.31	34.5	2	1.5	1.5	364.4	365.9	IW	
								3	1.5	1.5	365.9	367.4	HS, BGAS	
								4	1.28	1.28	367.4	368.68		
								CC(w/CC)	0.37	0.37	368.68	369.05	PAL	
								Totals:	6.15	6.15				
42X	11	225	382.1	391.6	9.5	6.51	68.5	1	1.5	1.5	372.5	374.0	IW	
								2	1.5	1.5	374.0	375.5	BACT, HS, BGAS	
								CC(w/CC)	0.31	0.31	375.5	375.81	PAL	
								Totals:	3.31	3.31				
43X	11	520	391.6	401.2	9.6	3.91	40.7	1	1.5	1.5	382.1	383.6		
								2	1.5	1.5	383.6	385.1	HS, BGAS	
								3	1.5	1.5	385.1	386.6		
								4	1.5	1.5	386.6	388.1		
								5	0.22	0.22	388.1	388.32		
								CC(w/5)	0.29	0.29	388.32	388.61	PAL	
								Totals:	6.51	6.51				
44X	11	750	401.2	410.8	9.6	9.15	95.3	1	1.5	1.5	391.6	393.1	IW	
								2	1.5	1.5	393.1	394.6	HS, BGAS	
								3	0.69	0.69	394.6	395.29		
								CC(w/3)	0.22	0.22	395.29	395.51	PAL	
								Totals:	3.91	3.91				
190-1178B-	12	1345	0.0	395.0	9.6	9.15	95.3	1	0.87	0.87	401.2	402.07		
								2	1.45	1.45	402.07	403.52		
								3	1.5	1.5	403.52	405.02		
								4	1.5	1.5	405.02	406.52		
								5	1.5	1.5	406.52	408.02	WRY, WRS, BACT	
								6	0.87	0.87	408.02	408.89	HS, BGAS, IW	
								CC(w/CC)	1.46	1.46	408.89	410.35	PAL	
Totals:	9.15	9.15												
Totals:					410.8	340.19	82.8							
190-1178B-	12	1345	0.0	395.0	395.0	0.00	0.0							
2R	12	1500	395.0	400.0	5.0	4.01	80.2	1	1.5	1.5	395.0	396.5		
								2	1.16	1.16	396.5	397.66	BACT, HS, BGAS, IW	
								3	0.34	0.34	397.7	398.0		
								4	0.86	0.86	398.0	398.86		
								CC(w/4)	0.15	0.15	398.86	399.01	PAL	
3R	12	1655	400.0	409.6	9.6	5.43	56.6	1	1.5	1.5	400.0	401.5		
								2	1.5	1.5	401.5	403.0	HS, BGAS	
								3	1.5	1.5	403.0	404.5	IW	
								4	0.67	0.67	404.5	405.17		
								CC(w/4)	0.26	0.26	405.17	405.43	PAL	
4R	12	1900	409.6	419.3	9.7	6.60	68.0	1	1.5	1.5	409.6	411.1		
								2	1.5	1.5	411.1	412.6		
								3	1.5	1.5	412.6	414.1	BACT, HS, BGAS, IW	
								4	1.25	1.25	414.1	415.35	IW	
								5	0.59	0.59	415.35	415.94		
CC(w/5)	0.26	0.26	415.94	416.2	PAL									
5R	13	0215	419.3	429.0	9.7	4.91	50.6	1	1.5	1.5	419.3	420.8	IW, IW	
								2	1.5	1.5	420.8	422.3	HS, BGAS	
								3	1.5	1.5	422.3	423.8		
								4	0.2	0.2	423.8	424.0		
								CC(w/4)	0.21	0.21	424.0	424.21	PAL	
Totals:	4.91	4.91												

Table T2 (continued).

Core	Date (July 2000)	Time (local)	Core depth (mbsf)		Length (m)		Recovery (%)	Section	Length (m)		Section depth (mbsf)		Catwalk samples	Comment
			Top	Bottom	Cored	Recovered			Liner	Curated	Top	Bottom		
6R	13	0405	429.0	438.6	9.6	6.23	64.9							
								1	1.5	1.5	429.0	430.5	IW	
								2	1.5	1.5	430.5	432.0	HS, BGAS	
								3	1.5	1.5	432.0	433.5		
								4	1.51	1.51	433.5	435.01	BACT	
								CC(w/CC)	0.22	0.22	435.01	435.23	PAL	
								Totals:	6.23	6.23				
7R	13	0540	438.6	448.2	9.6	9.39	97.8							
								1	1.5	1.5	438.6	440.1	IW	
								2	1.5	1.5	440.1	441.6		
								3	1.5	1.5	441.6	443.1		
								4	1.5	1.5	443.1	444.6	HS, BGAS	
								5	1.5	1.5	444.6	446.1		
								6	1.5	1.5	446.1	447.6		
								CC(w/CC)	0.39	0.39	447.6	447.99	PAL	
								Totals:	9.39	9.39				
8R	13	0715	448.2	457.8	9.6	9.40	97.9							
								1	1.5	1.5	448.2	449.7	HS, BGAS	
								2	1.5	1.5	449.7	451.2		
								3	1.5	1.5	451.2	452.7		
								4	1.5	1.5	452.7	454.2		
								5	1.5	1.5	454.2	455.7		
								6	1.5	1.5	455.7	457.2		
								7	0.19	0.19	457.2	457.39		
								CC(w/7)	0.21	0.21	457.39	457.6	PAL	
								Totals:	9.4	9.4				
9R	13	0840	457.8	467.4	9.6	6.96	72.5							
								1	1.5	1.5	457.8	459.3		
								2	1.5	1.5	459.3	460.8	BACT, IW	
								3	1.5	1.5	460.8	462.3	HS, BGAS	
								4	1.5	1.5	462.3	463.8		
								5	0.69	0.69	463.8	464.49		
								CC(w/5)	0.27	0.27	464.49	464.76	PAL	
								Totals:	6.96	6.96				
10R	13	1015	467.4	477.1	9.7	4.92	50.7							
								1	0.81	0.81	467.4	468.21	IW	
								2	1.5	1.5	468.21	469.71	HS, BGAS	
								3	1.5	1.5	469.71	471.21		
								4	0.85	0.85	471.21	472.06		
								CC(w/4)	0.26	0.26	472.06	472.32	PAL	
								Totals:	4.92	4.92				
11R	13	1205	477.1	486.7	9.6	6.92	72.1							
								1	1.5	1.5	477.1	478.6		
								2	1.5	1.5	478.6	480.1	HS, BGAS	
								3	1.5	1.5	480.1	481.6		
								4	1.5	1.5	481.6	483.1		
								5	0.62	0.62	483.1	483.72		
								CC(w/5)	0.3	0.3	483.72	484.02	PAL	
								Totals:	6.92	6.92				
12R	13	1350	486.7	496.4	9.7	6.72	69.3							
								1	1.5	1.5	486.7	488.2		
								2	1.5	1.5	488.2	489.7		
								3	1.5	1.5	489.7	491.2		
								4	1.5	1.5	491.2	492.7	HS, BGAS, IW	
								5	0.41	0.41	492.7	493.11		
								CC(w/5)	0.31	0.31	493.11	493.42	PAL	
								Totals:	6.72	6.72				
13R	13	1620	496.4	506.0	9.6	2.67	27.8							
								1	1.5	1.5	496.4	497.9	BACT, IW	
								2	0.83	0.83	497.9	498.73	HS, BGAS	
								CC(w/2)	0.34	0.34	498.73	499.07	PAL	
								Totals:	2.67	2.67				
14R	13	1805	506.0	515.6	9.6	3.18	33.1							
								1	1.5	1.5	506.0	507.5	BACT, WRY, WRS, WR	
								2	1.43	1.43	507.5	508.93	HS, BGAS	
								CC(w/CC)	0.25	0.25	508.93	509.18	PAL	
								Totals:	3.18	3.18				

Table T2 (continued).

Core	Date (July 2000)	Time (local)	Core depth (mbsf)		Length (m)		Recovery (%)	Section	Length (m)		Section depth (mbsf)		Catwalk samples	Comment
			Top	Bottom	Cored	Recovered			Liner	Curated	Top	Bottom		
15R	13	1955	515.6	525.2	9.6	8.58	89.4							
								1	1.5	1.5	515.6	517.1		
								2	1.5	1.5	517.1	518.6		
								3	1.5	1.5	518.6	520.1	IW	
								4	1.5	1.5	520.1	521.6	HS, BGAS, WRC	
								5	1.5	1.5	521.6	523.1	WRTB	
								6	0.83	0.83	523.1	523.93		
								CC(w/6)	0.25	0.25	523.93	524.18	PAL	
								Totals:	8.58	8.58				
16R	13	2130	525.2	534.8	9.6	7.30	76.0							
								1	1.5	1.5	525.2	526.7		
								2	1.5	1.5	526.7	528.2	HS, BGAS	
								3	1.55	1.55	528.2	529.75	WRMT, HS, BGAS	
								4	1.45	1.45	529.75	531.2		
								5	0.96	0.96	531.2	532.16		
								CC(w/CC)	0.34	0.34	532.16	532.5	PAL	
								Totals:	7.3	7.3				
17R	13	2335	534.8	544.4	9.6	5.07	52.8							
								1	1.47	1.47	534.8	536.27	IW	
								2	1.5	1.5	536.27	537.77		
								3	1	1	537.77	538.77	HS, BGAS	
								4	0.78	0.78	538.77	539.55	BACT	
								CC(w/4)	0.32	0.32	539.55	539.87	PAL	
								Totals:	5.07	5.07				
18R	14	0145	544.4	554.0	9.6	6.68	69.6							
								1	1.5	1.5	544.4	545.9		
								2	1.5	1.5	545.9	547.4		
								3	1.5	1.5	547.4	548.9	HS, BGAS	
								4	1.5	1.5	548.9	550.4		
								5	0.44	0.44	550.4	550.84		
								CC(w/5)	0.24	0.24	550.84	551.08	PAL, WRTB	
								Totals:	6.68	6.68				
19R	14	0325	554.0	563.6	9.6	5.92	61.7							
								1	1.5	1.5	554	555.5		
								2	1.5	1.5	555.5	557	SMTCR	
								3	1.5	1.5	557	558.5	SMTCR, HS, BGAS	
								4	1.14	1.14	558.5	559.64	SMTCR	
								CC(w/4)	0.28	0.28	559.64	559.92	PAL	
								Totals:	5.92	5.92				
20R	14	0530	563.6	573.3	9.7	6.18	63.7							
								1	1.5	1.5	563.6	565.1		
								2	1.5	1.5	565.1	566.6		
								3	1.5	1.5	566.6	568.1	HS, BGAS	
								4	0.4	0.4	568.1	568.5	IW	
								5	1.02	1.02	568.5	569.52		
								CC(w/5)	0.26	0.26	569.52	569.78	PAL	
								Totals:	6.18	6.18				
21R	14	0755	573.3	582.9	9.6	5.98	62.3							
								1	1.5	1.5	573.3	574.8	BACT	
								2	1.5	1.5	574.8	576.3		
								3	1.5	1.5	576.3	577.8	HS, BGAS	
								4	1.25	1.25	577.8	579.05		
								CC(w/4)	0.23	0.23	579.05	579.28	PAL	
								Totals:	5.98	5.98				
22R	14	0955	582.9	592.5	9.6	5.24	54.6							
								1	1.38	1.38	582.9	584.28		
								2	1.5	1.5	584.28	585.78	IW	
								3	1.5	1.5	585.78	587.28	HS, BGAS	
								4	0.6	0.6	587.28	587.88		
								CC(w/CC)	0.26	0.26	587.88	588.14	PAL	
								Totals:	5.24	5.24				
23R	14	1205	592.5	602.1	9.6	3.97	41.4							
								1	1.5	1.5	592.5	594	BACT, WRY	
								2	1.5	1.5	594	595.5	HS, BGAS	
								3	0.69	0.69	595.5	596.19		
								CC(w/3)	0.28	0.28	596.19	596.47	PAL	
								Totals:	3.97	3.97				

Table T2 (continued).

Core	Date (July 2000)	Time (local)	Core depth (mbsf)		Length (m)		Recovery (%)	Section	Length (m)		Section depth (mbsf)		Catwalk samples	Comment	
			Top	Bottom	Cored	Recovered			Liner	Curated	Top	Bottom			
24R	14	1415	602.1	611.7	9.6	5.74	59.8								
								1	1.5	1.5	602.1	603.6			
								2	1.5	1.5	603.6	605.1	IW		
								3	1.5	1.5	605.1	606.6	HS, BGAS		
								4	1.02	1.02	606.6	607.62			
								CC(w/4)	0.22	0.22	607.62	607.84	PAL		
								Totals:	5.74	5.74					
25R	14	1640	611.7	621.4	9.7	3.42	35.3								
								1	1.5	1.5	611.7	613.2			
								2	1.0	1.0	613.2	614.2	HS, BGAS		
								3	0.64	0.64	614.2	614.84			
								CC(w/3)	0.28	0.28	614.84	615.12	PAL		
								Totals:	3.42	3.42					
26R	14	1900	621.4	631.0	9.6	3.22	33.5								
								1	1.5	1.5	621.4	622.9	IW		
								2	1.4	1.4	622.9	624.3	HS, BGAS		
								CC(w/CC)	0.32	0.32	624.3	624.62	PAL		
								Totals:	3.22	3.22					
27R	14	2115	631.0	640.7	9.7	4.24	43.7								
								1	1.5	1.5	631.0	632.5	IW, IW		
								2	1.5	1.5	632.5	634.0	HS, BGAS, BACT		
								3	0.78	0.78	634.0	634.78			
								CC(w/3)	0.46	0.46	634.78	635.24	PAL		
								Totals:	4.24	4.24					
28R	14	2340	640.7	650.4	9.7	4.60	47.4								
								1	1.5	1.5	640.7	642.2			
								2	1.5	1.5	642.2	643.7	HS, BGAS		
								3	1.3	1.3	643.7	645.0			
								CC(w/CC)	0.3	0.3	645.0	645.3			
								Totals:	4.6	4.6					
29R	15	0155	650.4	660.0	9.6	4.03	42.0								
								1	1.5	1.5	650.4	651.9	BACT		
								2	1.5	1.5	651.9	653.4	HS, BGAS		
								3	0.73	0.73	653.4	654.13			
								CC(w/3)	0.3	0.3	654.13	654.43	WRS, PAL		
								Totals:	4.03	4.03					
30R	15	0355	660.0	669.6	9.6	4.87	50.7								
								1	1.5	1.5	660.0	661.5	HS, BGAS		
								2	1.5	1.5	661.5	663.0			
								3	1.5	1.5	663.0	664.5			
								CC(w/CC)	0.37	0.37	664.5	664.87	PAL		
								Totals:	4.87	4.87					
31R	15	0545	669.6	679.2	9.6	3.58	37.3								
								1	1.5	1.5	669.6	671.1	HS, BGAS		
								2	1.5	1.5	671.1	672.6			
								3	0.33	0.33	672.6	672.93			
								CC(w/3)	0.25	0.25	672.93	673.18	PAL		
								Totals:	3.58	3.58					
Totals:					679.2	165.96	24.40								

Notes: Catwalk samples: IW = interstitial water, HS = headspace, PAL = paleontology, VAC = vacutainer. All other abbreviations are sample codes for postcruise research (see the "Sample Codes" database query). CC = core catcher (number in parenthesis indicated which section the core catcher is stored with). This table is also available in ASCII format.

**Table T3.** Summary of stratigraphic relations, Site 1178.

Unit	Facies name	Interval (cm)		Depth (mbsf)		Thickness (m)	Stratigraphic age	Lithologic description	Processes of formation
		Top	Bottom	Top	Bottom				
IA	Upper slope apron	190-1178A-1H-1, 0	190-1178A-12X-1, 0	0.00	94.40	94.40	Quaternary to Pliocene	Hemipelagic, nannofossil-rich mud, sandy mud, volcanic ash; intervals of contorted stratification	Hemipelagic settling, volcanic ash falls; deformed by slumping
IB	Middle slope apron	12X-1, 0	15X-3, 80	94.40	127.00	32.60	Pliocene	Hemipelagic mud and sandy mud, abundant silty sand turbidites, minor mud-supported gravel, lapilli gravel; intervals of contorted stratification	Hemipelagic settling, sandy mudflows, turbidity currents, debris flows
IC	Lower slope apron	15X-3, 80	23X-1, 0	127.00	199.20	72.20	Pliocene to late Miocene	Hemipelagic mud (locally nannofossil rich), sandy mud, minor volcanic ash and lapilli-gravel; intervals of contorted stratification, strongly deformed mud toward base	Hemipelagic settling, debris flows, rare ash falls; deformed by slumping
IIA	Accreted axial trench-wedge facies	190-1178A-23X-1, 0	190-1178B-4R-1, 140	199.20	411.00	211.80	late Miocene	Hemipelagic mudstone, sandy mudstone, abundant sand and silty sand turbidites, rare pebbly mudstone; highly deformed	Hemipelagic settling, frequent turbidity currents, debris flows; accreted by frontal offscraping
IIB	Accreted outer trench-wedge facies	190-1178B-4R-1, 140	190-1178B-20R-1, 35	411.00	563.95	152.95	late Miocene	Hemipelagic mudstone, sandy mudstone, sporadic silt to sandy silt turbidites; highly deformed	Hemipelagic settling, occasional turbidity currents; accreted by frontal offscraping
IIC	Accreted axial trench-wedge facies	20R-1, 35	31R-CC, 25	563.95	673.18	109.23	late Miocene	Hemipelagic mudstone, sandy mudstone, abundant sand and silty sand turbidites; highly deformed	Hemipelagic settling, frequent turbidity currents; accreted by frontal offscraping

**Table T4.** Peak intensities and peak areas from X-ray diffraction analysis of bulk-powder sediment samples, Holes 1178A and 1178B. (Continued on next page.)

Core, section, interval (cm)	Depth (mbsf)	X-ray diffraction peak intensity (cps)								X-ray diffraction peak area (total counts)							
		Smectite + chlorite	Illite	Chlorite + kaolinite	(101) Quartz	Plagioclase	Calcite	(100) Quartz	(101) Cristobalite	Smectite + chlorite	Illite	Chlorite + kaolinite	(101) Quartz	Plagioclase	Calcite	(100) Quartz	(101) Cristobalite
190-1178A-																	
1H-1, 136-137	1.36	31	72	72	1,813	472	1,047	289	107	961	1,706	1,396	23,473	12,731	13,757	4,052	1,702
2H-4, 136-137	8.76	36	101	115	1,765	354	1,653	345	87	804	2,193	2,284	23,785	9,615	23,115	4,569	1,292
3H-4, 135-136	18.25	45	78	81	1,908	428	823	328	137	1,738	1,815	1,619	23,998	9,736	10,997	4,419	1,940
4H-6, 132-133	29.72	47	91	108	2,675	471	457	480	108	1,648	2,029	2,241	34,829	14,368	6,609	6,365	1,558
5H-4, 135-136	37.25	48	92	104	2,358	502	536	431	174	1,706	2,151	2,462	30,972	12,615	8,218	6,065	2,103
6H-4, 135-136	46.75	54	107	131	2,839	744	394	473	141	1,799	2,584	2,747	36,513	16,556	5,563	6,250	1,890
7H-3, 138-139	54.78	48	92	107	2,182	350	614	387	125	2,137	2,217	2,305	28,937	10,707	8,294	5,269	1,662
8H-4, 133-134	63.33	52	105	117	2,411	383	524	424	127	2,013	2,562	2,569	32,368	12,007	7,335	5,865	1,674
9X-5, 132-133	72.06	44	90	86	2,485	405	592	379	116	1,912	2,221	1,877	31,731	10,729	8,343	5,359	1,585
11X-4, 126-127	90.56	51	100	107	2,812	456	209	542	118	1,684	2,598	2,693	36,115	11,881	2,861	7,176	1,680
12X-5, 134-135	101.65	49	108	118	3,637	494	243	595	106	1,909	2,923	2,492	46,236	14,947	3,366	7,592	1,418
13X-4, 130-131	109.80	53	105	105	2,872	551	280	550	136	1,742	3,540	2,713	37,173	17,004	4,027	7,418	1,960
13X-5, 121-122	111.21	43	93	100	3,048	630	362	756	126	1,291	3,142	2,362	37,408	15,693	4,851	9,359	1,659
14X-4, 133-134	119.43	51	138	120	2,964	491	348	471	163	2,263	3,539	2,662	38,064	12,663	5,113	6,559	2,116
15X-4, 132-133	129.02	57	121	146	2,635	701	204	469	220	2,109	3,239	3,182	34,763	17,088	2,854	6,416	2,799
16X-4, 128-129	138.48	51	114	108	2,382	455	231	492	105	2,421	3,427	2,690	31,979	13,796	3,664	6,860	1,496
17X-2, 127-128	144.97	58	114	107	2,487	500	156	493	122	3,038	2,652	2,595	33,149	14,147	2,256	7,269	1,752
18X-4, 128-129	156.44	50	112	105	2,746	432	143	428	126	2,981	3,206	2,814	35,094	11,791	2,226	6,146	1,642
19X-3, 123-124	165.63	53	113	109	2,339	400	110	426	121	1,951	3,408	2,844	31,700	11,860	1,826	6,052	1,895
20X-5, 53-54	176.11	45	94	92	2,348	387	504	419	109	1,769	2,876	2,023	31,802	10,552	7,045	6,217	1,715
21X-4, 119-120	186.09	43	101	79	2,364	487	717	462	104	2,342	2,739	1,939	30,620	10,746	10,665	6,262	1,335
22X-1, 103-104	190.83	47	119	98	2,638	548	366	474	125	1,567	3,450	2,105	35,268	12,508	5,374	6,716	1,766
22X-4, 8-9	194.38	41	97	71	3,190	475	515	581	96	1,683	2,597	1,632	40,907	11,874	7,799	7,493	1,237
23X-2, 120-121	201.90	43	112	95	3,671	796	61	489	153	2,236	3,441	2,738	46,358	18,432	1,021	7,302	1,884
24X-1, 122-123	210.02	41	125	85	2,573	434	83	522	219	2,189	4,460	2,612	35,101	13,367	1,614	7,675	3,044
25X-2, 117-118	221.04	60	120	127	2,468	425	279	445	130	2,772	3,078	3,224	33,665	11,369	4,126	6,393	1,762
27X-3, 123-124	242.03	56	126	116	2,066	640	120	361	105	2,869	4,108	3,558	28,815	13,241	1,716	5,875	1,504
28X-4, 129-130	253.19	57	133	115	2,320	458	139	395	117	3,037	3,378	2,888	32,483	11,243	1,977	6,201	1,698
29X-3, 124-125	260.95	45	121	108	2,303	377	99	444	119	2,589	2,760	3,129	30,797	10,584	1,583	6,800	1,690
31X-4, 116-117	281.86	43	88	78	2,232	361	125	405	122	1,685	3,588	2,735	29,498	9,770	1,798	6,099	1,684
32X-4, 122-123	291.07	77	159	152	2,285	431	152	578	289	3,071	3,820	3,606	31,995	11,409	2,146	7,537	3,130
33X-5, 121-122	302.71	42	68	68	1,749	316	104	272	76	2,804	2,255	2,079	32,944	11,134	2,375	6,362	1,610
34X-3, 122-123	309.32	57	110	113	2,183	354	69	425	106	3,596	3,006	3,089	30,791	11,393	1,055	6,620	1,609
35X-4, 123-124	320.53	45	88	82	2,030	341	121	382	110	3,672	2,002	2,229	27,152	9,791	1,557	6,306	1,565
36X-1, 84-85	325.24	49	112	97	2,524	482	103	457	100	2,832	2,790	2,995	35,603	12,671	1,496	7,263	1,543
36X-1, 89-90	325.29	54	109	95	3,670	844	0	625	136	2,413	2,239	2,317	49,321	25,642	0	8,041	1,866
36X-1, 91-92	325.31	54	106	104	2,345	494	0	433	116	3,660	2,967	3,123	34,209	13,299	0	7,054	2,022
36X-5, 124-125	331.64	66	127	121	3,012	641	110	481	148	2,853	3,431	2,907	39,743	18,138	1,714	6,753	2,006
37X-5, 119-120	341.19	68	131	125	2,685	422	144	554	127	3,626	3,073	2,979	36,712	12,308	2,305	7,728	1,947
38X-3, 126-127	347.86	69	112	126	2,059	597	211	413	111	3,065	3,229	3,158	28,922	16,104	2,915	6,101	1,824
39X-1, 19-20	353.39	36	82	78	2,840	460	129	433	116	1,190	2,781	1,962	40,124	13,689	2,449	6,879	1,626
40X-2, 116-117	365.56	46	85	95	5,552	623	0	1,143	109	1,245	3,171	2,152	68,035	14,727	0	13,447	1,330
41X-1, 93-94	373.43	44	72	82	1,985	368	227	383	113	2,051	2,016	2,014	26,642	9,859	3,286	5,752	1,550
42X-3, 96-97	386.06	44	86	79	2,368	640	85	398	124	3,609	2,199	2,274	31,354	13,669	1,457	6,114	1,823
43X-1, 125-126	392.85	49	96	96	2,170	411	86	408	101	2,142	3,127	2,832	29,280	10,705	1,364	5,911	1,401
44X-5, 121-122	407.73	54	108	130	2,060	355	152	739	86	2,313	2,906	3,313	30,832	9,507	2,154	9,074	1,112

Table T4 (continued).

Core, section, interval (cm)	Depth (mbsf)	X-ray diffraction peak intensity (cps)								X-ray diffraction peak area (total counts)							
		Smectite + chlorite	Illite	Chlorite + kaolinite	(101) Quartz	Plagioclase	Calcite	(100) Quartz	(101) Cristobalite	Smectite + chlorite	Illite	Chlorite + kaolinite	(101) Quartz	Plagioclase	Calcite	(100) Quartz	(101) Cristobalite
190-1178B-																	
2R-2, 94-95	397.44	44	85	74	1,740	290	237	314	90	3,290	3,453	1,913	23,901	8,660	3,679	5,178	1,511
3R-3, 146-147	404.46	36	130	104	1,944	348	75	381	106	872	4,210	3,015	27,301	9,482	1,099	6,155	1,445
4R-2, 148-149	412.58	54	146	149	2,758	595	0	563	131	1,485	4,690	3,276	37,843	15,174	0	7,478	1,625
4R-3, 24-25	412.84	31	86	56	2,031	1,077	62	312	263	938	6,117	1,182	26,565	28,516	1,151	4,997	3,736
4R-3, 125-126	413.85	60	152	137	2,815	593	0	493	116	1,504	4,666	2,948	37,819	14,669	0	6,921	1,448
5R-1, 116-117	420.46	58	105	116	1,837	269	227	364	115	1,819	3,160	3,204	25,271	8,818	3,277	5,693	1,450
6R-1, 34-35	429.34	54	124	128	2,116	393	101	390	101	1,796	3,946	3,145	29,355	11,763	1,425	5,654	1,488
6R-1, 123-124	430.23	33	98	46	1,465	489	0	300	247	4,595	4,066	1,191	19,691	16,837	0	5,904	4,534
8R-5, 149-150	455.69	54	150	118	3,247	473	78	526	169	1,887	3,629	2,759	43,901	13,546	1,087	7,399	2,119
8R-6, 68-69	456.38	51	128	130	2,906	432	0	444	125	2,076	4,311	2,873	38,259	12,486	0	6,405	1,448
9R-2, 115-116	460.45	43	109	110	2,107	620	146	397	92	2,352	3,804	2,750	29,141	14,055	2,067	6,543	1,165
10R-1, 45-46	467.85	50	113	110	2,807	405	26	528	106	1,333	4,087	3,010	37,404	12,461	298	7,543	1,491
11R-1, 89-90	477.99	30	87	79	4,080	767	86	744	135	588	2,950	1,737	51,412	20,441	1,495	9,494	1,558
12R-4, 112-113	492.32	42	103	96	2,371	377	62	452	105	1,199	4,241	2,611	32,247	11,077	1,197	6,654	1,336
13R-2, 80-81	498.70	40	96	85	3,154	676	75	559	127	866	3,753	1,836	41,230	16,881	1,140	8,008	1,707
14R-1, 94-95	506.94	51	125	125	2,461	414	44	465	119	1,718	4,265	3,048	33,933	11,941	838	6,530	1,374

**Table T5.** Normalized relative mineral abundances based on X-ray diffraction analysis of random bulk-sediment powders, Site 1178. (Continued on next page).

Unit	Core, section, interval (cm)	Depth (mbsf)	Normalized relative abundance (wt%)			
			Total clay minerals	Quartz	Plagioclase	Calcite
I	190-1178A-					
	1H-1, 136-137	1.36	26	26	17	31
	2H-4, 136-137	8.76	26	20	11	43
	3H-4, 135-136	18.25	33	29	13	25
	4H-6, 132-133	29.72	32	37	18	12
	5H-4, 135-136	37.25	34	34	16	16
	6H-4, 135-136	46.75	35	36	20	9
	7H-3, 138-139	54.78	37	33	14	17
	8H-4, 133-134	63.33	38	34	15	13
	9X-5, 132-133	72.06	35	35	13	16
	11X-4, 126-127	90.56	40	40	16	4
	12X-5, 134-135	101.65	38	43	16	4
	13X-4, 130-131	109.80	42	34	19	5
	13X-5, 121-122	111.21	38	36	19	7
	14X-4, 133-134	119.43	44	35	14	7
	15X-4, 132-133	129.02	42	34	20	3
	16X-4, 128-129	138.48	46	33	16	5
	17X-2, 127-128	144.97	44	37	17	2
	18X-4, 128-129	156.44	48	37	13	1
	19X-3, 123-124	165.63	48	35	16	1
	20X-5, 53-54	176.11	40	34	13	13
	21X-4, 119-120	186.09	38	31	12	19
	22X-1, 103-104	190.83	42	34	15	9
	22X-4, 8-9	194.38	35	39	13	13
	Mean Unit I:		38	34	16	12
II	190-1178A-					
	23X-2, 120-121	201.90	41	41	19	0
	24X-1, 122-123	210.02	52	33	15	0
	25X-2, 117-118	221.04	45	36	13	6
	27X-3, 123-124	242.03	55	30	16	0
	28X-4, 129-130	253.19	50	36	13	1
	29X-3, 124-125	260.95	48	38	14	1
	31X-4, 116-117	281.86	52	34	14	1
	32X-4, 122-123	291.07	53	33	13	1
	33X-5, 121-122	302.71	43	41	14	2
	34X-3, 122-123	309.32	51	36	13	0
	35X-4, 123-124	320.53	48	39	13	1
	36X-1, 84-85	325.24	45	40	15	0
	36X-1, 89-90	325.29	31	43	25	0
	36X-1, 91-92	325.31	48	37	15	0
	36X-5, 124-125	331.64	44	37	19	0
	37X-5, 119-120	341.19	47	38	13	1
	38X-3, 126-127	347.86	47	31	19	3
	39X-1, 19-20	353.39	38	42	18	3
	40X-2, 116-117	365.56	34	53	14	0
	41X-1, 93-94	373.43	41	37	15	6
	42X-3, 96-97	386.06	45	39	16	0
	43X-1, 125-126	392.85	50	35	15	0
	44X-5, 121-122	407.73	48	37	13	2
	190-1178B-					
	2R-2, 94-95	397.44	55	30	10	5
	3R-3, 146-147	404.46	56	29	15	0
	4R-2, 148-149	412.58	50	33	17	0
	4R-3, 24-25	412.84	52	18	30	0
	4R-3, 125-126	413.85	50	33	17	0
	5R-1, 116-117	420.46	50	31	13	6
	6R-1, 34-35	429.34	53	31	16	0
	6R-1, 123-124	430.23	58	24	18	0
	8R-5, 149-150	455.69	44	41	15	0
	8R-6, 68-69	456.38	51	36	14	0
	9R-2, 115-116	460.45	51	31	17	1
	10R-1, 45-46	467.85	49	36	16	0
	11R-1, 89-90	477.99	32	45	23	0

**Table T5 (continued).**

Unit	Core, section, interval (cm)	Depth (mbsf)	Normalized relative abundance (wt%)			
			Total clay minerals	Quartz	Plagioclase	Calcite
	12R-4, 112-113	492.32	53	33	15	0
	13R-2, 80-81	498.70	42	38	20	0
	14R-1, 94-95	506.94	52	33	15	0
	Mean Unit II:		47	36	16	1

Table T6. Structural data, Hole 1178A. (See table notes. Continued on next seven pages.)

Core, section, interval (cm)	Depth (mbsf)	Cr az. (°)	Cr dip (°)	Pm az.	Pm plunge	Identifier	Notes
190-1178A-							
1H	0						
2H	2.90	0	0			Bedding	
3H	12.40	0	0			Bedding	
4H-6, 31-35	28.71	335	30	299	30	Bedding	
4H-7, 20-21	30.10	299	22	263	22	Bedding	
4H-7, 69-70	30.59	274	52	238	52	Bedding	
5H-2, 50-63	33.40	160	62	246	62	Bedding	
5H-3, 68-72	35.08	154	35	240	35	Bedding	
5H-3, 110-115	35.50	183	36	269	36	Bedding	
5H-4, 123-130	37.13	165	51	251	51	Bedding	
5H-6, 99-101	39.89	286	42	12	42	Bedding	
5H-7, 63-80	41.03					Fold	In ash layer
6H-2, 50-60	42.90	20	74	108	74	Bedding	
6H-3, 50-65	44.40	15	61	103	61	Bedding	
6H-4, 65-73	46.05	20	54	108	54	Bedding	
6H-5, 60-73	47.50	356	64	84	64	Bedding	
6H-5, 139-145	48.29	14	61	102	61	Bedding	
7H-2, 144-148	53.34	325	45	71	45	Bedding	
7H-2, 65-67	52.55	0	14	106	14	Bedding	
7H-4, 135-137	56.25	0	8	106	8	Bedding	
7H-4, 49-72	55.39					Fold?	Possibly core induced
8H-3, 69-72	61.19	301	39	261	39	Bedding	
8H-2, 106-106	60.06	0	90			Bedding	
8H-4, 33-40	62.33					Fold	
8H-5, 110-120	64.60					Fold?	Possibly core induced
9X	65.60						No structures
10X							Empty core
11X	84.80						Highly biscuited
12X-1, 1-140	94.41						Comminuted biscuited material
12X-2, 6-50	95.87					Bedding	Vertical with some horizontal axis folds
12X-3, 37-41	97.68	58	66			Bedding	Small biscuit size, reorientation not possible
12X-4, 20-21	99.01	0	0			Bedding	
12X-5, 4-47	100.35	15	48			Bedding	Fissility and/or lamination
12X-6, 45-54	102.26	331	47			Bedding	Fissility and/or lamination
12X-6, 62-64	102.43	126	18			Bedding	Fissility and/or lamination
13X-3, 38-41	107.38					Bedding	Fissility and/or lamination
13X-4	108.50						Highly broken core, drilling induced
13X-5	110.00						Highly broken core, drilling induced
13X-6, 85-97	112.35	33	65			Bedding	
14X-3, 34-35	116.94	0	0			Bedding	Fissility and/or lamination
14X-4, 81-82	118.91	28	20			Bedding	Fissility and/or lamination
14X-6, 57-59	121.67	326	36			Bedding	Fissility and/or lamination
15X-3, 65-70	126.85	329	77			Bedding	Fissility and/or lamination
15X-3, 52-57	126.72	118	81			Bedding	Fissility and/or lamination
15X-5, 35-37	129.55	5	86			Bedding	Fissility and/or lamination
16X-2, 52-53	134.72	0	0			Bedding	Highly biscuited
17X	142.20	0	0			Bedding	Highly biscuited
18X	151.80						Highly biscuited
19X	161.40						Highly biscuited
20X	171.00						Highly biscuited
20X-2, 108-110	172.42	175	45	150	45	Black seam	(106-112)
20X-2, 108-110	172.42	162	36	137	36	Black seam	(106-112)
20X-2, 108-110	172.42	238	60	213	60	Bedding	Zoophycos (106-112)
20X-2, 113-118	172.47	230	62	205	62	Bedding	Zoophycos (113-118)
20X-4, 101-103	175.35	232	45	224	45	Normal fault	3- to 4-mm offset (97-104)
20X-4, 100-103	175.34	333	38	325	38	Bedding	Zoophycos (97-104)
20X-4, 101-102	175.35					Black seam	(97-104)
21X-5, 53-53	186.93	273	50		50	Bedding	Zoophycos (51-55)
21X-6, 45-45	188.35	270	3		3	Black seam	(45-49)
22X-1, 131-135	191.11	330	87		87	Fault	2-mm displacement (131-135)
22X-1, 54-57	190.34	90	90	30	90	Fault	>20-mm displacement (57-64)
22X-1, 54-57	190.34	150	42	90	42	Bedding	Zoophycos (57-64)
22X-2, 59-66	191.89	90	90	65	90	Fault	>2-mm displacement (59-66)
22X-2, 59-66	191.89	240	63	215	63	Fault or fracture	(59-66)
22X-2, 104-107	192.34	311	29	243	29	Fault	>20-mm displacement (102-107)
22X-2, 110-110	192.40	264	44	222	44	Black seam	(108-113)
22X-3, 0-62	192.80					Brecciated zone	
23X	199.20	0	0		0	Bedding	Highly broken silt layers

Table T6 (continued).

Core, section, interval (cm)	Depth (mbsf)	Cr az. (°)	Cr dip (°)	Pm az.	Pm plunge	Identifier	Notes
23X-1, 35-40	199.55					Black seam	Subvertical
24X	208.80	0	0		0	Bedding	Highly broken silt layers
25X	218.40	0	0		0	Bedding	Highly broken silt layers
26X	228.10	0	0		0	Bedding	
26X-1, 0-53	228.10					Soft sediment deformation	Possibly liquefaction and/or drilling disturbance
27X-3, 33-35	241.13	317	28	117	28	Bedding	
27X-4, 101-103	243.31	90	63		63	Fault	Apparent orientation only
27X-4, 101-105	243.31	0	5		5	Bedding	Slightly kinked
27X-6, 101-105	246.31	180	30		30	Bedding	
27X-6, 105-108	246.35	21	45		45	Fracture	
27X-7, 15-19	246.75	219	31		31	Bedding	
28X-4, 8-10	251.98	313	36	305	36	Bedding	
28X-4, 60-61	252.50	105	29	227	29	Bedding	
28X-6, 57-59	255.47	341	35		35	Bedding	
29X	257.00						Biscuited massive silty clay
30X-3, 96-98	270.16	0	17	315	17	Bedding	
30X-4, 103-106	271.73	330	23		23	Bedding	
30X-5, 15-18	272.35	314	35	56	35	Bedding	
30X-5, 25-27	272.45	323	16		16	Bedding	
30X-5, 71-74	272.91	306	32		32	Bedding	
31X-1	276.20						
31X-2, 92-96	278.62	8	26		26	Bedding	
31X-3, 66-70	279.86	205	19		19	Bedding	
31X-4, 54-63	281.24	346	31	196	31	Bedding	Bedding with parallel fissility
31X-5, 14-22	282.24					Fractures	Irregular hairline fractures, drilling induced?
32X-1, 35-37	286.25	33	14		14	Bedding	
32X-1, 83-84	286.73	240	8		8	Bedding	
32X-2	287.40						Irregular arrays of hairline fracture inside biscuits
32X-3, 22-29	288.57	303	37		37	Bedding	Parallel fissility
32X-3, 138-143	289.73	304	30		30	Bedding	
32X-5, 40-44	291.75	203	27		27	Bedding	
32X-6, 49-52	293.34	187	28	162	28	Bedding	
32X-6, 123-140	294.08	332	77	307	77	Fault	Constrasting material crossing biscuits
33X-1, 143-145	296.93	332	22	2	22	Bedding	
33X-2, 26-28	297.26	119	41	239	41	Bedding	
33X-2, 109-112	298.09	342	24		24	Bedding	
33X-4, 17-19	300.17	311	19		19	Bedding	
33X-4, 55-58	300.55	320	25		25	Bedding	
33X-5, 33-36	301.83	339	23		23	Bedding	
33X-6, 110-112	304.10	162	30	322	30	Bedding	
34X-2, 33-42	306.93	142	67	117	67	Fault	
34X-2, 121-126	307.81	259	32	313	32	Fissility	(121-126)
34X-3, 102-106	309.12	25	27	230	27	Fissility	(102-106)
35X-2, 19-27	316.49	213	34	350	34	Bedding	(19-32)
35X-2, 123-127	317.53	0	24	164	24	Bedding	(123-127)
35X-3, 115-118	318.95	0	0		0	Bedding	(115-118)
35X-4, 42-46	319.72	0	28		28	Bedding	(42-54)
35X-4, 93-97	320.23	180	23	315	23	Bedding	(92-99)
35X-6, 48-49	322.78	0	12		12	Bedding	
36X-1, 117-124	325.57	144	34		34	Bedding	(117-125)
36X-2, 133-136	327.23	205	27	165	27	Bedding	(128-135)
36X-5, 34-37	330.74	180	26	165	26	Bedding	(34-44)
37X-1, 127-128	335.27	341	15		15	Bedding	
37X-1, 130-132	335.30	310	60		60	Fault?	
37X-1, 135-137	335.35	217	40		40	Normal fault	20-mm displacement
37X-1, 137-139	335.37	338	26		26	Bedding	
37X-1, 146-150	335.46	37	38		38	Fault	
37X-3, 5-10	337.05	332	42		42	Dipping contact	(3-13?)
37X-4, 30-33	338.80	19	40		40	Fault	(30-33)
37X-4, 30-33	338.80	141	30		30	Bedding	(30-33)
37X-5, 77-79	340.77	35	31		31	Bedding	
37X-6, 102-104	342.52	69	47		47	Normal fault	>40-mm displacement
37X-6, 103-104	342.53	126	30		30	Bedding	
38X-1, 58-60	344.18	304	16	320	16	Bedding	(57-62)
38X-2, 41-44	345.51	180	28		28	Color band	(40-44)
38X-2, 131-132	346.41	226	29	231	29	Color band	(130-133)
38X-3, 75-76	347.35	221	19	224	19	Bedding	(71-79)
38X-4, 27-28	348.37	312	25		25	Bedding	(26-30)
39X	353.20						No structures

Table T6 (continued).

Core, section, interval (cm)	Depth (mbsf)	Cr az. (°)	Cr dip (°)	Pm az.	Pm plunge	Identifier	Notes
40X-1, 13-140	363.03					Sediment breccia	
40X	362.90	0	0		0	Bedding	
40X-4, 112-114	368.52	152	50		50	Deformation band	(110-116)
41X	372.50	0	0		0	Bedding	
41X-1, 104-108	373.54					Inclined fracture set	
41X-2, 126-130	375.26					Veins	Filled with drilling (?) mud
41X-3, 12-13		11	24		24	Normal fault	(2-16)
41X-3, 68-71						Brecciated zone	
42X	382.10	0	0		0	Bedding	
42X-3, 45-50	385.55					Fault	(44-50)
42X-3, 61-94	385.71					Veins	Filled with drilling (?) mud
42X-4, 57-76	387.17					Veins	Filled with drilling (?) mud
42X-4, 10-56	386.70					Fault	Disrupted and faulted interval, probably coring enhanced
43X-1, 66-69	392.26	90	47		47	Normal fault	Offset >17 mm
43X-1, 104-107	392.64	215	43		43	Fault	
43X-1, 109-114	392.69	323	16		16	Bedding	
44X-3, 102-107	404.54	291	26		26	Bedding	
44X-3, 140-147	404.92	195	30		30	Normal fault	10-mm offset, healed (140-144)
44X-4, 6-14	405.08					Fracture	Network of hairline fractures
44X-5, 17-18	406.69	0	12		12	Bedding	
44X-CC, 15-25	409.04	200	66		66	Fault	Average of 4 faults 4-mm offset each one (15-19)
190-1178B-							
2R-1, 36-49	395.36	339	31	229	31	Foliation	Millimeter-scale partings (36-49)
2R-1, 49-61	395.49	279	34	259	34	Foliation	(49-61)
2R-1, 80-112	395.80					Fracture set	2-cm fracture spacing
2R-1, 67-80	395.67	198	52		52	Foliation	(67-80)
2R-2, 54-80	397.04	0	42		42	Fault	Doubtful origin
2R-3, 10-20	397.76	180	22		22	Deformation band	Faultlike deformation band
2R-4, 0-80	398.00	6	41	266	41	Foliation	Slightly kinked (0-80)
2R-4, 49-59	398.49	189	60	89	60	Deformation band	Kinklike band (0-80)
3R-1, 112-114	401.12	139	38		38	Foliation	
3R-1, 112-114	401.12	150	43	70	43	Fracture set	(108-127)
3R-1, 110-111	401.10	109	23	29	23	Fracture set	(108-127)
3R-2, 88-90	402.38	45	32		32	Foliation	(82-125)
3R-2, 88-90	402.38	350	70		70	Fracture set	1- to 2-cm spacing, cuts foliation (82-125)
3R-3, 68-72	403.68	12	43		43	Bedding	(20-75)
3R-3, 52-53	403.52	12	64		64	Foliation	(20-75)
3R-3, 145-147	404.45	46	43		43	Foliation	(137-150)
3R-3, 144-145	404.44	94	75	259	75	Fracture set	(137-150)
3R-4, 0-4	404.50	37	47		47	Foliation	(0-34)
3R-4, 22-24	404.72	56	38		38	Bedding	(0-34)
4R-2, 10-17	411.20	249	21		21	Bedding	
4R-2, 34-37	411.44	265	59	235	59	Foliation	
4R-2, 34-37	411.44	103	32	73	32	Fracture set	
4R-2, 51-61	411.61	150	28		28	Foliation	
4R-2, 51-61	411.61	233	38		38	Foliation	Second measurement to suggest anastomosing aspect
4R-2, 61-118	411.71	345	15	135	15	Foliation	
4R-2, 119-150	412.29	327	75	152	75	Foliation	
4R-3, 23-34	412.83	340	52		52	Bedding	
4R-3, 40-66	413.00	315	79	160	79	Foliation	(15-67)
4R-3, 113-129	413.73	260	55	200	55	Foliation	
4R-4, 72-97	414.82	236	38	239	38	Foliation	
4R-4, 116-126	415.26	193	66	154	66	Foliation	
4R-5, 0-7	415.35	201	48		48	Foliation	
4R-5, 0-8	415.35	198	54		54	Bedding	
4R-5, 7-10	415.42	151	22		22	Fault	(0-10) Two parallel faults, no sense indication
4R-5, 21-30	415.56	217	57	261	57	Fault	(0-43)
5R-1, 13-15	419.43	24	24		24	Foliation	
5R-1, 25-29	419.55	0	41	290	41	Fracture set	
5R-1, 29.5-30	419.595	180	6	110	6	Fracture set	
5R-1, 33-33.5	419.63	30	8		8	Fracture set	
5R-1, 44-50	419.74	10	40	30	40	Foliation	
5R-1, 56-57	419.86	26	22		22	Fracture set	
5R-1, 80-83	420.10	316	34		34	Bedding	Color band
5R-2, 5-6	420.85	118	20	53	20	Bedding	Color band
5R-2, 5-6	420.85	155	30	90	30	Fracture set	
5R-2, 7-9	420.87	154	11	89	11	Fracture set	Slicks: 0-10 degree azimuth
5R-2, 7-9	420.87	111	37	46	37	Fracture set	Slicks: 45-60 degree azimuth
5R-2, 24-25	421.04	21	39	261	39	Fracture set	No slicks
5R-2, 27-28	421.07	52	24	292	24	Fracture set	Bedding parallel

Table T6 (continued).

Core, section, interval (cm)	Depth (mbsf)	Cr az. (°)	Cr dip (°)	Pm az.	Pm plunge	Identifier	Notes
5R-2, 37-40	421.17	0	28	240	28	Bedding	
5R-2, 37-40	421.17	17	57	257	57	Fracture set	
5R-3, 0-7	422.30	216	44	146	44	Fracture set	
5R-3, 0-7	422.30	172	67	102	67	Fracture set	
5R-3, 0-7	422.30	220	55	150	55	Foliation	
5R-3, 0-7	422.30	309	13	239	13	Fracture set	
5R-3, 10-13	422.40	215	39	155	39	Fracture set	
5R-3, 26-27	422.56	0	35		35	Fracture set	
5R-3, 28-30	422.58	41	32	241	32	Fracture set	
5R-3, 48-53	422.78	5	65		65	Fracture set	
5R-3, 54-56	422.84	202	39		39	Fracture set	
5R-3, 57-60	422.87	356	55	231	55	Fracture set	
5R-3, 54-55	422.84	270	79		79	Fracture set	
5R-3, 99-99	423.29	328	34		34	Fracture set	
5R-3, 108-113	423.38	328	34		34	Fracture set	
5R-3, 135-139	423.65	330	28	220	28	Bedding	
6R-1, 51-54	429.51	213	44		44	Bedding	(46-56)
6R-1, 69-70	429.69	30	33		33	Foliation	
6R-1, 124-126	430.24	343	29	223	29	Foliation	
6R-2, 13-18	430.63	30	44		44	Foliation	
6R-2, 35-36	430.85	332	28	212	28	Foliation	
6R-2, 69-70	431.19	334	11		11	Foliation	
6R-2, 96-96	431.46	90	22		22	Foliation	
6R-2, 130-135	431.80	210	75	70	75	Foliation	
6R-3, 6-7	432.06	180	48		48	Foliation	
6R-3, 53-53	432.53	296	24	246	24	Foliation	
6R-3, 116-118	433.16	205	32		32	Foliation	
6R-4, 6-7	433.56	0	25	270	25	Foliation	
6R-4, 26-29	433.76	120	39	220	39	Foliation	
6R-4, 61-63	434.11	180	12		12	Foliation	
6R-4, 75-76	434.25	180	40		40	Foliation	
6R-4, 128-129	434.78	65	32	215	32	Foliation	
7R-1, 21-25	438.81	187	23	167	23	Bedding	(21-32)
7R-1, 28-29	438.88	229	32	209	32	Fracture set	(21-32)
7R-1, 34-38	438.94	328	43		43	Fracture set	
7R-1, 44-49	439.04	191	55	221	55	Fracture set	
7R-1, 47-48	439.07	119	10	144	10	Foliation	
7R-1, 76-77	439.36	28	20		20	Fracture set	
7R-1, 76-77	439.36	82	60		60	Fracture set	
7R-1, 81-81	439.41	180	21	220	21	Fracture set	
7R-1, 82-83	439.42	179	64	219	64	Fracture set	
7R-2, 11-14	440.21	125	43		43	Fracture set	
7R-2, 17-20	440.27	226	54		54	Fracture set	
7R-2, 38-38	440.48	110	32	120	32	Foliation	
7R-2, 39-40	440.49	26	40	36	40	Fracture set	
7R-2, 86-87	440.96	270	24	260	24	Fracture set	
7R-2, 85-87	440.95	183	33	173	33	Fracture set	
7R-2, 100-102	441.10	180	19	260	19	Bedding	
7R-3, 18-24	441.78	191	40	226	40	Fracture set	(13-26)
7R-3, 18-24	441.78	157	15	192	15	Foliation	(13-26)
7R-3, 23-26	441.83	0	25	35	25	Foliation	(13-26)
7R-3, 80-84	442.40	151	49		49	Fracture set	(68-86)
7R-3, 76-78	442.36	140	23		23	Fracture set	(68-86)
7R-3, 106-109	442.66	151	37		37		
7R-4, 3-10	443.13	346	62		62	Fracture set	(3-10)
7R-4, 3-10	443.13	99	23		23	Foliation	(3-10)
7R-6, 56-56	446.66	255	31	195	31	Fracture set	(82-106)
7R-6, 56-56	446.66	161	40	101	40	Fracture set	(82-106)
7R-6, 82-84	446.92	299	30	239	30	Bedding	(82-106)
7R-6, 86-93	446.96	180	6	120	6	Bedding	(82-106)
7R-6, 86-93	446.96	200	60	140	60	Normal fault	(82-106)
7R-6, 110-113	447.20	311	19	251	19	Bedding	(82-106)
7R-6, 106-116	447.16	177	56	117	56	Normal fault	(82-106)
8R-1, 38-40	448.58	286	50	241	50	Foliation	
8R-1, 86-87	449.06	47	24	225	24	Foliation	(84-100)
8R-2, 90-90	450.60	74	36		36	Foliation	(76-100) following 2 fracture sets cut foliation
8R-2, 81-86	450.51	216	36		36	Fracture set	(76-100) following 2 fracture sets cut foliation
8R-2, 84-86	450.54	30	28		28	Fracture set	(76-100) following 2 fracture sets cut foliation
8R-3, 87-89	452.07	55	46	215	46	Foliation	(70-120)

Table T6 (continued).

Core, section, interval (cm)	Depth (mbsf)	Cr az. (°)	Cr dip (°)	Pm az.	Pm plunge	Identifier	Notes
8R-3, 106-108	452.26	0	18	160	18	Bedding	(70-120)
8R-4, 30-30	453.00	8	58	168	58	Foliation	(10-60)
8R-4, 42-42	453.12	33	35	193	35	Foliation	(10-60)
8R-4, 133-134	454.03	283	43		43	Bedding	(131-146)
8R-4, 131-132	454.01	281	64		64	Foliation	(131-146)
8R-6, 110-112	456.80	135	33	195	33	Bedding	(95-134)
8R-CC, 10-15	457.49	13	24	68	24	Deformation band	Set of two submillimeter thickness, dark seams
9R-1, 97-100	458.77	156	29	216	29	Foliation	(94-110)
9R-1, 103-105	458.83	355	12	55	12	Fracture set	(94-110)
9R-2, 28-29	459.58	258	27		27	Fracture set	(17-50)
9R-2, 33-34	459.63	102	58		58	Foliation	(17-50)
9R-3, 127-129	462.07	220	23	170	23	Bedding	(125-145)
9R-4, 140-145	463.70	13	36	223	36	Bedding	(110-150)
9R-5, 2-10	463.82	10	54	100	54	Bedding	(0-30)
9R-5, 18-18	463.98	16	7	106	7	Fracture set	(0-30) 1-cm spacing
9R-5, 23-23	464.03	5	68	95	68	Foliation	(0-30)
9R-5, 25-27	464.05	12	45	102	45	Fault	(0-30)
10R-1, 5-20	467.45	180	27		27	Foliation	
10R-2, 60-60	468.81	218	38		38	Foliation	(46-73) 2- to 3-cm spacing
10R-2, 63-63	468.84	205	65		65	Fracture set	(46-73) 2- to 3-cm spacing
10R-2, 120-150	469.41	45	7		7	Fracture set	(120-150) 2-cm spacing
10R-2, 120-150	469.41	140	62		62	Fracture set	(120-150) 1-cm spacing
10R-3, 23-65	469.94	18	40	177	40	Foliation	(23-65) curved (continuous) foliations
10R-3, 23-65	469.94	5	76	164	76	Foliation	(23-65) curved (continuous) foliations
10R-3, 23-65	469.94	29	29	188	29	Foliation	(23-65) curved (continuous) foliations
10R-3, 77-89	470.48	220	28		28	Foliation	Apparently parallel to bedding
10R-3, 124-125	470.95	256	46	196	46	Bedding	(113-133)
10R-3, 124-125	470.95	245	65	185	65	Foliation	(113-133) foliation oblique to bedding
10R-3, 126-128	470.97	247	47	187	47	Fracture	(113-133) slickenlines in dip direction
10R-4, 26-30	471.47	349	58	239	58	Foliation	(0-48)
11R-1, 89-90	477.99	340	22	270	22	Foliation	(67-95)
11R-2, 34-36	478.94	250	56	154	56	Fracture set	(20-43)
11R-2, 121-124	479.81	203	53	113	53	Fracture set	(86-130) dominant fracture orientation
11R-2, 135-150	479.95					Sand	
11R-3, 73-75	480.83	147	32	167	32	Foliation	Main foliation plan
11R-4, 0-52	481.60					Sand	Disaggregated, but slight foliation
11R-4, 16-18	481.76	156	68	161	68	Deformation band	(13-21)
11R-4, 53-57	482.13	146	33	181	33	Bed?	(50-86)
11R-4, 87-+	482.47					Sand	Disaggregated, but slight foliation
12R-1, 29-33	486.99	165	76	115	76	Foliation	(7-35)
12R-1, 24-27	486.94	140	44	89	44	Fracture set	(7-35)
12R-1, 50-53	487.20	175	85		85	Foliation	(49-67)
12R-2, 35-57	488.55	22	41		41	Fracture set	(35-57) spacing 1-20 mm, predominant 1 mm
12R-2, 35-57	488.55	180	12		12	Fracture set	(35-57) spacing 5-10 mm
12R-2, 60-61	488.80	330	28		28	Fracture set	(35-57) spacing 1-3 mm
12R-2, 62-63	488.82	63	45		45	Fracture set	(35-57) spacing 1-3 mm
12R-2, 82-88	489.02	156	59		59	Fracture set	(69-97) spacing 5-10 mm
12R-2, 72-76	488.92	30	64		64	Fracture set	(69-97) spacing 1 cm
12R-2, 72-76	488.92	273	31		31	Fracture set	(69-97) spacing 5-10 cm
12R-2, 77-79	488.97	343	51		51	Fracture set	(69-97) spacing 5 cm?
12R-2, 87-88	489.07	64	37		37	Fracture set	(69-97) spacing 0.2-5mm
12R-2, 87-88	489.07	9	18		18	Fracture set	(69-97)
12R-3, 117-120	490.87	180	34		34	Foliation	Fissility?
12R-4, 60-82	491.80					Scaly mudstone	
12R-4, 94-95	492.14	0	90		90	Fracture	Silt/sand, irregular, spaced fracture
12R-4, 90-99	492.10	270	45		45	Fracture	Silt/sand, irregular, spaced fracture
12R-4, 83-85	492.03	169	43		43	Fracture	Silt/sand, irregular, spaced fracture
12R-4, 92-93	492.12	22	34		34	Fracture	Silt/sand, irregular, spaced fracture
12R-4, 93-97	492.13	149	46		46	Fracture	Silt/sand, irregular, spaced fracture
12R-5, 15-21	492.85					Fracture set	Near-vertical, slickenlined surfaces
13R-1, 0-62	496.40	170	51		51	Foliation	(22-62)
13R-1, 0-62	496.40	324	43		43	Fracture set	(22-62)
13R-1, 100-110	497.40	180	69		69	Foliation	Apparently bedding parallel
13R-1, 21-26	496.61	281	35		35	Fracture set	(10-30) >4-cm spacing
13R-1, 21-26	496.61	180	53		53	Fracture set	(10-30) 1- to 10-mm spacing
13R-2, 0-20	497.90	193	35	113	35	Fracture	Intersecting
13R-2, 0-20	497.90	172	63	92	63	Fracture	Intersecting
13R-2, 0-20	497.90	193	35	113	35	Fracture	Intersecting
13R-2, 0-20	497.90	193	35	113	35	Fracture	Intersecting

Table T6 (continued).

Core, section, interval (cm)	Depth (mbsf)	Cr az. (°)	Cr dip (°)	Pm az.	Pm plunge	Identifier	Notes
14R-1, 36-50	506.36	10	70	90	70	Foliation	(36-66)
14R-1, 0-22	506.00					Sand	
14R-1, 22-30	506.22					Angular blocks	
14R-1, 30-33	506.30	85	30		30	Bedding	(30-60)
14R-1, 40-44	506.40	0	0		0	Bedding	(30-60) determined on core face, or also x-section?
14R-2, 98-100	508.48	152	41		41	Bedding	(91-109)
14R-2, 98-100	508.48	63	61		61	Foliation	(91-109)
14R-2, 90-144	508.40					Angular blocks	
15R-1, 16-22	515.76	167	13	287	13	Bedding, fissility	(20-37)
15R-2, 63-64	517.73	39	14	127	14	Bedding	(58-73)
15R-2, 140-141	518.50	138	149		149	Bedding	(138-149)
15R-3, 92-93	519.52	50	17	285	17	Bedding	(74-110)
15R-4, 20-21	520.30	0	0		0	Bedding	
15R-4, 45-46	520.55	42	13	282	13	Bedding	Bedding parallel fissility?
15R-5, 52-53	522.12	138	12	273	12	Bedding	(49-72)
15R-5, 126-127	522.86	166	16	266	16	Bedding	(121-147)
16R-1, 23-24	525.43	135	17	295	17	Bedding, fissility	(23-39)
16R-1, 84-86	526.04	258	18	270	18	Fissility	(84-110)
16R-1, 134-135	526.54	230	28		28	Fissility	(134-139)
16R-2, 14-15	526.84	216	13	270	13	Fissility	(8-15)
16R-2, 50-51	527.20	225	15	210	15	Fissility	(40-53)
16R-2, 122-124	527.92	162	16		16	Bedding, fissility	(122-128)
16R-3, 10-12	528.30	154	22		22	Bedding, fissility	(0-12)
16R-3, 108-109	529.28	80	16		16	Bedding, fissility	(108-125)
16R-4, 55-58	530.30	0	21	245	21	Bedding	(55-91)
16R-4, 100-102	530.75	0	15	220	15	Bedding	(90-103)
16R-4, 131-134	531.06	180	25		25	Bedding, fissility	((130-140)
16R-5, 33-34	531.53	353	30	308	30	Bedding	(30-44)
16R-5, 76-78	531.96	336	24	187	24	Bedding	(74-85)
17R-1, 40-42	535.20	28	30	268	30	Foliation	(34-32)
17R-1, 69-70	535.49	55	20	245	20	Foliation	(46-74)
17R-1, 73-74	535.53	55	20	235	20	Bedding	(73-95)
17R-2, 32-33	536.59	297	21	287	21	Bedding	(31-40)
17R-2, 83-85	537.10	326	24	321	24	Bedding	(71-100)
17R-2, 137-139	537.64	309	22		22	Bedding	(135-150)
17R-2, 132-134	537.59	123	21		21	Foliation	(135-150)
17R-3, 0-14	537.77	0	9	315	9	Bedding	(0-140)
17R-3, 32-33	538.09	17	29	227	29	Foliation	(16-60)
17R-3, 50-51	538.27	281	28	276	28	Bedding	(44-60)
17R-4, 10-11	538.87	135	6		6	Foliation	(0-23)
17R-4, 34-34	539.11	275	20	255	20	Bedding	(26-61)
18R-1, 13-15	544.53	213	31	103	31	Bedding	(12-15)
18R-1, 39-40	544.79	52	25	225	25	Foliation	(39-45)
18R-1, 55-56	544.95	318	13		13	Bedding	(54-59)
18R-1, 76-77	545.16	69	19	179	19	Foliation	(72-77)
18R-1, 124-125	545.64	95	12	260	12	Foliation	(124-130)
18R-2, 17-18	546.07	225	10	145	10	Bedding	(13-21)
18R-3, 76-77	548.16	300	28	75	28	Bedding	(67-86)
18R-3, 109-110	548.49	325	17	235	17	Foliation	(108-110)
18R-4, 54-56	549.44	312	13		13	Bedding	(50-60)
18R-5, 10-11	550.50	64	11		11	Bedding	(6-19)
19R-1, 18-19	554.18	107	36		36	Bedding	(12-19)
19R-1, 43-44	554.43	119	18		18	Bedding	(37-46)
19R-1, 86-89	554.86	351	37	206	37	Foliation	(86-97)
19R-1, 128-130	555.28	345	28	225	28	Bedding	(117-131)
19R-2, 23-25	555.73	58	40		40	Bedding	(21-27)
19R-2, 29-32	555.79	56	42	113	42	Foliation	(29-47)
19R-2, 69-71	556.19	133	25	233	25	Foliation	(47-42)
19R-3, 44-48	557.44	346	36		36	Bedding	(38-48)
19R-3, 67-69	557.67	297	38	177	38	Bedding	(64-70)
19R-4, 30-33	558.80	121	34	216	34	Bedding	(30-37)
20R-1, 8-10	563.68	251	23	221	23	Bedding	(0-10)
20R-1, 119-123	564.79	343	33	213	33	Bedding	(119-128)
20R-1, 129-132	564.89	342	30	265	30	Foliation	(129-143)
20R-2, 64-68	565.74	301	39	231	39	Foliation	(63-84)
20R-2, 117-121	566.27	0	36	275	36	Foliation	(117-141)
20R-5, 8-9	568.58	180	16		16	Bedding	(0-9)
20R-5, 20-35	568.70					Foliation	Vertical
21R-1, 22-24	573.52	148	25		25	Foliation	(21-26)

Table T6 (continued).

Core, section, interval (cm)	Depth (mbsf)	Cr az. (°)	Cr dip (°)	Pm az.	Pm plunge	Identifier	Notes
21R-1, 122-126	574.52	175	36	50	36	Foliation	(118-127)
21R-1, 9-9	573.39	120	14	190	14	Fracture	(0-24)
21R-1, 13-14	573.43	341	15	51	15	Fracture	(0-24)
21R-1, 18-19	573.48	48	12	118	12	Fracture	(0-24)
21R-2, 19-22	574.99	168	31	158	31	Foliation	(0-22)
21R-2, 101-104	575.81	0	34	190	34	Bedding	(101-119)
21R-2, 107-110	575.87	333	36	163	36	Foliation	(101-119)
21R-2, 120-122	576.00	0	15		15	Fracture	Polished and slickenlined
21R-2, 124-126	576.04	341	21		21	Fracture	Polished and slickenlined
21R-2, 132-133	576.12	0	8		8	Fracture	Polished and slickenlined
21R-3, 21-24	576.51	317	38	157	38	Bedding	(8-24)
21R-3, 73-76	577.03	58	40	191	40	Foliation	(73-84)
21R-3, 97-100	577.27	0	0		0	Foliation	
21R-3, 119-120	577.49	100	49	225	49	Bedding	(123-129)
21R-3, 131-135	577.61	138	33	263	33	Bedding	(123-129)
21R-4, 0-15	577.80	0	0	180	0	Bed and fissility	Horizontal
21R-4, 20-23	578.00	40	48		48	Foliation	(20-28)
21R-4, 90-98	578.70	0	90		90	Foliation	
22R-1, 37-38	583.27	252	19		19	Bedding	
22R-1, 46-138	583.36					Foliation	
22R-1, 85-87	583.75	342	29	207	29	Fissility	Intensely disaggregated fissility (342-29)
22R-2, 0-49	584.28					Foliation	Several millimeter scaly mudstone
22R-2, 21-25	584.49	126	36	61	36	Foliation	(18-45)
22R-3, 47-52	586.25	200	38	275	38	Bedding	(46-72)
22R-4, 4-7	587.32	337	39		39	Bedding	(4-13)
23R-1, 30-69	592.80	197	36		36	Bedding/fissility	(30-69)
23R-2, 51-64	594.51	17	31		31	Bedding/fissility	(51-64)
23R-2, 83-110	594.83		90		90	Foliation	3-mm spacing in sands
23R-2, 98-102	594.98	0	0		0	Veins	Sediment-filled vein, crosscuts foliation
23R-3, 25-29	595.75	346	31		31	Bedding/fissility	(0-31)
23R-3, 61-66	596.11	0	0		0	Veins	Sediment-filled vein, crosscuts foliation
24R-1, 20-23	602.30	180	30	260	30	Bedding/fissility	(0-70)
24R-1, 123-150	603.33	4	38	274	38	Bedding/fissility	(123-150)
24R-2, 39-55	603.99	7	35		35	Bedding/fissility	(39-55)
24R-2, 56-68	604.16	204	28	219	28	Bedding/fissility	(56-68)
24R-2, 83-111	604.43	180	36	230	36	Bedding/fissility	(83-111)
24R-2, 122-132	604.82	173	37	213	37	Bedding/fissility	(122-132)
24R-3, 4-28	605.14	135	39	165	39	Bedding/fissility	(4-28)
24R-3, 36-46	605.46	31	35		35	Bedding/fissility	(36-46)
24R-3, 94-108	606.04	155	41		41	Bedding/fissility	(94-108)
24R-3, 122-140	606.32	167	76	172	76	Fracture set	(122-140)
24R-3, 122-140	606.32	172	76	177	76	Fracture set	(122-140)
24R-3, 122-140	606.32	168	34	173	34	Fracture set	(122-140)
25R-1, 104-108	612.74	295	44		44	Bedding	
25R-2, 80-81	614.00	278	60	113	60	Bedding	(76-87)
25R-3, 5-10	614.25	332	69	77	69	Bedding	(0-17)
25R-3, 20-37	614.40	0	0	45	0	Bedding	
25R-3, 46-50	614.66	0	0		0	Bedding	
26R-1, 30-31	621.70	0	30	290	30	Bedding/fissility	(0-58)
26R-1, 35-38	621.75	180	10	110	10	Fracture set	(0-58)
26R-1, 106-109	622.46	37	33		33	Foliation	(80-120)
26R-2, 14-19	623.04	10	56		56	Bedding	Turbidite sand
26R-2, 42-46	623.32	331	42		42	Fracture set	(29-52)
26R-2, 46-51	623.36	42	57		57	Fracture set	(29-52)
26R-2, 69-71	623.59	193	29		29	Fracture set	(65-94)
26R-2, 99-101	623.89	232	32	177	32	Fracture set	(94-117)
26R-2, 110-113	624.00	188	50	133	50	Bedding	Well defined
27R-1, 0-150	631.00					Breccia	Incipient
27R-2, 10-18	632.60	23	42		42	Foliated breccia	
27R-2, 30-33	632.80					Faults	
27R-3, 40-48	634.40	25	61		61	Fault	
27R-CC	634.79					Web structure	Weakly developed
28R-1, 29-31	640.99	194	41	74	41	Foliation	(1-32)
28R-1, 62-64	641.32	213	39	143	39	Foliation	(39-74)
28R-1, 65-66	641.35	201	19		19	Fractures	
28R-1	640.71	193	29	128	29	Foliation	(88-109)
28R-2, 35-36	642.55	191	64	321	64	Fracture set	(33-75)
28R-2, 44-45	642.64	212	19	342	19	Fracture set	(33-75)
28R-3, 40-41	644.10	0	30		30	Fissility	(39-55)

Table T6 (continued).

Core, section, interval (cm)	Depth (mbsf)	Cr az. (°)	Cr dip (°)	Pm az.	Pm plunge	Identifier	Notes
28R-3, 45-46	644.15	0	30		30	Bedding	(39-55)
29R-1, 10-13	650.50	318	33	263	33	Foliation	(4-17)
29R-1, 15-17	650.55	156	24	61	24	Fracture set	(17-29) fracture 1
29R-1, 45-47	650.85	137	28		28	Fracture set	Fracture 1
29R-1, 70-71	651.10	116	9	266	9	Fracture set	Fracture 1
29R-1, 86-91	651.26	5	48		48	Fracture set	(86-91) fracture 2
29R-1, 90-91	651.30	167	13	22	13	Fracture set	(90-95) fracture 1
29R-1, 94-95	651.34	135	13	350	13	Fracture set	(90-95) fracture 1
29R-1, 97-100	651.37	24	45	224	45	Fracture set	(97-100) fracture 2
29R-1, 100-101	651.40	152	20	352	20	Fracture set	Fracture 1
29R-1, 100-102	651.40	19	35	209	35	Fracture set	(100-102) fracture 2
29R-1, 102-106	651.42	0	45	190	45	Fracture set	(102-106) fracture 2
29R-1, 110-112	651.50	23	36		36	Foliation	(110-112)
29R-1, 116-119	651.56	11	45		45	Foliation	(116-119)
29R-1, 140-143	651.80	162	41	222	41	Foliation	(140-143)
29R-2, 10-14	652.00	40	37		37	Foliation	(10-14)
29R-2, 25-27	652.15	205	23	225	23	Fracture	
29R-2, 96-100	652.86	33	39		39	Foliation	
29R-2, 123-150	653.13					Foliation	Vertical
29R-3, 19-24	653.59	286	65	166	65	Fracture	Fracture 1
29R-3, 22-29	653.62	14	34	254	34	Fracture	Fracture 1
29R-3, 35-36	653.75	342	32	222	32	Fracture	Fracture 1
29R-3, 39-41	653.79	294	48	174	48	Fracture	Fracture 7
29R-3, 26-27	653.66	0	5	240	5	Fracture	Fracture 2
29R-3, 29-30	653.69	296	11	176	11	Fracture	Fracture 2
29R-3, 26-40	653.66	180	64	60	64	Fracture	Fracture 3
29R-3, 40-43	653.80	356	24	236	24	Fracture	Fracture 1
29R-3, 42-47	653.82	19	41	259	41	Fracture	Fracture 1
29R-3, 51-53	653.91	222	15	102	15	Fracture	Fracture 5
29R-3, 56-58	653.96	33	50		50	Fracture	
29R-3, 48-53	653.88	353	42		42	Fracture	Fracture 1
30R-1, 45-55	660.45					Brecciated zone	Polished and slickenlined
30R-1, 134-137	661.34	227	38	132	38	Foliation	(133-137)
30R-3, 60-63	663.60	206	38	216	38	Fracture set	Fracture 1
30R-3, 62-62	663.62	270	23	280	23	Fracture set	Fracture 2
30R-3, 63-67	663.63	208	52	218	52	Fracture set	Fracture 1
30R-3, 68-69	663.68	180	6	190	6	Fracture set	Fracture 2
30R-3, 43-45	663.43	318	32		32	Foliation	(38-45)
31R-1, 10-11	669.70	320	18		18	Fracture set	Fracture 1
31R-1, 10-17	669.70	349	56		56	Fracture set	Fracture 2
31R-1, 7-17	669.67	348	66		66	Fracture set	Fracture 2
31R-1, 17-17	669.77	278	14		14	Fracture set	Fracture 3
31R-1, 21-21	669.81	180	0		0	Fracture set	Fracture 3
31R-1, 27-28	669.87	230	42		42	Foliation	
31R-1, 49-50	670.09	227	38	117	38	Foliation	
31R-2, 12-15	671.22	180	34		34	Foliation	
31R-3, 7-9	672.67	209	29	154	29	Bedding	

Notes: Cr az. = azimuth of plane in core reference frame, Cr dip = dip of plane in core reference frame, Pm az. = azimuth of plane in paleomagnetism reference frame, Pm plunge = plunge of plane in paleomagnetism reference frame. Paired values in parentheses in Notes column record coherent interval of intact drill biscuit used in paleomagnetic reorientation. This table is also available in [ASCII](#) format.

Table T7. Nannofossil events recognized, Site 1178.

Nannofossil zones	Datum events	Age (Ma)	Depth (mbsf)
NN21a	FAD <i>Emiliania huxleyi</i>	0.26	7.60 ± 4.71
NN20	LAD <i>Pseudoemiliania lacunosa</i>	0.46	7.60 ± 4.71
NN17	LAD <i>Discoaster surculus</i>	2.55	17.31 ± 5.00
NN16	LAD <i>Reticulofenestra pseudoumbilicus</i> (>7 µm)	3.75	54.05 ± 3.47
NN15	LAD <i>Amaurolithus</i> spp.	5.05	116.13 ± 2.72
NN13	FAD <i>Ceratolithus cristatus</i>	5.05	198.95 ± 5.58
NN12	LAD <i>Discoaster quinqueringus</i>	5.54	198.95 ± 5.58
NN11b	FAD <i>Amaurolithus primus</i>	7.4	351.98 ± 1.41
NN12	LAD <i>Discoaster quinqueringus</i>	5.54	414.77 ± 1.42
NN11b	FAD <i>Amaurolithus primus</i>	7.4	528.33 ± 4.16
NN10b	LAD <i>Reticulofenestra pseudoumbilicus</i> (>7 µm)	9.0	528.33 ± 4.16
NN12	LAD <i>Discoaster quinqueringus</i>	5.54	659.64 ± 5.22

Note: LAD = last appearance datum, FAD = first appearance datum.

**Table T8.** Interval and depth constraints of calcareous nannofossil events, Site 1178.

Event	Interval (cm)		Depth (mbsf)	
	Top	Bottom	Top	Bottom
	190-1178A-	190-1178A-		
B <i>Emiliana huxleyi</i>		1H-CC		2.89
T <i>Pseudoemiliana lacunosa</i>	1H-CC	2H-CC	2.89	12.31
T <i>Discoaster surculus</i>	2H-CC	3H-CC	12.31	22.30
T <i>Reticulofenestra pseudoumbilicus</i> (>7 µm)	6H-CC	7H-CC	50.58	57.52
T <i>Amaurolithus</i> spp.	13X-CC	14X-4, 75-76	113.40	118.85
B <i>Ceratolithus cristatus</i>	22X-3, 57-58	23X-CC	193.37	204.53
T <i>Discoaster quinqueramus</i>	22X-3, 57-58	23X-CC	193.37	204.53
B <i>Amaurolithus primus</i>	38X-CC	39X-1, 19-20	350.57	353.39
	190-1178B-	190-1178B-		
T <i>Discoaster quinqueramus</i>	4R-CC	5R-3, 12-13	416.19	422.42
B <i>Amaurolithus primus</i>	15R-CC	16R-CC	524.17	532.49
T <i>Reticulofenestra pseudoumbilicus</i> (>7 µm)	15R-CC	16R-CC	524.17	532.49
T <i>Discoaster quinqueramus</i>	29R-CC	30R-CC	654.42	664.86

Note: B = bottom occurrence, T = top occurrence.

**Table T9.** Epoch boundaries, Site 1178.

Boundary	Depth (mbsf)	Event
Pleistocene/Pliocene	17.31 ± 5.00	T <i>Discoaster surculus</i> *
Pliocene/late Miocene	198.95 ± 5.58	B <i>Ceratolithus cristatus</i>

Notes: B = bottom occurrence, T = top occurrence. \* = due to unconformity











Table T10 (continued).

Epoch	Zone	Core, section, interval (cm)	Depth (mbsf)	Preservation		Abundance	Fossil Taxa
				M	R		
late Miocene	NN11b	13R-CC		M	R		<i>Helicosphaera orientalis</i>
		14R-CC		M	F		<i>Helicosphaera sellii</i>
		15R-CC		M	C		<i>Helicosphaera stalis</i>
		16R-CC		P	R		<i>Minylitha convallis</i>
		17R-CC		P	R		<i>Neosphaera coccolithomorpha</i>
		18R-CC		P	F		<i>Pontosphaera discopora</i>
		19R-CC		M	C		<i>Pontosphaera japonica</i>
		20R-CC		P	F		<i>Pontosphaera multipora</i>
		21R-CC		P	B		<i>Pseudoemiliania lacunosa</i>
	NN10a	22R-CC		P	R		<i>Pseudoemiliania ovata</i>
		23R-CC		P	R		<i>Reticulofenestra haqii</i>
		24R-CC		P	R		<i>Reticulofenestra minuta</i>
		25R-CC		P	R		<i>Reticulofenestra minutula</i>
		26R-CC		P	R		<i>Reticulofenestra pseudoumbilicus (&gt;7 µm)</i>
		27R-CC		P	F		<i>Reticulofenestra pseudoumbilicus (5-7 µm)</i>
		28R-CC		P	R		<i>Reticulofenestra</i> with 'pseudobar'
		29R-CC		P	F		<i>Rhabdosphaera clavigera</i>
		30R-CC		M	C		<i>Rhabdosphaera clavigera</i> var. <i>stylifera</i>
	NN11b	31R-CC		P	C		<i>Scapholithus fossilis</i>
							<i>Scyphosphaera</i> spp.
							<i>Sphenolithus abies</i>
						<i>Sphenolithus grandis</i>	
						<i>Sphenolithus moriformis</i>	
						<i>Sphenolithus</i> spp.	
						<i>Syracosphaera pulchra</i>	
						<i>Syracosphaera</i> spp.	
						<i>Triquetrorhabdulus rioi</i>	
						<i>Triquetrorhabdulus rugosus</i>	
						<i>Umbellosphaera irregularis</i>	
						<i>Umbellosphaera tenuis</i>	
						<i>Umbilicosphaera hultburtiana</i>	
					<i>Umbilicosphaera jafari</i>		
					<i>Umbilicosphaera rotula</i>		
					<i>Umbilicosphaera sibogae</i> var. <i>foliosa</i>		
					<i>Umbilicosphaera sibogae</i> var. <i>sibogae</i>		

**Table T11.** Depths and ages of magnetic chrons and subchrons, Holes 1178A and 1178B.

Depth (mbsf)	Polarity	Chron	Subchron	Age (Ma)
0.05	N	Brunhes		
8.5	N	Gauss		
43.65	R		C2An.2r	3.22
53.65	N		C2An.2n	3.33
89.05	R	Gilbert		3.58
323.3	N	C3A		5.894
353.5	N	C3B?		6.935
405.42	N	C4	C4r.1n	8.225
408.94	R		END of C4r.1n	8.257

Note: N = normal, R = reversed.

Table T12. Pore fluid composition, Site 1178.

Hole, core, section, interval (cm)	Depth (mbsf)	Alk (T) (mM)	Cl (T) (mM)	SO <sub>4</sub> (I) (mM)	Mg (T) (mM)	Ca (T) (mM)	Si (S) (μM)	NH <sub>4</sub> (S) (mM)
190-1178A-								
1H-1, 140-150	1.40	3.6	549.0	27.69	52.7	9.96	575	0.10
2H-4, 140-150	8.80	6.0	551.0	21.85	50.0	7.48	583	
3H-4, 140-150	18.30	11.8	559.0	14.24	46.3	5.52	671	1.43
4H-6, 140-150	29.80	18.3	561.5	1.45	39.8	3.29	854	
5H-4, 140-150	37.30	17.5	560.0	1.08	39.0	3.32	829	2.91
6H-4, 140-150	46.80	18.4	559.5	0.06	39.1	3.58	704	
7H-3, 140-150	54.80	19.3	558.0	0.34	38.0	3.72	821	5.21
8H-4, 140-150	63.40	20.1	551.5	0.40	37.6	3.89		
9X-5, 135-150	72.09	20.0	555.0	0.61	37.0	3.94	867	4.86
11X-4, 135-150	90.65	20.9	550.0	0.30	35.2	4.23	825	
12X-5, 135-150	101.66	20.2	547.0	0.37	32.7	5.19	825	7.04
13X-4, 135-150	109.85	20.9	544.0	0.33	32.1	5.51	875	
14X-4, 135-150	119.45	20.3	540.5	0.25	31.0	5.54	842	8.54
15X-4, 135-150	129.05	20.7	538.0	0.17	30.1	5.65	783	
16X-4, 130-150	138.50	21.3	540.0	0.09	28.9	6.19	838	10.25
17X-2, 130-150	145.00	21.4	544.5	0.19	28.4	6.35	767	
18X-4, 130-150	156.46	20.3	537.0	0.65	26.6	6.71	780	11.25
19X-3, 130-150	165.70	18.1	528.5	2.62	27.3	6.87	750	
20X-5, 60-80	176.18	17.1	526.0	1.79	25.9	6.63	859	11.96
21X-4, 130-150	186.20	17.6	541.5	0.14	24.8	6.52	843	
22X-3, 130-150	194.10	20.0	543.0	0.32	25.2	7.47	851	11.55
23X-2, 130-150	200.65	18.8	524.0	0.16	23.7	8.01	621	
24X-1, 130-150	202.00	17.7	524.0	1.43	22.3	9.02		11.39
25X-2, 130-150	210.10	18.6	547.5	0.35	22.2	9.48	759	
26X-1, 130-150	221.17	16.7	547.0	0.12	21.1	9.59	780	
27X-3, 130-150	242.10		546.5		21.1	9.94	671	
28X-4, 130-150	253.20	16.5	537.0	0.78	19.2	9.32	763	
29X-3, 125-145	260.96	15.2	527.0	0.40	22.6	7.39	776	
31X-4, 120-140	281.90		538.5	0.39	16.7	12.48	725	
32X-4, 125-150	291.10	13.1	538.5	0.25	17.3	13.53	725	
34X-3, 125-150	309.35		535.0	0.08	16.2	14.42	545	
35X-4, 125-150	320.55		528.0	0.00	16.3	15.16	478	
36X-5, 130-150	331.70		538.0	0.09	15.8	14.69	516	
37X-5, 125-150	341.25	7.8	521.0	0.37	15.8	15.17		
40X-2, 120-150	365.60		531.0	0.31	14.3	16.97		
41X-1, 0-13	372.50		522.5	0.74	12.3	16.95		
43X-1, 125-150	392.85		520.0	0.40	12.0	16.48		
44X-6, 0-20	408.02	3.7	517.0	0.40	11.8	16.52		
190-1178B-								
2R-2, 97-116	397.47		529.5	0.35	12.98	17.01		
3R-3, 0-18	403.00		528.5	1.60	11.81	16.72		
4R-3, 130-150	413.90		516.0	0.30	11.04	16.24		
5R-1, 0-8	419.30		508.0	0.26	11.47	15.61		
6R-1, 0-28	429.00			0.92				
7R-1, 110-150	439.70		492.0	1.61	11.03	15.84		
9R-2, 140-150	460.70		487.0	1.97	9.76	14.19		
10R-1, 48-81	467.88		470.0	0.92	8.79	13.29		
13R-1, 113-150	497.53		475.0	1.68	8.68	14.85		
15R-3, 110-150	519.70		471.0	1.25	8.07	13.59		
17R-1, 107-147	535.87	2.5	482.0		8.35	12.68		
20R-4, 0-40	568.10		481.0		7.50	11.66		
22R-2, 110-150	585.38		488.0		7.71	11.66		
24R-2, 0-40	603.60		492.0					

Note: Alk = alkalinity, T = titration, I = ion, S = spectrophotometry.

**Table T13.** Headspace gas and vacutainer analysis, Site 1178. (See table note. Continued on next page.)

Core, section, interval (cm)	Depth (mbsf)	Sample method	C <sub>1</sub> /C <sub>2</sub>	C <sub>1</sub> (ppm)	C <sub>2</sub> (ppm)	C <sub>2</sub> = (ppm)	C <sub>3</sub> (ppm)	C <sub>3</sub> = (ppm)
190-1178A-								
1H-2, 0-5	1.50	HS		2	0.0	0.0	0.0	0.0
2H-5, 0-5	8.90	HS		4	0.0	0.0	0.0	0.0
3H-5, 0-5	18.40	HS		12	0.0	0.0	0.0	0.0
4H-7, 0-5	29.90	HS	886	1,152	1.3	0.0	0.0	0.0
5H-4, 0-5	35.90	HS	2,015	3,627	1.8	0.0	0.0	0.0
6H-6, 0-5	48.40	HS	2,442	10,501	4.3	0.0	0.0	0.0
7H-2, 0-5	51.90	HS	2,516	12,330	4.9	0.0	0.0	0.0
8H-3, 0-5	60.50	HS	1,470	4,703	3.2	0.0	0.0	0.0
9X-6, 0-5	72.24	HS	1,724	7,931	4.6	0.0	0.0	0.0
11X-3, 0-5	87.80	HS	1,724	8,273	4.8	0.0	0.0	0.0
12X-3, 0-5	97.31	HS	1,489	8,487	5.7	0.0	0.0	0.0
13X-4, 0-5	108.50	HS	939	4,881	5.2	0.0	1.8	0.0
14X-5, 0-5	119.60	HS	1,087	8,047	7.4	0.0	1.0	0.0
15X-5, 0-5	129.20	HS	693	4,159	6.0	0.0	1.2	0.0
16X-5, 0-5	138.70	HS	774	4,332	5.6	0.0	1.0	0.0
16X-5, 30-31	139.00	VAC	3,012	956,611	317.6	0.0	20.5	0.0
17X-3, 0-5	145.20	HS	655	5,308	8.1	0.0	1.3	0.0
17X-4, 110-111	147.80	VAC	1,192	947,270	795.0	0.0	19.6	0.0
18X-4, 0-5	155.16	HS	567	4,705	8.3	0.5	2.3	0.0
19X-4, 0-5	165.90	HS	758	6,821	9.0	0.4	1.6	0.0
20X-4, 0-5	174.34	HS	567	2,323	4.1	0.6	1.0	0.0
21X-5, 0-5	186.40	HS	987	5,033	5.1	0.0	0.8	0.0
22X-3, 0-5	192.80	HS	523	1,725	3.3	0.0	0.0	0.0
23X-3, 0-5	202.20	HS	1,066	10,339	9.7	0.0	0.3	0.0
24X-2, 0-5	210.30	HS	1,065	4,154	3.9	0.0	0.0	0.0
25X-3, 0-5	221.37	HS	637	765	1.2	0.0	0.0	0.0
26X-2, 0-5	229.60	HS	788	946	1.2	0.0	3.7	0.0
27X-5, 0-5	243.80	HS	919	827	0.9	0.0	4.1	0.0
28X-5, 0-5	253.40	HS	515	1,082	2.1	0.4	10.5	0.0
29X-4, 0-5	261.16	HS	515	2,110	4.1	0.0	12.2	0.0
30X-4, 0-5	270.70	HS	592	2,368	4.0	0.5	14.9	0.0
31X-5, 0-5	282.10	HS	536	4,284	8.0	0.0	6.8	0.0
32X-5, 0-5	291.35	HS	493	1,183	2.4	0.4	10.6	0.0
33X-3, 0-5	298.50	HS	349	698	2.0	0.0	8.4	0.0
34X-3, 0-5	308.10	HS	558	2,902	5.2	0.0	20.0	0.0
35X-4, 0-5	319.30	HS	759	10,546	13.9	0.0	18.0	0.0
36X-5, 0-5	330.40	HS	336	3,426	10.2	0.6	58.8	0.0
37X-5, 0-5	340.00	HS	570	6,268	11.0	0.3	28.5	0.0
38X-3, 0-5	346.60	HS	530	3,814	7.2	0.4	34.3	0.0
39X-1, 0-5	353.20	HS	241	2,099	8.7	0.0	43.0	0.0
40X-3, 0-5	365.90	HS	284	2,155	7.6	0.0	39.1	0.0
41X-2, 0-5	374.00	HS	247	445	1.8	0.0	5.0	0.0
42X-2, 0-5	383.60	HS	217	1,216	5.6	0.0	31.5	0.0
43X-2, 0-5	393.10	HS	446	5,976	13.4	0.0	15.3	0.0
44X-6, 0-5	408.02	HS	138	470	3.4	0.0	23.7	0.0
190-1178B-								
2R-2, 0-5	396.50	HS	389	3,778	9.7	0.0	17.4	0.0
3R-2, 0-5	401.50	HS	415	9,667	23.3	0.0	28.6	0.0
4R-3, 0-5	412.60	HS	302	2,722	9.0	0.0	34.6	0.0
5R-2, 0-5	420.80	HS	284	2,835	10.0	0.0	44.3	0.0
6R-2, 0-5	430.50	HS	326	3,421	10.5	0.0	30.5	0.0
7R-4, 0-5	443.10	HS	252	2,543	10.1	0.0	45.1	0.0
8R-1, 0-5	448.20	HS	216	1,795	8.3	0.0	43.9	0.0
10R-2, 0-5	468.21	HS	126	1,404	11.1	0.0	5.9	0.0
11R-2, 0-5	478.60	HS	137	4,149	30.3	0.0	8.9	0.0
12R-4, 0-5	491.20	HS	136	4,491	33.0	0.0	24.9	0.0
13R-2, 0-5	497.90	HS	226	5,261	23.3	0.0	12.9	0.0
14R-2, 0-5	507.50	HS	248	8,952	36.1	0.0	36.3	0.0
15R-4, 0-5	520.10	HS	98	2,659	27.2	0.0	28.7	0.0
16R-2, 0-5	526.70	HS	139	6,585	47.3	0.0	35.9	0.0
17R-3, 0-5	537.77	HS	117	6,307	53.9	0.0	48.7	0.0
18R-3, 0-5	547.40	HS	114	2,596	22.7	0.0	31.4	0.0
19R-3, 0-5	557.00	HS	141	1,003	7.1	0.0	10.5	0.0
20R-3, 0-5	566.60	HS	115	16,240	141.3	0.0	121.5	0.0
21R-3, 0-5	576.30	HS	133	1,896	14.2	0.0	14.2	0.0
22R-3, 0-5	585.780	HS	88	1,268	14.4	0.0	22.9	0.0

**Table T13 (continued).**

Core, section, interval (cm)	Depth (mbsf)	Sample method	C <sub>1</sub> / C <sub>2</sub>	C <sub>1</sub> (ppm)	C <sub>2</sub> (ppm)	C <sub>2</sub> = (ppm)	C <sub>3</sub> (ppm)	C <sub>3</sub> = (ppm)
23R-2, 0-5	594.00	HS	138	2,679	19.4	0.0	12.2	0.0
24R-3, 0-5	605.10	HS	121	2,924	24.1	0.0	16.0	0.0
25R-2, 0-5	613.20	HS	114	13,526	118.9	0.0	75.3	0.0
26R-2, 0-5	622.90	HS	243	4,087	16.8	0.0	11.0	0.0
27R-2, 0-5	632.50	HS	127	4,156	32.8	0.0	26.9	0.0
28R-2, 0-5	642.20	HS	152	7,911	52.1	0.0	31.6	0.0
29R-2, 0-5	651.90	HS	90	2,194	24.3	0.0	22.9	0.0
30R-1, 0-5	660.00	HS	165	2,076	12.6	0.0	14.5	0.0
31R-1, 0-5	669.60	HS	92	397	4.3	0.0	6.8	0.0

Note: HS = headspace, VAC = vacutainer.

**Table T14.** Carbon, nitrogen, sulfur, and hydrogen analyses, Hole 1178A.

Core, section, interval (cm)	Depth (mbsf)	Inorganic C (wt%)	CaCO <sub>3</sub> (wt%)	TOC (wt%)	Organic C (wt%)	N (wt%)	S (wt%)	H (mg HC/g of sediment)
190-1178A-								
1H-1, 135-136	1.35	1.15	9.63	NA	NA	NA	NA	NA
2H-4, 137-138	8.77	2.73	22.81	NA	NA	NA	NA	NA
3H-4, 136-137	18.26	1.00	8.40	NA	NA	NA	NA	NA
4H-6, 133-134	29.73	0.75	6.25	NA	NA	NA	NA	NA
5H-4, 136-137	37.26	0.84	7.06	NA	NA	NA	NA	NA
6H-4, 134-135	46.74	0.69	5.77	1.38	0.69	NA	0.17	0.53
7H-3, 138-139	54.78	0.97	8.08	NA	NA	NA	NA	NA
8H-4, 134-135	63.34	0.92	7.74	NA	NA	NA	NA	NA
9X-5, 132-133	72.06	1.15	9.60	NA	NA	NA	NA	NA
11X-4, 127-128	90.57	0.40	3.40	1.24	0.84	NA	0.28	0.64
12X-5, 133-134	101.64	0.56	4.69	NA	NA	NA	NA	NA
13X-4, 131-132	109.81	0.25	2.15	1.02	0.76	NA	0.51	0.6
13X-5, 122-123	111.22	0.57	4.76	NA	NA	NA	NA	NA
14X-4, 133-134	119.43	0.68	5.66	NA	NA	NA	NA	NA
15X-4, 133-134	129.03	0.46	3.91	NA	NA	NA	NA	NA
16X-4, 128-129	138.48	0.46	3.89	NA	NA	NA	NA	NA
17X-2, 127-128	144.97	0.43	3.66	1.01	0.57	NA	0.26	0.61
18X-4, 129-130	156.45	0.47	3.92	NA	NA	NA	NA	NA
19X-3, 124-125	165.64	0.34	2.88	1.04	0.69	NA	0.2	0.72
20X-5, 54-55	176.12	0.63	5.27	NA	NA	NA	NA	NA
21X-4, 120-121	186.10	1.32	11.07	NA	NA	NA	NA	NA
22X-1, 103-104	190.83	0.69	5.81	NA	NA	NA	NA	NA
22X-4, 8-9	194.38	0.93	7.79	NA	NA	NA	NA	NA
23X-2, 121-122	201.91	0.18	1.52	0.76	0.58	NA	0.98	0.58
24X-1, 123-124	210.03	0.31	2.61	1.04	0.73	NA	0.87	0.73
25X-2, 117-118	221.04	0.64	5.36	NA	NA	NA	NA	NA
27X-3, 123-124	242.03	0.51	4.31	NA	NA	NA	NA	NA
28X-4, 128-129	253.18	0.57	4.82	NA	NA	NA	NA	NA
29X-3, 124-125	260.95	0.34	2.90	1.35	1	NA	1.45	0.81
31X-4, 116-117	281.86	0.40	3.36	NA	NA	NA	NA	NA
32X-4, 122-123	291.07	0.46	3.83	NA	NA	NA	NA	NA
33X-5, 120-121	302.70	0.59	4.96	NA	NA	NA	NA	NA
34X-3, 123-124	309.33	0.34	2.87	1.04	0.7	NA	0.13	0.66
35X-4, 124-125	320.54	0.43	3.63	NA	NA	NA	NA	NA
36X-5, 123-124	331.63	0.53	4.42	NA	NA	NA	NA	NA
37X-5, 118-119	341.18	0.32	2.67	0.82	0.5	NA	0.24	0.63
38X-3, 127-128	347.87	0.61	5.09	NA	NA	NA	NA	NA
39X-1, 19-20	353.39	0.77	6.46	NA	NA	NA	NA	NA
40X-2, 115-116	365.55	0.17	1.46	1.21	1.03	NA	0.33	0.4
41X-1, 94-95	373.44	0.92	7.72	NA	NA	NA	NA	NA
42X-3, 95-96	386.05	0.66	5.54	NA	NA	NA	NA	NA
43X-1, 124-125	392.84	0.56	4.69	NA	NA	NA	NA	NA
44X-5, 120-121	407.72	0.69	5.78	NA	NA	NA	NA	NA

Note: TOC = total organic carbon; HC = hydrocarbon.

**Table T15.** Total bacterial populations in sediments, Site 1178.

Depth (mbsf)	Bacterial cells (cells/cm <sup>3</sup> )	
	Hole A	Hole B
0.00	$4.75 \times 10^8$	
1.50	$2.41 \times 10^7$	
4.19	$1.27 \times 10^7$	
8.89	$6.08 \times 10^6$	
18.29	$1.01 \times 10^7$	
29.79	$1.66 \times 10^6$	
42.14	$2.07 \times 10^6$	
72.23	$1.07 \times 10^6$	
101.65	$5.89 \times 10^5$	
111.24	$5.25 \times 10^5$	
138.49	$2.09 \times 10^5$	
165.69	$1.66 \times 10^5$	
195.49	$1.28 \times 10^5$	
210.09	$7.13 \times 10^3$	
247.04	$8.28 \times 10^4$	
272.19	$4.71 \times 10^4$	
302.72	BD	
341.24	BD	
374.00	$3.94 \times 10^5$	
407.76	$5.93 \times 10^5$	
396.50		$6.48 \times 10^4$
413.89		$1.05 \times 10^5$
435.00		$3.40 \times 10^4$
460.49		$5.57 \times 10^5$
497.52		$6.22 \times 10^5$
506.94		BD
538.77		$9.85 \times 10^4$
574.79		BD
593.84		BD
633.99		$1.16 \times 10^4$

Note: BD = below detection ( $\sim 6 \times 10^4$  cells/cm<sup>3</sup>).

**Table T16.** Comparison of near-surface sediment bacterial populations at Site 1178 with data from nine other ODP sites with different overlying-water depths.

Location	ODP leg-site	Depth (mbsf)	Total bacteria (cells/cm <sup>3</sup> )
Peru margin	112-681	150	$1.05 \times 10^9$
Santa Barbara Basin	146-893	577	$1.27 \times 10^9$
Japan Sea	128-798	900	$7.82 \times 10^8$
Woodlark Basin	180-1115	1150	$2.83 \times 10^8$
Cascadia margin	146-890	1326	$6.95 \times 10^8$
Woodlark Basin	180-1109	2211	$3.28 \times 10^8$
Juan de Fuca Ridge	139-857	2419	$8.28 \times 10^8$
Cascadia margin	146-888	2516	$5.32 \times 10^8$
Lau Basin	135-834	2703	$6.12 \times 10^8$
Woodlark Basin	180-1108	3188	$2.67 \times 10^8$
Amazon Fan	155-940	3195	$5.62 \times 10^8$
Amazon Fan	155-934	3432	$6.04 \times 10^8$
Eastern Equatorial Pacific	138-851	3760	$2.08 \times 10^8$
Nankai Trough	190-1173	4791	$7.23 \times 10^7$
	190-1174	4751	$1.47 \times 10^8$
	190-1175	2998	$6.97 \times 10^7$
	190-1178	1742	$4.75 \times 10^8$

**Table T17.** Drilling fluid intrusion estimated based on PFT tracer experiments, Site 1178.

Core, section	Total sample weight (g)			Bulk density (g/cm <sup>3</sup> )	PFT peak area			Drilling fluid (μL)/sediment (g)		
	Outside	Quarter	Center		Outside	Quarter	Center	Outside	Quarter	Center
190-1178A-										
8H-1	18.57	19.23	19.53	1.76	1265.7	58.7	179.2	3.18	0.02	0.24
8H-3	19.01	18.97	19.40	1.76	1824.3	267.6	509.2	3.85	0.48	0.86
8H-5	19.63	19.64	24.94	1.76	279.6	199.2	158.1	0.40	0.26	0.06
11X-1	17.78	18.60	18.77	1.77	2161.4	58.0	434.0	8.59	0.03	0.92
11X-3	19.11	17.75	18.74	1.77	728.2	733.0	57.5	1.42	2.84	0.02
11X-5	20.83	19.26	18.80	1.77	784.9	569.0	240.1	0.91	1.03	0.45
190-1178B-										
19R-2	26.95	21.26	20.43	1.77	9256.0	240.3	51.5	4.18	0.22	0.00
19R-3	20.26	19.48	18.83	1.77	2612.6	4392.7	340.7	3.76	8.06	0.69
19R-4	18.37	17.57	20.07	1.77	150.7	90.6	7554.0	0.30	36.03	0.07

**Table T18.** Fluorescent microsphere tracer experiments, Site 1178A.

Core, section	Total sample weight (g)			Microspheres/sediment (g)			Microspheres/sediment (g)		
	Outside	Quarter	Center	Outside	Quarter	Center	Outside	Quarter	Center
190-1178A-									
11X-1	17.78	18.60	18.77	12	0	0	0.67	0.00	0.00
11X-3	19.11	17.75	18.74	3	1	0	0.16	0.06	0.00
11X-5	20.83	19.26	18.80	1	0	0	0.05	0.00	0.00

Table T19. Electrical conductivities and formation factor data for cubes, Hole 1178A. (See table note. Continued on next page.)

Core, section, interval (cm)	Depth (mbsf)	Conductivity (S/m)			Temp (°C)	Formation factor		
		x	y	z		x	y	z
190-1178A-								
20X-2, 109	172.43	0.91	0.88	0.86	25.0	5.80	6.01	6.17
21X-6, 29	188.19	0.89	0.85	0.83	25.1	5.95	6.23	6.38
22X-2, 125	192.55	0.78	0.71	0.77	24.8	6.80	7.41	6.88
24X-1, 26	209.06	0.89	0.79	0.80	24.8	5.91	6.65	6.63
25X-3, 114	222.51	0.82	0.76	0.83	24.9	6.43	6.98	6.40
25X-5, 43	224.73	0.80	0.79	0.69	25.0	6.66	6.74	7.63
26X-3, 41	231.51	0.81	0.79	0.58	25.0	6.53	6.74	9.19
27X-2, 91	240.21	0.79	0.86	0.72	25.0	6.70	6.20	7.32
27X-6, 95	246.25	0.79	0.76	0.66	25.0	6.74	6.96	8.08
28X-4, 113	253.03	0.65	0.70	0.45	25.0	8.12	7.56	11.73
28X-6, 78	255.68	0.59	0.71	0.47	25.0	9.05	7.45	11.28
29X-2, 80	259.30	0.84	0.79	0.40	24.7	6.24	6.70	13.03
29X-5, 72	263.36	0.49	0.54	0.55	24.7	10.74	9.75	9.60
30X-1, 99	267.59	0.68	0.76	0.64	24.7	7.80	6.94	8.21
30X-4, 48	271.18	0.71	0.72	0.61	24.7	7.37	7.30	8.58
31X-4, 101	281.71	0.79	0.75	0.65	24.7	6.71	7.02	8.05
31X-7, 127	285.79	0.68	0.64	0.58	24.7	7.72	8.23	9.15
32X-5, 68	292.03	0.68	0.67	0.52	24.9	7.77	7.89	10.13
33X-4, 143	301.43	0.62	0.66	0.46	24.9	8.55	8.07	11.62
33X-6, 15	303.15	0.65	0.77	0.49	24.7	8.07	6.87	10.85
34X-2, 88	307.48	0.72	0.91	0.62	24.7	7.33	5.81	8.51
34X-4, 9	309.69	0.74	0.66	0.52	24.7	7.16	7.95	10.23
34X-1, 139	306.49	0.75	0.66	0.68	25.2	7.13	8.08	7.83
35X-1, 88	315.68	0.66	0.61	0.58	25.1	8.00	8.74	9.22
35X-4, 120	320.50	0.73	0.69	0.55	25.2	7.28	7.75	9.64
36X-1, 48	324.88	0.80	0.79	0.60	24.4	6.52	6.67	8.74
36X-4, 148	330.38	0.74	0.65	0.53	24.3	7.11	8.10	9.83
37X-2, 45	335.95	0.63	0.77	0.53	24.4	8.26	6.84	9.86
37X-6, 77	342.27	0.67	0.68	0.57	24.4	7.81	7.76	9.23
38X-2, 71	345.81	0.57	0.68	0.51	24.5	9.28	7.77	10.32
38X-4, 64	348.74	0.57	0.64	0.51	24.5	9.19	8.15	10.34
39X-1, 20	353.40	0.89	0.91	0.80	24.6	5.88	5.80	6.60
40X-3, 108	366.98	0.85	0.77	0.60	24.6	6.20	6.79	8.76
40X-4, 111	368.51	0.57	0.60	0.40	24.8	9.27	8.81	13.35
41X-2, 6	374.06	0.69	0.66	0.58	24.8	7.63	8.05	9.18
43X-2, 37	393.47	0.77	0.81	0.56	24.5	6.84	6.46	9.39
44X-2, 103	403.10	0.63	0.61	0.38	24.8	8.35	8.65	13.96
44X-5, 70	407.22	0.74	0.61	0.45	24.8	7.11	8.70	11.66
190-1178B-								
2R-2, 93	397.43	0.67	0.52	0.63	25.8	8.08	10.39	8.51
3R-3, 62	403.62	0.70	0.56	0.60	25.8	7.72	9.53	8.99
4R-4, 31	414.41	0.61	0.70	0.53	25.5	8.77	7.69	10.10
4R-CC, 10	416.04	0.43	0.55	0.43	25.5	12.48	9.66	12.42
5R-1, 96	420.26	0.58	0.67	0.56	24.6	9.15	7.80	9.37
5R-3, 103	423.33	0.59	0.56	0.46	24.7	8.94	9.45	11.42
6R-1, 34	429.34	0.77	0.83	0.66	24.6	6.80	6.32	7.92
6R-4, 55	434.05	0.39	0.63	0.41	24.6	13.60	8.34	12.76
7R-2, 90	441.00	0.52	0.57	0.41	24.5	10.02	9.15	12.73
7R-6, 54	446.64	0.52	0.59	0.45	24.5	10.05	8.96	11.54
7R-CC, 19	447.79	0.61	0.56	0.45	24.5	8.66	9.43	11.58
8R-2, 10	449.80	0.52	0.58	0.38	24.8	10.10	9.17	13.88
8R-4, 142	454.12	0.74	0.71	0.54	24.8	7.14	7.46	9.71
8R-6, 35	456.05	0.54	0.52	0.45	24.8	9.73	10.21	11.64
9R-4, 96	463.26	0.66	0.54	0.54	24.8	8.02	9.83	9.72
10R-4, 4	471.25	0.53	0.54	0.44	24.8	10.01	9.86	11.98
11R-CC, 12	483.84	0.45	0.48	0.54	24.8	11.69	11.08	9.84
14R-2, 48	507.98	0.89	0.76	0.67	24.9	5.97	6.97	7.94
15R-3, 108	519.68	0.56	0.52	0.33	24.9	9.46	10.13	16.02
15R-6, 42	523.52	0.48	0.50	0.34	24.9	10.94	10.52	15.44
16R-1, 26	525.46	0.49	0.56	0.32	25.0	10.91	9.54	16.69
16R-3, 127	529.47	0.52	0.56	0.51	24.9	10.25	9.52	10.32
16R-5, 20	531.40	0.49	0.57	0.32	25.0	10.79	9.30	16.41
17R-2, 38	536.65	0.46	0.53	0.41	25.0	11.41	9.96	13.03
17R-4, 15	538.92	0.43	0.60	0.46	25.0	12.34	8.80	11.63
18R-1, 27	544.67	0.50	0.45	0.34	24.9	10.65	11.75	15.50
18R-3, 123	548.63	0.44	0.54	0.39	25.0	12.12	9.87	13.44
18R-4, 133	550.23	0.48	0.61	0.37	25.0	11.06	8.67	14.31

**Table T19 (continued).**

Core, section, interval (cm)	Depth (mbsf)	Conductivity (S/m)			Temp (°C)	Formation factor		
		x	y	z		x	y	z
19R-2, 10	555.60	0.46	0.52	0.38	24.4	11.40	10.16	13.73
19R-3, 79	557.79	0.39	0.50	0.34	24.5	13.59	10.59	15.40
20R-CC, 7	569.59	0.40	0.49	0.34	24.5	13.10	10.79	15.45
21R-4, 71	578.51	0.50	0.37	0.43	24.6	10.43	14.05	12.35
22R-3, 19	585.97	0.47	0.50	0.32	24.8	11.15	10.54	16.31
23R-1, 100	593.50	0.55	0.39	0.41	24.7	9.67	13.44	12.79
23R-3, 46	595.96	0.34	0.46	0.34	24.7	15.47	11.41	15.28
24R-3, 62	605.72	0.35	0.52	0.34	24.7	15.04	10.22	15.60
24R-4, 35	606.95	0.38	0.42	0.34	24.7	13.93	12.56	15.59
25R-1, 76	612.46	0.34	0.50	0.37	24.7	15.71	10.61	14.30
26R-CC, 13	624.43	0.45	0.42	0.31	24.7	11.74	12.65	16.95
27R-2, 30	632.80	0.43	0.42	0.31	24.9	12.38	12.68	17.10
28R-3, 92	644.62	0.35	0.41	0.25	24.6	14.83	12.70	20.80
29R-1, 101	651.41	0.44	0.41	0.27	24.5	11.83	12.88	19.48
29R-2, 94	652.84	0.54	0.50	0.31	24.5	9.72	10.46	16.91
30R-1, 36	660.36	0.47	0.37	0.29	24.7	11.24	14.11	18.22
30R-3, 88	663.88	0.47	0.47	0.32	24.7	11.13	11.13	16.66
30R-3, 86	663.86	0.42	0.32	0.36	25.2	12.71	16.53	14.59
31R-2, 141	672.51	0.49	0.43	0.32	25.4	10.94	12.46	16.88
31R-CC, 21	673.14	0.32	0.44	0.31	25.1	16.42	12.05	17.37

Note: Measurements on cubes were generally performed in directions x, y (orthogonal to core) and z (parallel to core). Measurements in italic were performed on samples cut following the main foliation. For those samples, z is orthogonal to the foliation and y is the intersection of the foliation plane with the core face.

**Table T20.** Formation factor data from the needle-probe method, Hole 1178A.

Core, section, interval (cm)	Depth (mbsf)	Lithologic type	Formation factor	
			y	z
190-1178A-				
1H-2, 86	2.36	Clayey silt	2.97	2.83
2H-2, 90	5.30	Clayey silt	2.70	2.89
2H-6, 91	11.31	Clayey silt	2.88	2.93
3H-2, 62	14.52	Clayey silt	3.12	3.30
3H-6, 58	20.48	Clayey silt	3.51	3.09
4H-3, 93	25.83	Clayey silt	4.64	4.77
4H-6, 127	29.67	Clayey silt	4.08	4.21
5H-2, 65	33.55	Clayey silt	3.68	3.72
5H-6, 60	39.50	Clayey silt	4.17	4.73
6H-2, 83	43.23	Clayey silt	4.01	4.62
6H-6, 68	49.08	Clayey silt	5.24	5.48
7H-1, 84	51.24	Clayey silt	5.16	5.29
7H-5, 70	57.10	Clayey silt	4.68	4.72
8H-2, 92	59.92	Clayey silt	4.93	5.09
8H-5, 41	63.91	Clayey silt	4.78	5.20

Note: y and z = probe axis.